The bony anatomy of Chadian *Synodontis* (Osteichthyes, Teleostei, Siluriformes, Mochokidae): interspecific variations and specific characters

Aurélie PINTON
Olga OTERO
Université Poitiers, Bâtiment des Sciences naturelles,
Faculté des Sciences fondamentales et appliquées,
Institut international de Paléoprimatologie, Paléontologie humaine :
Évolution et Paléoenvironnements (IPHEP), CNRS UMR 6046,
40 av. du Recteur Pineau, F-86022 Poitiers cedex (France)
aurelie.pinton@univ-poitiers.fr
olga.otero@univ-poitiers.fr

Pinton A. & Otero O. 2010. — The bony anatomy of Chadian *Synodontis* (Osteichthyes, Teleostei, Siluriformes, Mochokidae): interspecific variations and specific characters. *Zoosystema* 32 (2) : 173-231.

ABSTRACT
The genus *Synodontis* Cuvier, 1816 (Siluriformes, Mochokidae) numbers about 120 species and is exclusive to the freshwater of Africa except Maghreb and Cape Province. It is one of the most widespread catfish of African freshwater. The *Synodontis* fossil record covers the last 18 Myr and most of the *Synodontis* fossil bones are found in a disarticulated state. The identification of the fossils at a specific level is so far impossible, because we lack an osteological study of the species. Here, we present the study of the osteology of eleven *Synodontis* species living in Chad: *S. batensoda* Rüppell, 1832, *S. clarias* (Linnaeus, 1758), *S. courteti* Pellegrin, 1906, *S. eupterus* Boulenger, 1901, *S. filamentosus* Boulenger, 1901, *S. membranaceus* (Geoffroy Saint-Hilaire, 1809), *S. nigrita* Valenciennes, 1840, *S. ocellifer* Boulenger, 1900, *S. schall* (Bloch & Schneider, 1801), *S. sorex* Günther, 1864 and *S. violaceus* Pellegrin, 1919. Each species is characterized based on its bony anatomy. The morphological variability within and between the species is discussed. The entire skeleton is described, bone by bone. A total of 61 osteological characters, both qualitative and quantitative are established. We emphasize the bones that are well preserved in the fossil, i.e. the mesethmoid, the lateral ethmoid, the frontal, the supraoccipital, the cleithrum, the pectoral spine, the middle nucal plate and the dorsal spine. As a first result, the Chadian *Synodontis* species can be recognized on the basis of bony characters only. Second, we are also able to attribute isolated bones to nominative species or to a group of species. At last, we note that no osteological character legitimates the distinction of the genera *Hemisynodontis* Bleeker, 1862 and *Brachysynodontis* Bleeker, 1862.

KEY WORDS
Osteichthyes,
Teleostei,
Siluriformes,
Mochokidae,
Synodontis,
Africa,
Chad,
osteology,
morphometry,
species identification.

RÉSUMÉ
Anatomie osseuse de Synodontis *du Tchad (Osteichthyes, Teleostei, Siluriformes, Mochokidae) : variabilité intra-spécifique et caractéristiques spécifiques.*
Le genre *Synodontis* Cuvier, 1816 (Siluriformes, Mochokidae) comprend environ 120 espèces dont la distribution est restreinte à l'ensemble des eaux douces africaines, excepté le Maghreb et la province du Cap en Afrique du Sud. C'est l'un des poissons-chats les plus répandus en Afrique. Le registre fossile de *Synodontis* couvre les 18 derniers millions d'années et la majorité des restes fossiles se trouve à l'état désarticulé. L'identification d'espèces de *Synodontis* dans le registre fossile est à ce jour impossible parce qu'il n'existe pas d'étude ostéologique des espèces. Ici, nous présentons l'anatomie osseuse de 11 espèces de *Synodontis* présentes au Tchad : *S. batensoda* Rüppell, 1832, *S. clarias* (Linnaeus, 1758), *S. courteti* Pellegrin, 1906, *S. eupterus* Boulenger, 1901, *S. filamentosus* Boulenger, 1901, *S. membranaceus* (Geoffroy Saint-Hilaire, 1809), *S. nigrita* Valenciennes, 1840, *S. ocellifer* Boulenger, 1900, *S. schall* (Bloch & Schneider, 1801), *S. sorex* Günther, 1864 and *S. violaceus* Pellegrin, 1919. Chacune de ces espèces est caractérisée sur la base de son anatomie osseuse uniquement, et la variabilité morphologique existant au sein et entre chacune des espèces est discutée. Le squelette entier est décrit, os par os. Au total, 61 caractères, qualitatifs et quantitatifs sont établis. Nous insistons sur les os particulièrement bien préservés dans le registre fossile, c'est-à-dire le mésethmoïde, l'ethmoïde latéral, le frontal, le pariéto-supraoccipital, le cleithrum, l'épine pectorale, la seconde plaque nucale et l'épine dorsale. Comme premier résultat, il apparaît que les espèces de *Synodontis* peuvent être reconnues sur la base seule de leur anatomie osseuse. Ensuite, nous sommes capables d'attribuer des os isolés à une espèce ou à un groupe d'espèces. Enfin, aucun des caractères ostéologiques établis ne légitime la distinction des genres *Hemisynodontis* Bleeker, 1862 et *Brachysynodontis* Bleeker, 1862.

MOTS CLÉS
Osteichthyes, Teleostei, Siluriformes, Mochokidae, *Synodontis*, Afrique, Tchad, ostéologie, morphométrie, identification des espèces.

INTRODUCTION

The genus *Synodontis* Cuvier, 1816 belongs to the catfish family Mochokidae Jordan, 1923. With about 120 species exclusive to the freshwaters of Africa except Maghreb and Cape Province, it is one of the most diversified catfish genera in Africa (Poll 1971). Some living species are restricted to a single stream, whereas others overlap several drainage basins (Poll 1971). In the ichtyological provinces where the *Synodontis* genus is distributed, a high level of endemicity is observed. For instance, in the Congo province, 34 of the 41 *Synodontis* species are endemic. According to Poll (1971), *Synodontis* high level of endemicity supports a long-time history in the hydrographical network dependent on the geological context. This long-time history is confirmed by the richness of the fossil record which starts in the Early Miocene of Chalouf, Egypt (*c.* 18 Myr). So far, fossil remains have been reported in eastern and Central Africa, and also in Maghreb (Priem 1920; Greenwood 1951, 1972, 1973; Greenwood & Howes 1975; Van Couvering 1977; Schwartz 1983; Gaudant 1987; Stewart 1990, 2003a, b; Van Neer 1992, 1994; Brunet *et al.* 2000; Vignaud *et al*. 2002; Otero *et al*. 2009, in press).

The wide distribution of the modern *Synodontis* genus, its high level of endemicity as well as its richness in the fossil record make it of primary interest in order to study past diversity and to reconstruct the paleobiogeography of African drainage basins

during the Neogene (23-2.5 Myr). Due to the lack of osteological study of the species, most of the fossil specimens are identified only at the familial or generic levels, which prevents the reconstruction of the history of the group. From this perspective, the identification of fossil *Synodontis* at a specific level is crucial. It is one of the first steps to reconstruct the history of the group in the freshwater basins in Africa.

Most of the fossil fish from continental outcrops are found disarticulated, with the exception of some lake and swamp deposits. In the case of *Synodontis*, partial neurocrania or connected skulls are known but rare, and most of its fossil record is composed of isolated bones. More frequently, we found mesethmoid, frontals, supraoccipitals, cleithra, pectoral spines, nucal shield bones and dorsal spines. The only existing osteological description of *Synodontis* is the study by Taverne & Aloulou-Triki (1974), who only considered common features of several modern species in order to define the genus. Studies on soft characters, including meristematic ones (fins), as well as brief description of the body of the pectoral spine and of the humeral plate of *Synodontis* were carried out by Poll (1971) and Paugy & Roberts (1992) in order to identify extant species. So far, the possibility to identify species based on osteological characters only has never been tested. However, both the diversity of shapes observed among the fossils and a preliminary study on the fin spines (Pinton *et al*. 2006) support that the analysis of qualitative and quantitative characters might allow the identification of isolated bones at a specific level.

Of the over 100 species of *Synodontis*, we focus on the 11 Chadian ones to be able to determine the fossils that have been collected in the Neogene deposits of the Chad basin (Vignaud *et al.* 2002; Otero *et al.* in press). Moreover, these species represent a third of the genus diversity in the Nilo-Sudan province, where they are widely distributed. We describe the bony anatomy of each nominal species and we estimate the amount of variability in the bony morphology within the genus and among the species. The entire skeleton is described, bone by bone. We focus on the elements that exhibit specific characteristics, and on the bones that preserve well in the fossil. To describe the bone shape and when pertinent for species determination, we discuss the distribution of quantitative characters that complement the qualitative observations made. These characters defined on modern specimens would allow the attribution of fossil remains. They allow also the discussion of the validity of osteological arguments to attribute the species *Synodontis batensoda* Rüppel, 1892 and *S. membranaceus* (Geoffroy Saint-Hilaire, 1809) to separate genera, i.e. *Brachysynodontis* Bleeker, 1862 and *Hemisynodontis* Bleeker, 1862. We emphasize illustration of the characters observed.

MATERIALS AND METHODS

The material belongs to 11 *Synodontis* species reported from Chad country by various authors: *S. batensoda* (n = 16), *S. clarias* (Linnaeus, 1758) (n = 17), *S. courteti* Pellegrin, 1906 (n = 9), *S. eupterus* Boulenger, 1901 (n = 2), *S. filamentosus* Boulenger, 1901 (n = 7), *S. membranaceus* (n = 13), *S. nigrita* Valenciennes, 1840 (n = 12), *S. schall* (Bloch & Schneider, 1801) (n = 25), *S. sorex* Günther, 1864 (n = 13) and *S. violaceus* Pellegrin, 1919 (n = 10). These 10 species are present in Chad country, in the Chadian basin. The species *Synodontis ocellifer* Boulenger, 1900 (n = 5) is also included in the study. It inhabits Chad country in the Lac Lere which belongs to the Niger basin. Conversely, the species *Synodontis frontosus* Vaillant, 1895 is not included despite being reported in the Chadian waters by Blache (1964). Indeed, this species is known endemic in the Nile River and its supposed presence in Chad probably results from a misidentification (Poll 1971; Paugy pers. comm.). The studied material is listed in Table 1.

The fresh specimens were prepared as dry skeletons either by boiling or letting them decompose naturally. In the latter case, the bony elements are not articulated and we exclude meristic data for these specimens. Observations were conducted under a stereomicroscope. Linear measurements were taken using a digital calliper or on stereomicroscope photographs, except for the cleithra, on

TABLE 1. — List of the *Synodontis* Cuvier, 1816 dry-skeleton material studied. The material is deposited in the Centre de Valorisation des Collections de l'Université de Poitiers (CVCU).

Species	Collection number	Standard length (mm)	Origin	Species	Collection number	Standard length (mm)	Origin
S. membranaceus	UP-BA-2999	225	Chad basin	*S. clarias*	UP-BA-3065	173	Niger basin
S. membranaceus	UP-BA-3000	230	Chad basin	*S. clarias*	UP-BA-3066	155	Niger basin
S. membranaceus	UP-BA-3001	235	Chad basin	*S. clarias*	UP-BA-3067	170	Chad basin
S. membranaceus	UP-BA-3002	245	Chad basin	*S. clarias*	UP-BA-3068	140	Chad basin
S. membranaceus	UP-BA-3003	200	Chad basin	*S. clarias*	UP-BA-3069	145	Chad basin
S. membranaceus	UP-BA-3004	195	Niger basin	*S. clarias*	UP-BA-3070	135	Chad basin
S. membranaceus	UP-BA-3005	130	Chad basin	*S. schall*	UP-BA-3071	120	Chad basin
S. membranaceus	UP-BA-3006	135	Chad basin	*S. schall*	UP-BA-3072	120	Chad basin
S. membranaceus	UP-BA-3007	130	Chad basin	*S. schall*	UP-BA-3073	125	Chad basin
S. membranaceus	UP-BA-3008	140	Chad basin	*S. schall*	UP-BA-3074	120	Chad basin
S. membranaceus	UP-BA-3009	140	Chad basin	*S. schall*	UP-BA-3075	110	Chad basin
S. membranaceus	UP-BA-3010	145	Chad basin	*S. schall*	UP-BA-3076	115	Chad basin
S. membranaceus	UP-BA-3011	145	Chad basin	*S. schall*	UP-BA-3077	120	Chad basin
S. sorex	UP-BA-3012	148	Chad basin	*S. schall*	UP-BA-3078	125	Chad basin
S. sorex	UP-BA-3013	150	Chad basin	*S. schall*	UP-BA-3079	140	Niger basin
S. sorex	UP-BA-3014	158	Chad basin	*S. schall*	UP-BA-3080	153	Niger basin
S. sorex	UP-BA-3015	180	Chad basin	*S. schall*	UP-BA-3081	138	Niger basin
S. sorex	UP-BA-3016	200	Chad basin	*S. schall*	UP-BA-3082	180	Niger basin
S. sorex	UP-BA-3017	156	Chad basin	*S. schall*	UP-BA-3083	142	Niger basin
S. sorex	UP-BA-3018	195	Chad basin	*S. schall*	UP-BA-3084	153	Niger basin
S. sorex	UP-BA-3019	165	Niger basin	*S. schall*	UP-BA-3085	140	Niger basin
S. sorex	UP-BA-3020	158	Niger basin	*S. schall*	UP-BA-3086	150	Niger basin
S. sorex	UP-BA-3021	185	Niger basin	*S. schall*	UP-BA-3087	165	Niger basin
S. sorex	UP-BA-3022	152	Niger basin	*S. schall*	UP-BA-3088	150	Senegal basin
S. sorex	UP-BA-3023	145	Niger basin	*S. schall*	UP-BA-3089	120	Senegal basin
S. sorex	UP-BA-3024	163	Niger basin	*S. schall*	UP-BA-3090	130	Senegal basin
S. batensoda	UP-BA-3025	123	Chad basin	*S. schall*	UP-BA-3091	125	Senegal basin
S. batensoda	UP-BA-3026	125	Chad basin	*S. schall*	UP-BA-3092	135	Senegal basin
S. batensoda	UP-BA-3027	126	Chad basin	*S. schall*	UP-BA-3093	135	Senegal basin
S. batensoda	UP-BA-3028	126	Chad basin	*S. schall*	UP-BA-3094	155	Senegal basin
S. batensoda	UP-BA-3029	130	Chad basin	*S. schall*	UP-BA-3095	250	Senegal basin
S. batensoda	UP-BA-3030	137	Chad basin	*S. filamentosus*	UP-BA-3096	110	Chad basin
S. batensoda	UP-BA-3031	105	Chad basin	*S. filamentosus*	UP-BA-3097	115	Chad basin
S. batensoda	UP-BA-3032	135	Chad basin	*S. filamentosus*	UP-BA-3098	140	Niger basin
S. batensoda	UP-BA-3033	135	Chad basin	*S. filamentosus*	UP-BA-3099	150	Niger basin
S. batensoda	UP-BA-3034	145	Chad basin	*S. filamentosus*	UP-BA-3100	130	Niger basin
S. batensoda	UP-BA-3035	115	Niger basin	*S. filamentosus*	UP-BA-3101	125	Niger basin
S. batensoda	UP-BA-3036	130	Niger basin	*S. filamentosus*	UP-BA-3102	135	Niger basin
S. batensoda	UP-BA-3037	110	Niger basin	*S. courteti*	UP-BA-3103	240	Chad basin
S. batensoda	UP-BA-3038	115	Niger basin	*S. courteti*	UP-BA-3104	225	Chad basin
S. batensoda	UP-BA-3039	120	Niger basin	*S. courteti*	UP-BA-3105	225	Niger basin
S. batensoda	UP-BA-3040	125	Niger basin	*S. courteti*	UP-BA-3106	165	Niger basin
S. nigrita	UP-BA-3041	60	Chad basin	*S. courteti*	UP-BA-3107	280	Niger basin
S. nigrita	UP-BA-3042	60	Chad basin	*S. courteti*	UP-BA-3108	170	Niger basin
S. nigrita	UP-BA-3043	60	Chad basin	*S. courteti*	UP-BA-3109	190	Niger basin
S. nigrita	UP-BA-3044	60	Chad basin	*S. courteti*	UP-BA-3110	230	Chad basin
S. nigrita	UP-BA-3045	60	Chad basin	*S. courteti*	UP-BA-3111	230	Chad basin
S. nigrita	UP-BA-3046	60	Chad basin	*S. violaceus*	UP-BA-3112	125	Niger basin
S. nigrita	UP-BA-3047	65	Chad basin	*S. violaceus*	UP-BA-3113	175	Niger basin
S. nigrita	UP-BA-3048	65	Chad basin	*S. violaceus*	UP-BA-3114	115	Niger basin
S. nigrita	UP-BA-3049	65	Chad basin	*S. violaceus*	UP-BA-3115	125	Niger basin
S. nigrita	UP-BA-3050	65	Chad basin	*S. violaceus*	UP-BA-3116	135	Niger basin
S. nigrita	UP-BA-3051	65	Chad basin	*S. violaceus*	UP-BA-3117	165	Niger basin

TABLE 1. — Continuation.

Species	Collection number	Standard length (mm)	Origin	Species	Collection number	Standard length (mm)	Origin
S. nigrita	UP-BA-3052	70	Chad basin	*S. violaceus*	UP-BA-3118	180	Senegal basin
S. clarias	UP-BA-3053	135	Chad basin	*S. violaceus*	UP-BA-3119	175	Senegal basin
S. clarias	UP-BA-3054	150	Chad basin	*S. violaceus*	UP-BA-3120	175	Senegal basin
S. clarias	UP-BA-3055	155	Chad basin	*S. violaceus*	UP-BA-3121	180	Chad basin
S. clarias	UP-BA-3056	155	Chad basin	*S. ocellifer*	UP-BA-3122	150	Senegal basin
S. clarias	UP-BA-3057	150	Chad basin	*S. ocellifer*	UP-BA-3123	140	Senegal basin
S. clarias	UP-BA-3058	160	Chad basin	*S. ocellifer*	UP-BA-3124	165	Senegal basin
S. clarias	UP-BA-3059	165	Chad basin	*S. ocellifer*	UP-BA-3125	160	Senegal basin
S. clarias	UP-BA-3060	155	Chad basin	*S. ocellifer*	UP-BA-3126	140	Senegal basin
S. clarias	UP-BA-3061	170	Chad basin	*S. eupterus*	UP-BA-3127	100	Chad basin
S. clarias	UP-BA-3062	145	Chad basin	*S. eupterus*	UP-BA-3128	115	Chad basin
S. clarias	UP-BA-3063	115	Niger basin				

which studies were performed on a Gateway 2000 computer using the free UTHSCSA Image Tool program (developed at the University of Texas Health Science Center at San Antonio, Texas and available from the Internet by anonymous FTP from ftp://maxrad6.uthscsa.edu). Differences in the shape between the bones of different *Synodontis* species were assessed for both qualitative and quantitative variations. For quantitative differences, we used log-shape-ratios following Mosimann's method (Mosimann 1970), so that the size effect is removed on each observation on an individual basis, using a calculated index for the individual size. This index is the geometric mean which is the nth root of the product of the n variables. The procedure is applied on log transformed data because of size heterogeneity among the group. Finally, each individual is adjusted for size by taking the difference of each log variable with log size, which is the log-shape-ratio. We used an analysis of variance (ANOVA) with Tukey's post hoc test for Honestly Significant Differences (HSD). The statistical analysis was run with the CCS: STATISTICA package to test the significance of the variable values between the species. We used a significant level at $P < 0.05$. Finally, we calculated a Euclidean distance matrix based on 46 linear measurements to describe the morphological resemblance of the head among the species through a principal component analysis. Osteological terminology follows Mo (1991).

OSTEOLOGICAL ANATOMY OF MODERN CHADIAN *SYNODONTIS* SPECIES

GENERAL FEATURES OF THE NEUROCRANIUM (FIG. 1)

According to Mo (1991), the neurocranium of *Synodontis* is characterized by a mesethmoid which is anteriorly thickened and round or convex and a reduced epioccipital. Moreover, there is no extrascapula; the supraoccipital is truncated posteriorly where it connects the wide nucal shield; a single fontanel develops anteriorly between the frontals; and a fenestra opens between the lateral ethmoid and the orbitosphenoid.

THE MESETHMOID (FIGS 2; 3; APPENDIX 1)

Unlike the rest of the neurocranial roof, the ethmoid region is dorsally ornamented with ridges instead of tubercles. The mesethmoid constitutes the anterior part of the skull roof. Posteriorly, it articulates through an interdigitated suture with the two frontals on both lateral sides of the anterior tip of the fontanel (Fig. 2A, B). Ventrally, in its anterior half, the mesethmoid exhibits two wings that develop laterally on both sides of the vomerine surface, where the maxilla-palatine complex lies (Fig. 2C). Both lateral ethmoids articulate with the mesethmoid along its posterolateral edges and through ventral projections (Fig. 2B, C).

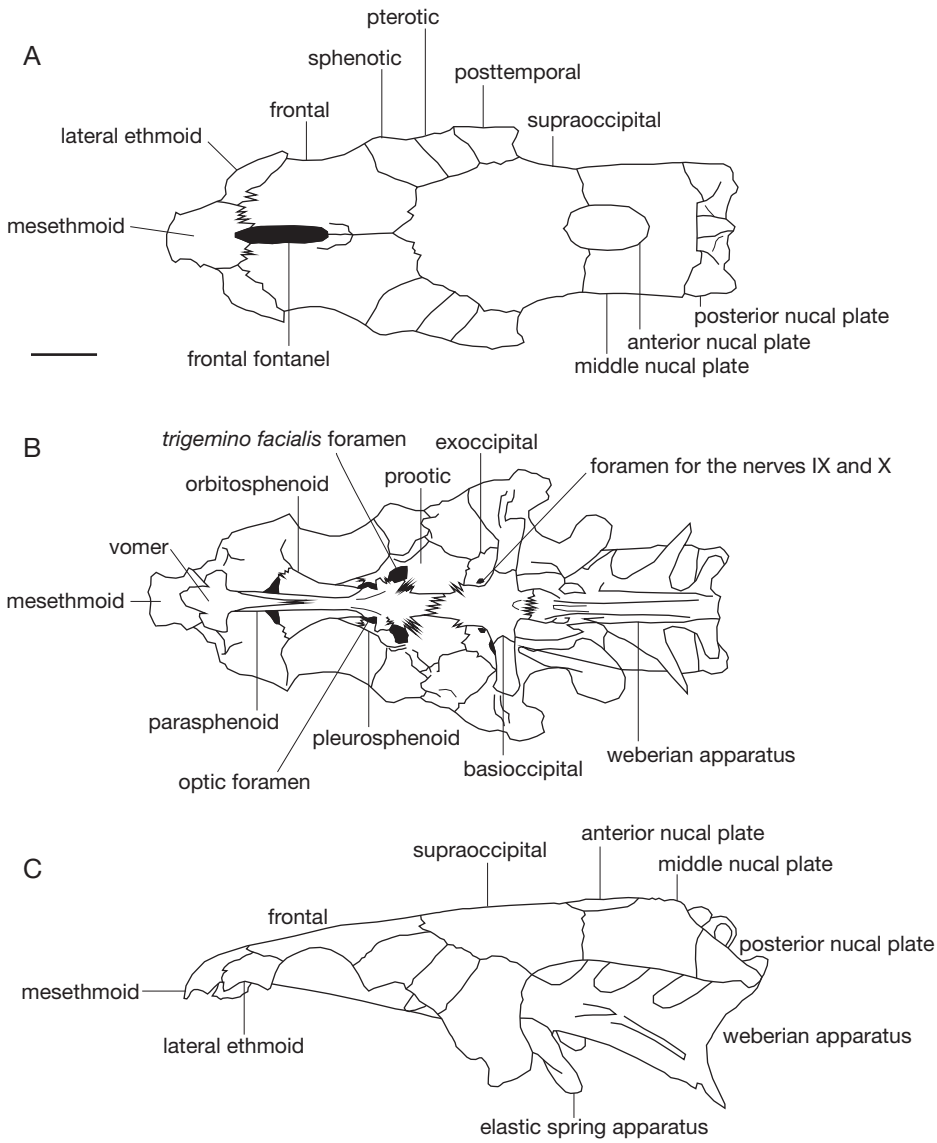

FIG. 1. — The neurocranium in *Synodontis* Cuvier, 1816, exemplified in *S. schall* (Bloch & Schneider, 1801): **A**, dorsal view; **B**, ventral view; **C**, lateral view. Scale bar: 20 mm.

In dorsal view (Fig. 2D-I) the mesethmoid globally displays a quadrangular shape in *Synodontis courteti*, *S. ocellifer*, *S. eupterus* and *S. filamentosus* (Fig. 2G-I), and a trapezoidal shape in all other species studied, including *S. clarias*, *S. sorex* and *S. membranaceus* (Fig. 2D-F). Two types of trapezoidal shapes are observed: the anterior edge is the largest in *S. membranaceus* (Fig. 2F) and *S. violaceus*, whereas the anterior edge is shorter in the remaining species, such as *S. clarias*, and *S. sorex* (Fig. 2D, E). Moreover, there is an anterior constriction at about one third of the mesethmoid length in every Chadian *Synodontis* except in all *S. clarias* studied (Fig. 2D) and in some *S. schall* specimens. Finally,

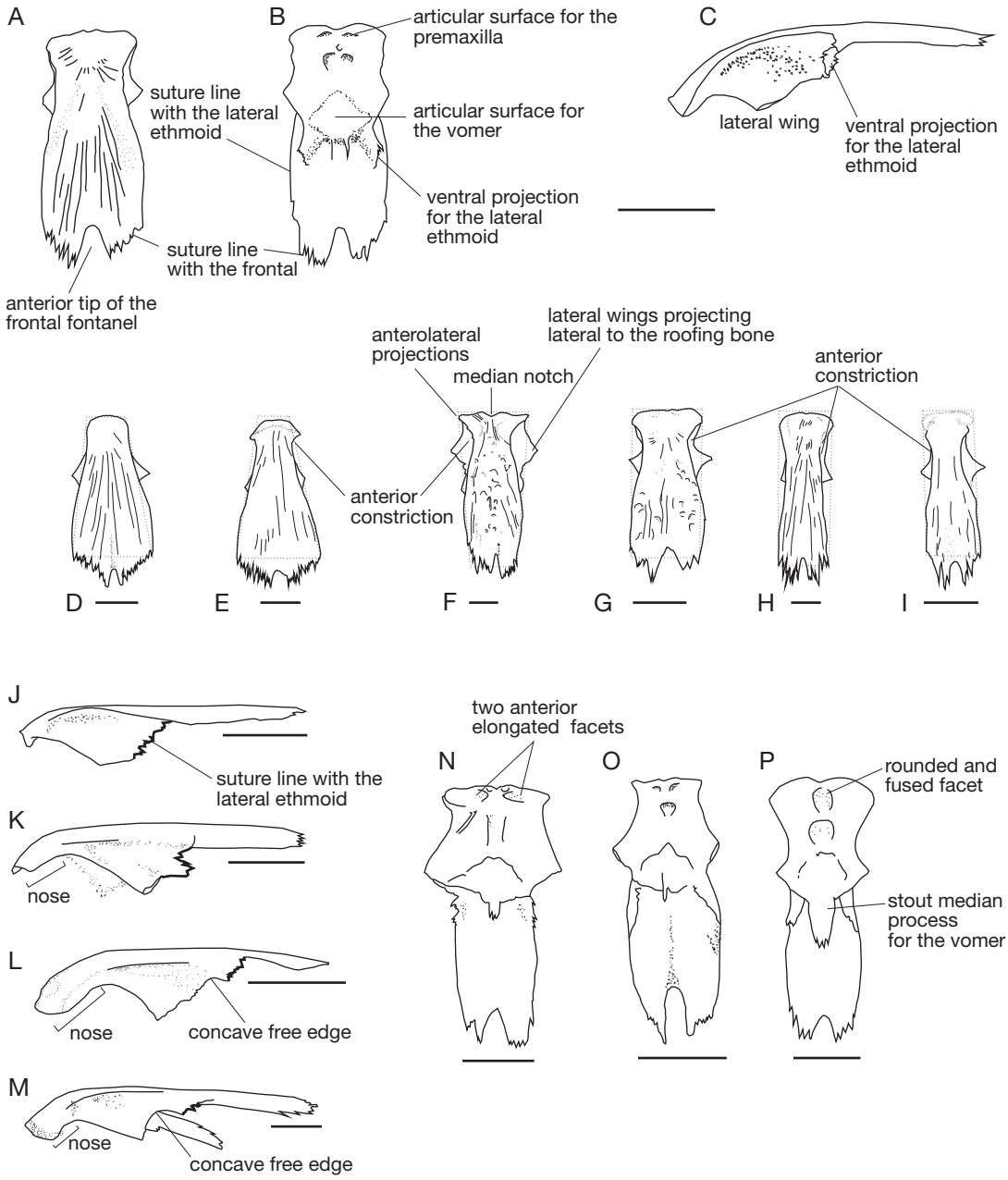

FIG. 2. — The mesethmoid of *Synodontis* Cuvier, 1816 species: **A**-**C**, main features exemplified in *S. schall* (Bloch & Schneider, 1801); **A**, dorsal view; **B**, ventral view; **C**, lateral view; **D**-**I**, mesethmoids in dorsal views; **D**, *S. clarias* (Linnaeus, 1758); **E**, *S. sorex* Günther, 1864; **F**, *S. membranaceus* (Geoffroy Saint-Hilaire, 1809); **G**, *S. ocellifer* Boulenger, 1900; **H**, *S. courteti* Pellegrin, 1906; **I**, *S. filamentosus* Boulenger, 1901; **J**-**M**, mesethmoids in lateral views; **J**, *S. membranaceus*; **K**, *S. clarias*; **L**, *S. violaceus* Pellegrin, 1919; **M**, *S. courteti*; **N**-**P**, mesethmoids in ventral views; **N**, *S. membranaceus*; **O**, *S. batensoda* Rüppell, 1832; **P**, *S. violaceus.* Scale bars: 5 mm.

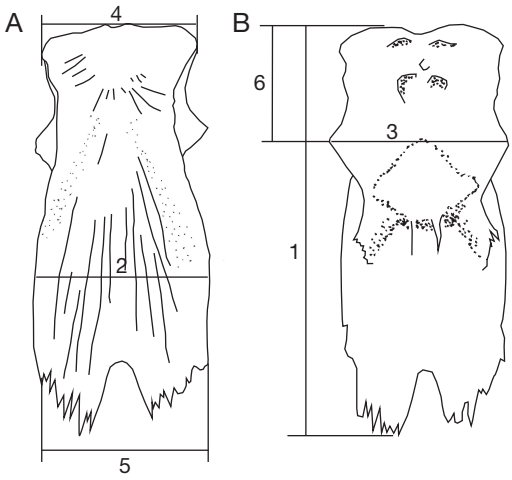

FIG. 3. — Linear measurements taken on the mesethmoids, shown in *Synodontis schall* (Bloch & Schneider, 1801): **A**, dorsal view; **B**, ventral view. Measurements: **1**, maximum length; **2**, maximum width of the whole bone; **3**, width of the lateral wings; **4**, width of the anterior edge of the bone; **5**, width of the bone at the suture with the frontals; **6**, length from the anterior edge of the mesethmoid to the level of the maximum width of the lateral wings.

in *S. membranaceus* only, the two anterolateral projections develop on both side of a minute median anterior notch and the lateral wings project clearly lateral to the edge of the roofing bone (Fig. 2F).

In lateral view, the mesethmoid of *Synodontis violaceus*, *S. clarias*, *S. courteti* (Fig. 2K-M), *S. filamentosus* and *S. sorex* exhibit a "nose" due to a more posterior position of the insertion of the lateral wings. Moreover, the ventral surface for the articulation with the lateral ethmoid is either continuous with the lateral wings (in most of the species, e.g., Fig. 2J, K) or they are separated from each other by a concave free edge in *S. violaceus*, *S. courteti* (Fig. 2L, M) and *S. sorex*.

Ventrally (Fig. 2N-P), there are two anterior facets where the upper jaw ligaments attach. Their shape varies according to the species. In *Synodontis membranaceus*, they are elongated (Fig. 2N), whereas they are rounded in the other species (e.g., Fig. 2O, P); in *S. violaceus* (Fig. 2P) and *S. filamentosus* only, they fuse medially. Additionally, in *Synodontis sorex* and *S. clarias*, the facets are poorly marked. Posterior to these facets, two depressions develop within a small median fossa (Fig. 2N, O), except in *S. membranaceus* which lacks the depression and the fossa (Fig. 2N). In the specimens of *S. membranaceus* that are larger than 200 mm in standard length, the vomer and the mesethmoid are fused, whereas the head of the vomer is autogenous and sutures with the mesethmoid between the two lateral wings in other *Synodontis* species. Finally, in *Synodontis courteti*, *S. filamentosus* and *S. violaceus*, a stout median process develops posteriorly towards the parasphenoid and supports the anterior part of the body of the vomer (Fig. 2P).

Six linear measurements on the mesethmoid (Fig. 3) transformed into log-shape ratios, and one log transformed variable enabled us to distinguish species and/or groups of species (Appendix 1). The most evident characters are as follows.

The log-shape ratios based on the width of the suture with the frontal bones (Appendix 1: variable 5) and the width of the lateral wings (Appendix 1: 3) statistically isolate *Synodontis membranaceus* because its mesethmoid presents a relatively shorter suture line and extended lateral wings. Because of the trapezoidal outline of their mesethmoid (Fig. 3B), *S. membranaceus* and *S. violaceus* share high values of the log transformed variable "width of the anterior edge of the bone/maximum width of the whole bone" (Appendix 1: 7).

Synodontis sorex and *S. clarias* also are distinguished statistically for this log variable because they exhibit a trapezoidal outline of the mesethmoid with the base corresponding to the posterior edge. Moreover, *S. clarias* was kept apart statistically from the other species by the values of the log transformed variables constructed on the width of the anterior edge and on the maximum width of the bone (Appendix 1), because it displays a relatively wide mesethmoid with a narrow anterior edge.

Synodontis filamentosus and *S. courteti* do not differ statistically from each other. They both exhibit a long mesethmoid (Appendix 1: 1) and a fairly short suture with the frontals (Appendix 1: 5); their lateral wings are not extended laterally (Appendix 1: 3), whereas the length from the anterior edge of the mesethmoid to the level of the maximum width of the lateral wings is relatively great (Appendix 1: 6). Moreover, these two species exhibit a nose and a general quadrangular shape of the bone (Appendix 1: 7).

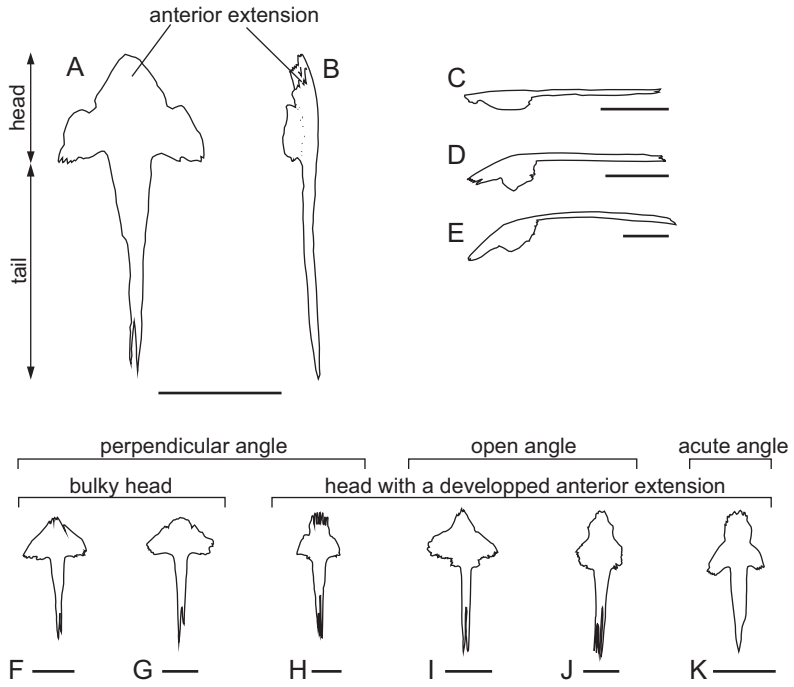

FIG. 4. — The vomer of *Synodontis* Cuvier, 1816 species: **A**, **B**, main features exemplified in *S. schall* (Bloch & Schneider, 1801); **A**, dorsal view; **B**, lateral view; **C**-**E**, vomers in lateral views; **C**, *S. batensoda* Rüppell, 1832; **D**, *S. clarias* (Linnaeus, 1758); **E**, *S. sorex* Günther, 1864; **F**-**K**, vomers in dorsal views; **F**, *S. batensoda*; **G**, *S. membranaceus* (Geoffroy Saint-Hilaire, 1809); **H**, *S. courteti* Pellegrin, 1906; **I**, *S. clarias*; **J**, *S. sorex*; **K**, *S. filamentosus* Boulenger, 1901. Scale bars: 5 mm.

Synodontis batensoda is statistically associated with *S. membranaceus*, *S. filamentosus*, *S. courteti* and *S. violaceus* for the log-shape ratio constructed from the maximum length (Appendix 1: 1), whereas it is separated from them by the log-shape ratio constructed from the maximum width (Appendix 1: 2) in relation with its relatively long and wide mesethmoid.

Synodontis ocellifer and *S. schall* resemble each other by the short length of their mesethmoids (Appendix 1: 1), a large suture with the frontals (Appendix 1: 5); their lateral wings are fairly extended laterally (Appendix 1: 3) and the length from the anterior edge of the mesethmoid to the level of the maximum width of the lateral wings is short (Appendix 1: 6). The log-shape ratio values presented by the dimensions of the mesethmoid of *S. eupterus* fall within the confidence interval of *S. schall* and *S. ocellifer*. At last, *S. nigrita* differs from all of them only by the log-shape ratio using the total length of the bone (Appendix 1: 1).

THE VOMER (FIG. 4)

The vomer is toothless. It globally exhibits an arrow-like shape (Fig. 4A, B), with a head that lies on the ventral face of the mesethmoid, and a tail that extends backwards onto the parasphenoid. The dorsal surface of the vomer is straight in most of the species (Fig. 4C), but bent ventrally only in *Synodontis clarias* and *S. sorex* (Fig. 4D, E).The shape of the head varies depending on the species, with a marked anterior extension in all of the species (Fig. 4H-K), except in *S. membranaceus* and *S. batensoda* in which the head is bulky (Fig. 4F, G). The angle formed by the posterior edge of the head and the median plane of the vomer is an acute angle in *S. filamentosus* (Fig. 4K) and *S. violaceus*, an open angle in *S. clarias* and *S. sorex* (Fig. 4I, J) and a right angle in the other species studied (Fig. 4F-H).

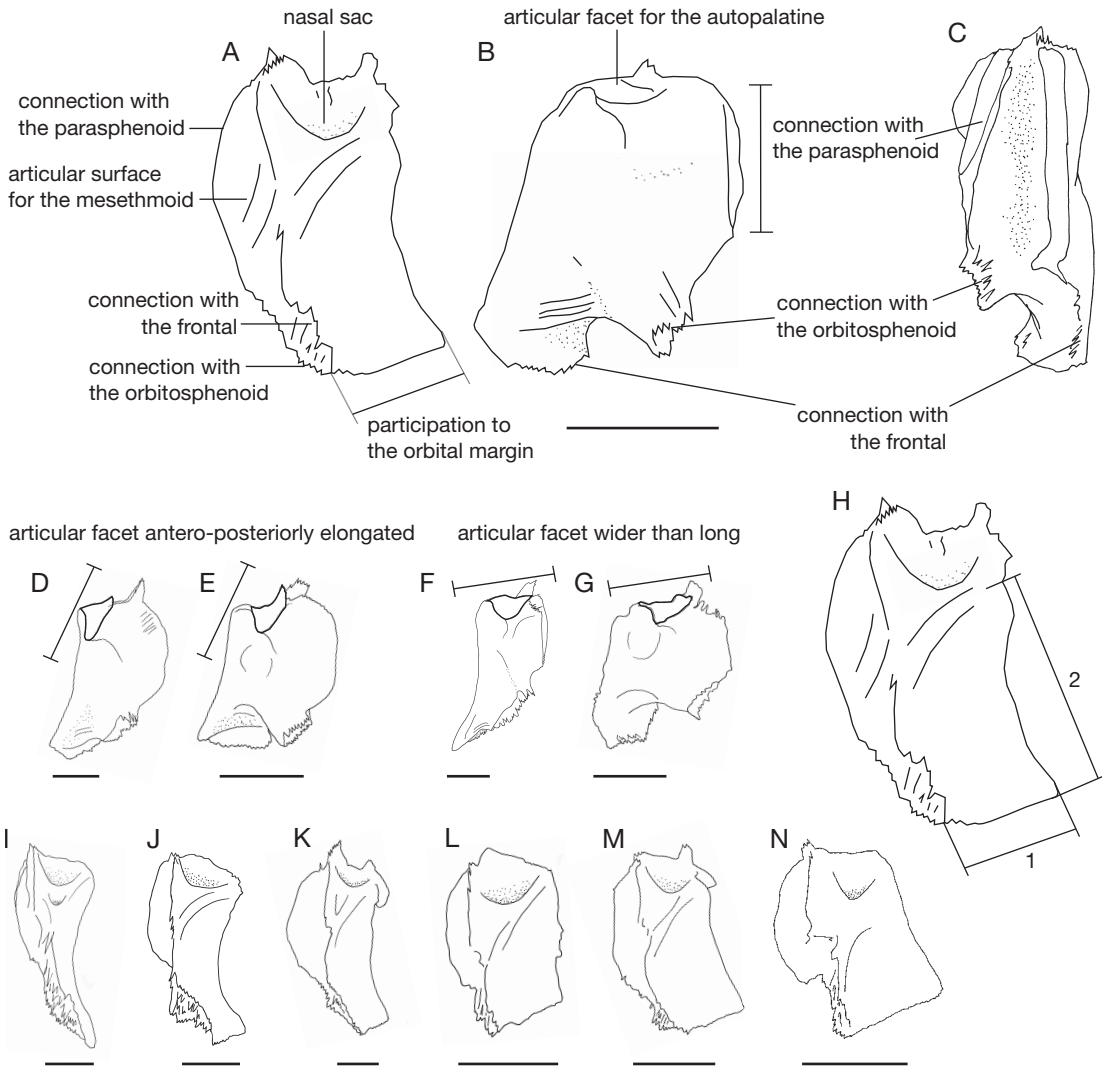

FIG. 5. — The lateral ethmoid of *Synodontis* Cuvier, 1816 species: **A**-**C**, main features of the lateral ethmoids, exemplified in *S. schall* (Bloch & Schneider, 1801) (right lateral ethmoid); **A**, medio-dorsal view; **B**, ventral view; **C**, lateral view; **D**-**G**, lateral ethmoids in ventral views; **D**, *S. sorex* Günther, 1864; **E**, *S. clarias* (Linnaeus, 1758); **F**, *S. courteti* Pellegrin, 1906; **G**, *S. ocellifer* Boulenger, 1900; **H**, linear measurements taken on the lateral ethmoids, shown in *S. schall* in medio-dorsal view; **1**, width of the free posterior edge; **2**, length of the lateral margin; **I**-**N**, lateral ethmoids in dorsal views; **I**, *S. courteti*; **J**, *S. violaceus* Pellegrin, 1919; **K**, *S. sorex*; **L**, *S. filamentosus* Boulenger, 1901; **M**, *S. clarias*; **N**, *S. eupterus* Boulenger, 1901. Scale bars: 5 mm.

THE LATERAL ETHMOID (FIG. 5; APPENDIX 2)

In its dorsal part, the lateral ethmoid sutures anteriorly with the posterior part of the mesethmoid, and posteriorly it sutures to the frontal anterior to the orbit and forms part of the orbital margin (Fig. 5A, C). It is free of dermal ornamentation in *Synodontis courteti* and in *S. violaceus*. Laterally, the posterior part of the lacrymal, the second infraorbital and the anterior part of the third infraorbital lie along the margin of the ethmoid. Ventrally, the two lateral ethmoids suture with the anterior tip of the parasphenoid at the front, and with the

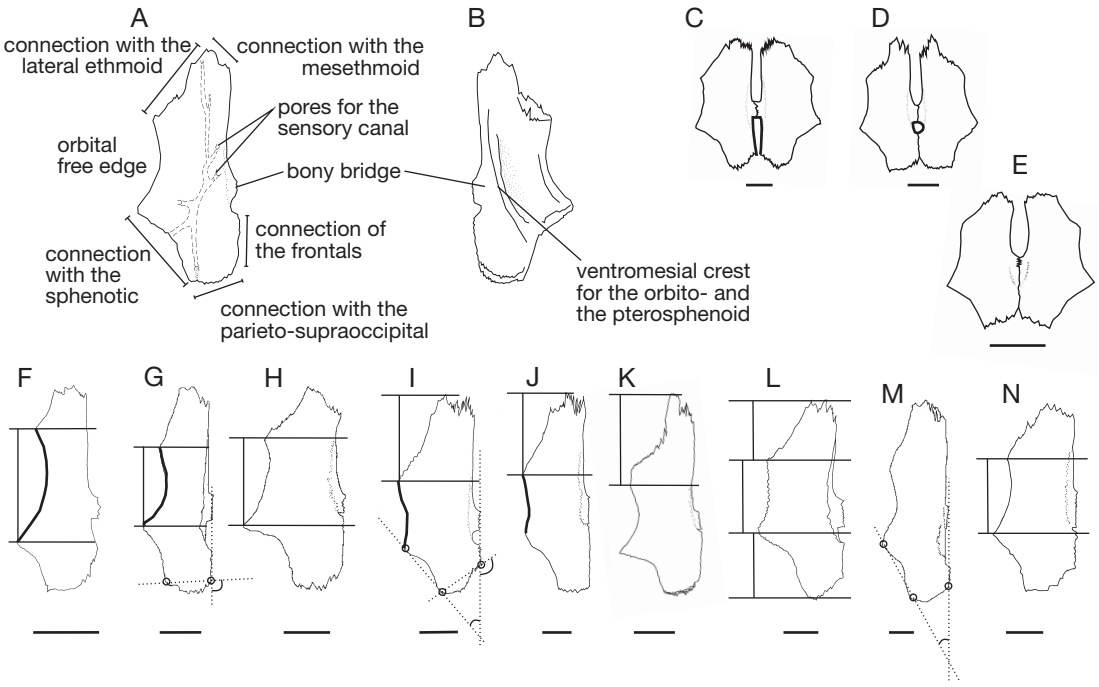

FIG. 6. — The frontal of *Synodontis* Cuvier, 1816 species: **A**, **B**, main features exemplified in *S. schall* (Bloch & Schneider, 1801) (left frontal); **A**, dorsal view; **B**, ventral view; **C**-**E**, the three states observed in the extension of the frontal fontanel (dorsal view); **C**, state 1 observed in *S. clarias* (Linnaeus, 1758); **D**, state 2 in *S. nigrita* Valenciennes, 1840; **E**, state 3 in *S. schall*; **F**-**N**, left frontals in dorsal views with main characteristics of each species pointed out (see the text for more details); **F**, *S. filamentosus* Boulenger, 1901; **G**, *S. batensoda* Rüppell, 1832; **H**, *S. ocellifer* Boulenger, 1900; **I**, *S. sorex* Günther, 1864; **J**, *S. courteti* Pellegrin, 1906; **K**, *S. violaceus* Pellegrin, 1919; **L**, *S. clarias*; **M**, *S. membranaceus* (Geoffroy Saint-Hilaire, 1809); **N**, *S. eupterus* Boulenger, 1901. Scale bars: 5 mm.

lateral flanges of the orbitosphenoid at the back (Fig. 5B, C). The nasal sac is placed at the front of the bone (Fig. 5A) and the olfactory foramen for nerve I opens anteriorly at the anterior edge. The articular facet for the palatine is placed ventrally on an anteromesial pillar (Fig. 5B). It is generally wider than long (Fig. 5F, G), except in *S. sorex* and *S. clarias* where it is antero-posteriorly elongated (Fig. 5D, E). Moreover, in the latter two species, the anteromesial pillar that bears the articular facet for the palatine projects ventrally. The lateral ethmoid segment of the supraorbital branch of the sensory canal runs in a bony tube that opens dorsally in front of the frontal.

Two linear measurements on the lateral ethmoid allow us to distinguish the lateral ethmoid of the Chadian *Synodontis* species according to their general shape (Fig. 5H). Using the log ratio "width of the free posterior edge/length of the lateral margin", three groups are distinct (Appendix 2). *Synodontis courteti* has a short posterior edge and a long lateral margin (Fig. 5I). *Synodontis violaceus* and *S. sorex* exhibit a reduced posterior edge and their lateral margins are extended but less than in *S. courteti* (Fig. 5J, K). The other species unite in a group due to the relatively large posterior edge and short lateral margin of their lateral ethmoid (Fig. 5L-N). Among this group, *S. eupterus* exhibits the widest free posterior edge (Fig. 5N).

THE FRONTAL (FIGS 6-8; APPENDICES 3, 4; TABLE 2)

Laterally, the frontals of *Synodontis* connect with the mesethmoid anteriorly and with the lateral ethmoid, and behind the orbit they connect with the sphenotic and with the supraoccipital at the

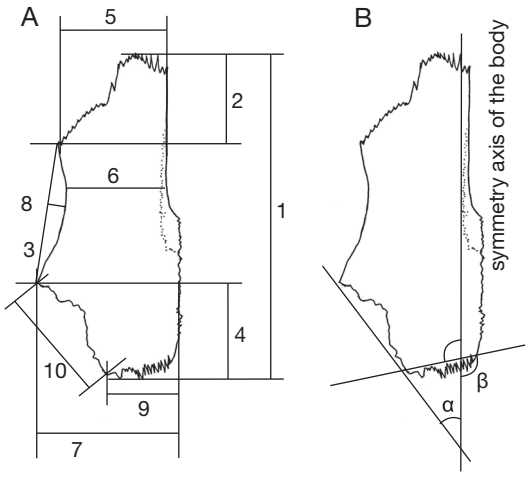

FIG. 7. — Linear and angular measurements taken on the frontals, shown in *Synodontis schall* (Bloch & Schneider, 1801) (dorsal view): **A**, linear measurements; **1**, total length; **2**, ante-orbital length; **3**, orbital edge length; **4**, post-orbital length; **5**, ante-orbital width; **6**, orbital width; **7**, post-orbital width; **8**, depth of the orbital edge; **9**, length of the frontal vs supraoccipital suture line; **10**, length of the frontal vs sphenotic suture line; **B**, measurements of the angles **α** and **β** of the frontals.

TABLE 2. — Percentage of the three states observed for the frontal fontanel development of *Synodontis* Cuvier, 1816 shown in Figure 7. See in the text for further explanations.

Species (no. of specimens)	no dorsal contact between the frontals (1)	the dorsal contact of the two frontals	
		covers the bony bridge (2)	does not cover the bony bridge (3)
S. membranaceus (12)	0	100	0
S. sorex (13)	23	77	0
S. batensoda (16)	0	100	0
S. nigrita (12)	0	0	100
S. clarias (20)	90	10	0
S. schall (28)	3	79	18
S. filamentosus (7)	14	86	0
S. courteti (9)	0	78	22
S. violaceus (10)	0	100	0
S. ocellifer (5)	0	75	25
S. eupterus (2)	0	100	0

back, through more or less interdigitated sutures (Fig. 6). The sensory canal enters the frontal at its anterior edge. On the roof, at about the middle of the bone, the inter-frontal branch divides and opens near the bony bridge (Fig. 6A). Posteriorly, the canal divides into three branches: one supraoccipital, one sphenotic and one orbital. Depending on the individuals, the supraoccipital branch may or may not open in a short pitline (Fig. 6A). Ventrally, the frontal articulates with the orbitosphenoid and the pterosphenoid through a ventromesial crest made of double ventral lamina. It borders the sphenotic branch of the sensory canal (Fig. 6B). Finally, the two frontals connect medially by a bony bridge and possibly by their dorsal roof posteriorly (Fig. 6C-E), depending on the extension of the frontal fontanel.

The bony bridge is located at about two thirds of the frontal maximal length except in *Synodontis sorex* in which it is placed further posteriorly. The frontal fontanel starts in a notch at the posterior edge of the mesethmoid and separates both frontals from each other either anteriorly or all along their length. The extension of the frontal fontanel varies intra- and interspecifically with three states identified (Fig. 6C-E; Table 2): 1) the frontal fontanel extends all along the frontals and ends in a median notch in the supraoccipital; the frontals connect medially through the bony bridge only (Fig. 6C); 2) the frontal fontanel extends only in front of the bony bridge (Fig. 6E); and 3) in an intermediate case, the frontal fontanel is found behind the level of the bony bridge but the frontals suture posteriorly (Fig. 6D). In the latter case, the fontanel length behind the bony bridge is smaller than 2% of the total length of the frontal in *S. ocellifer*; it comprises between 2% and 8% in *S. schall*, *S. violaceus*, *S. courteti*, *S. eupterus* and *S. filamentosus*, and between 8% and 15% in *S. sorex*, *S. batensoda* and *S. membranaceus*, and it exceeds 25% in *S. clarias*.

More generally, the frontal shape varies in its general proportions depending on the species. This is notably the case for the position of the orbit, the size of the orbit, the inter-orbital width and also the direction of the suture lines with the sphenotic and with the supraoccipital. To evaluate the position and size of the orbit on the lateral margin of the frontal bone, we compared the preorbital length, the orbital length and the postorbital length with each other (Fig. 7, dimension 2, 4 and [1-(2+4)];

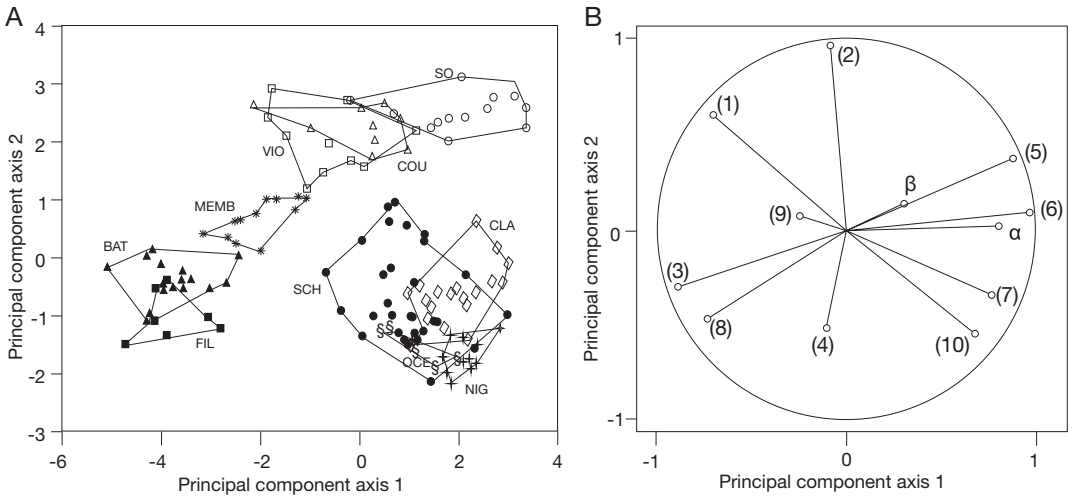

FIG. 8. — **A**, distribution of the frontals of the Chadian *Synodontis* Cuvier, 1816 specimens on the first two axis of the principal component analysis obtained from the correlation matrix of ten log-shape ratio and the tangent of the angles **α** and **β** (Fig. 7, Appendix 2); **B**, correlation circle showing the contribution of each variable on each axis. The axis 1 explains 43,45% of the overall variation and the axis 2 explains 19.87%. Abbreviations and symbols: **FIL** (■), *S. filamentosus* Boulenger, 1901; **BAT** (▲), *S. batensoda* Rüppell, 1832; **OCE** (§), *S. ocellifer* Boulenger, 1900; **SO** (○), *S. sorex* Günther, 1864; **COU** (△), *S. courteti* Pellegrin, 1906; **VIO** (□), *S. violaceus* Pellegrin, 1919; **CLA** (◇), *S. clarias* (Linnaeus, 1758); **MEMB** (✱), *S. membranaceus* (Geoffroy Saint-Hilaire, 1809); **NIG** (+), *S. nigrita* Valenciennes, 1840; **SCH** (●), *S. schall* (Bloch & Schneider, 1801).

Appendix 3). In *Synodontis sorex*, *S. courteti* and *S. violaceus*, the orbit is in a posterior position with a preorbital length which exceeds 40% of the total length of the frontal (Fig. 6I-K; Appendix 3), whereas it is in a median position in the other species (Fig. 6F-H, L-N; Appendix 3). The orbital edge of the frontal is large in *S. batensoda*, *S. ocellifer*, *S. nigrita*, *S. schall*, *S. eupterus* and even represents half of the total bone length in *S. filamentosus* (Fig. 6F-H, N; Appendix 3). For the latter two species, this can be related to the large diameter of the eye (more than 24% when compared with the head length) used by Paugy & Roberts (1992) in their identification key of the Western African species. *Synodontis clarias* and *S. membranaceus* are characterized by close dimensions of the preorbital, orbital and postorbital part of the frontal (Fig. 9L, M; Appendix 3). The Chadian species also differ in the minimum orbital width, and the pre- and postorbital maximum width of the frontal. *Synodontis filamentosus* and *S. batensoda* have a markedly narrow inter-orbital width and a deep orbital edge (Fig. 6F, G); whereas the frontal of *S. nigrita* and of *S. clarias* have large inter-orbital widths with a nearly straight orbital edge (Fig. 6L). These results can be related to those obtained by comparing the inter-orbital distance with the head length and width in the identification key of Paugy & Roberts (1992). The other species show intermediate widths of the bone (Fig. 6H-K), with a straight orbital edge in *S. sorex* and *S. courteti* (Fig. 6I, J). Moreover, the frontal in *S. filamentosus*, *S. batensoda*, *S. ocellifer*, and *S. eupterus* shows a small anterior width when compared with the posterior one (Fig. 6F-H, N). The angles drawn by the frontal/sphenotic suture (Fig. 7B: α) and frontal/supraoccipital suture (Fig. 7B: β) with the sagittal plane of the body vary respectively from 25 to 45° (Fig. 6I, M; Appendix 3) and from 102 to 133° (Fig. 6G, I; Appendix 3). For α, two groups arose (Appendix 3): it is either acute (mean lower than 30.5°) in *S. membranaceus*, *S. batensoda*, *S. filamentosus*, *S. eupterus* and *S. courteti*, or open in the other species (mean higher than 36.5°). The values of β are statistically different between *S. sorex* (higher than 130° average) and the other *Synodontis* species (lower than 120°), which

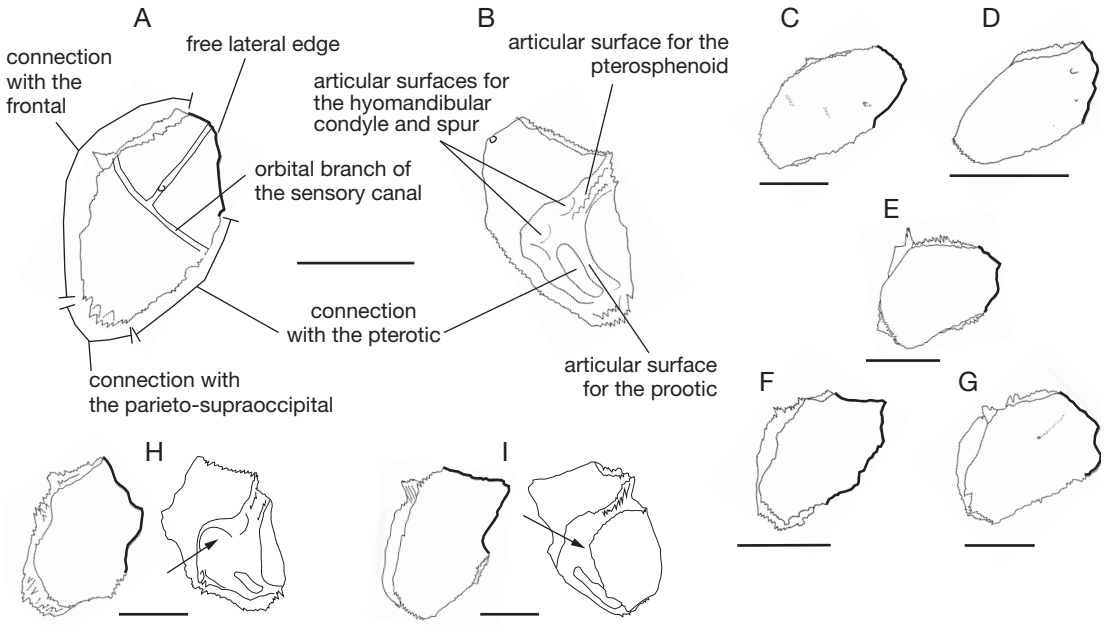

FIG. 9. — The sphenotic of *Synodontis* Cuvier, 1816 species: **A**, **B**, main features of the sphenotic exemplified in *S. schall* (Bloch & Schneider, 1801); **A**, outer view; **B**, inner view; **C**-**G**, sphenotic in outer views; **C**, *S. ocellifer* Boulenger, 1900; **D**, *S. nigrita* Valenciennes, 1840; **E**, *S. violaceus* Pellegrin, 1919; **F**, *S. batensoda* Rüppell, 1832; **G**, *S. sorex* Günther, 1864; **H**, **I**, sphenotic in outer and inner views; **H**, *S. courteti* Pellegrin, 1906; **I**, *S. membranaceus* (Geoffroy Saint-Hilaire, 1809). The arrows are for the articular surface for the condyle of the hyomandibula. Scale bars: 5 mm.

corresponds to an anteriormost insertion of the supraoccipital between the frontals in *S. sorex*.

Together with the use of the frontal proportions and the direction of the sutures, we propose the use of log-shape ratios based on the same linear measurements and some additional ones (Fig. 7) to distinguish the frontals of the Chadian species of *Synodontis* (Appendix 4). Groups of species can be statistically separated from each other by the values obtained from certain dimensions (Fig. 8).

Synodontis eupterus, *S. filamentosus* and S. *batensoda* resemble each other by their deep orbit (Appendix 4: variable 8). Moreover, *S. filamentosus* and *S. batensoda* are distinguished by having the narrowest frontal bones (Appendix 4: 6), and the largest orbital length (Appendix 4: 3) measured among the Chadian species. The latter two species differ by the log-shape ratio constructed from the ante- and postorbital widths, because *S. filamentosus* is larger posteriorly (Appendix 4: 5), and narrower anteriorly (Appendix 4: 7). In *S. filamentosus* and *S. eupterus*, the suture line between the frontals and the supraoccipital is relatively longer than in *S. batensoda* and most of the other species (Appendix 4: 9).

Synodontis sorex, *S. membranaceus*, *S. violaceus* and *S. courteti* are segregated by their large preorbital length (Appendix 4: 2) which corresponds to the posterior position of the orbit (see above). Together with a large β angle (see above), *S. sorex* is distinguished by its larger preorbital width (Appendix 4: 5). On the other hand, *S. membranaceus* differs from *S. courteti* and *S. violaceus* by a narrower postorbital width (Appendix 4: 7). Indeed, together with *S. batensoda*, they are the species that exhibit the narrowest frontal posteriorly (Appendix 4: 7). The frontals of *S. courteti* and *S. violaceus* are distinguished from each other by the depth of the orbital region (Appendix 4: 8), in relation to the difference observed in its outline (see above).

Finally, *Synodontis nigrita*, *S. clarias*, *S. ocellifer*, *S. eupterus* and *S. schall* are separated from the rest

because of their relatively short frontal as in *S. sorex* (Appendix 4: 1) and their short preorbital length as in *S. filamentosus* (Appendix 4: 2). Among them, only *S. nigrita* is set apart by weakest values of the log-shape ratio constructed from the maximum length (Appendix 4: 1).

The sphenotic (Fig. 9)

The sphenotic shows a roughly pentagonal outline in external view (Fig. 9A). It sutures with the frontal anteriorly and anteromedially, the supraoccipital medially and the pterotic posteriorly, whereas a free V-shaped lateral edge borders the orbit anteriorly (Fig. 9A). The sensory canal runs in a bony tube from the frontal to the pterotic onto the sphenotic and it opens in the middle of the bone; it gives off the infraorbital branch that opens at the pointed edge of the V, just above the fourth infraorbital (Fig. 9A). Internally, the sphenotic sutures with the pterosphenoid, the prootic and the pterotic through a ventral projection (Fig. 9B). Together with the latter two bones, the sphenotic delimits an elongated and shallow fossa where the dorsal condyle of the hyomandibula articulates (Fig. 9B). The anterodorsal spur of the hyomandibula enters a second deeper and shorter fossa in the middle of the ventral projection of the sphenotic (Fig. 9B).

The intra-specific variations in the outline of the sphenotic overlap the interspecific variations so that no taxa can be distinguished through log-shape ratios based on the sphenotic dimensions. The V-shape of the free edge of the bone is more or less flattened and the whole elongation of the sphenotic follows the overall shape of the neurocranium. For instance, in *Synodontis schall*, *S. ocellifer*, *S. eupterus* and *S. nigrita* (Fig. 9C, D), it is rather more slender whereas it is stouter in *S. violaceus* and *S. courteti* (Fig. 9H, E) which have a more dorso-ventrally flattened skull. The orbital margin varies in its position, from vertical in *S. membranaceus* and *S. batensoda* (Fig. 9I, F) to oblique in the other species (Fig. 9A, C-E, G, H). Finally, in internal view, the articular surface for the hyomandibula varies in its relative size from the smallest in *S. membranaceus* (Fig. 9I) to the largest in *S. courteti* (Fig. 9H).

The pterotic (Fig. 10)

The pterotic is a roughly quadrangular bone in external view, which participates in forming the cranial roof. Three sides of the pterotic suture with other bones: the sphenotic anteriorly, the supraoccipital medially and the posttemporal posteriorly. The fourth and lateral side of the pterotic projects above the process for the hyomandibula (Fig. 10A).

At the base of the process for the hyomandibula, a short surface forms part of the articulation of the dorsal condyle of the hyomandibula together with the sphenotic and the prootic (Fig. 10B). A thin internal bony plate connects to the wall of the braincase. It encloses the semicircular canal that receives the ampulla of the inner ear in the funnel-like structure. In front of the funnel-like structure, the thin internal bony plate sutures with the exoccipital (Fig. 10B) and with the prootic ventrally (Fig. 10C). On the skull roof, the sensory canal passes from the sphenotic to the posttemporal and onto the pterotic, and in the middle of the bone it gives off the preopercular lateral branch.

The articulation with the supraoccipital may be reduced by the presence of a temporal fenestra at the junction of the pterotic, supraoccipital, and posttemporal, which is only the case in *Synodontis courteti* and *S. violaceus* (Fig. 10D, see supraoccipital). Finally, the roof of the bone may or may not cover the process for the hyomandibula, depending on the species. In *S. clarias* and *S. sorex*, the process is hidden (Fig. 10G, H), whereas it is always seen in outer view in *S. eupterus*, *S. filamentosus*, *S. courteti*, *S. membranaceus*, *S. batensoda* and *S. violaceus* (Fig. 10E, F).

The supraoccipital (Figs 11, 12; Appendix 5)

The supraoccipital is the large bone that covers and dorso-posteriorly closes the braincase. As part of the skull roof it articulates with the two frontals anteriorly, and with the sphenotic, the pterotic and the posttemporal laterally (Fig. 11A). Posterior to the posttemporal, the lateral margin is free and the supraoccipital sutures posteriorly with the nucal shield, i.e. with the anterior nucal plate in a median notch and with the two anterior edges of the middle nucal plate on both sides (Fig. 11A). The sensory canal opens into two antero-posteriorly directed

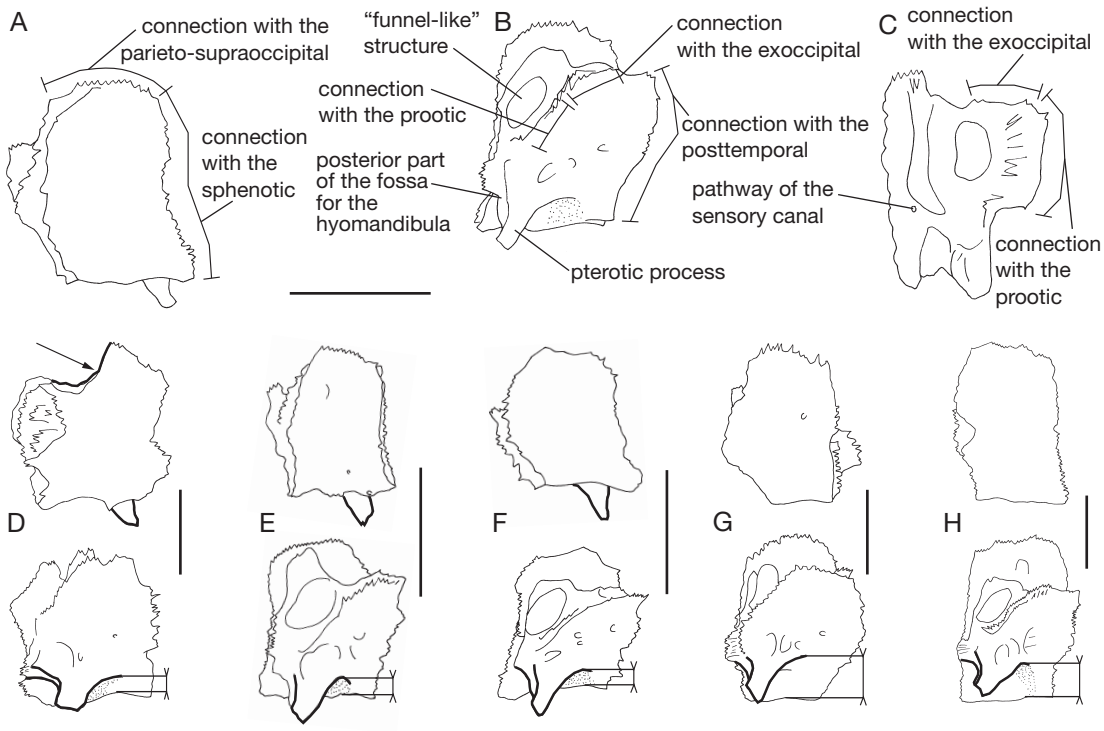

Fig. 10. — The pterotic of *Synodontis* Cuvier, 1816 species: **A**-**C**, main features of the pterotic exemplified in *S. schall* (Bloch & Schneider, 1801); **A**, outer view; **B**, inner view; **C**, median view; **D**-**H**, pterotic in outer and inner views; **D**, *S. courteti* Pellegrin, 1906; **E**, *S. filamentosus* Boulenger, 1901; **F**, *S. batensoda* Rüppell, 1832; **G**, *S. sorex* Günther, 1864; **H**, *S. clarias* (Linnaeus, 1758). The arrow is for the temporal fenestra edge. The process outline is blackened. Note the roof lateral development over the process in both outer and inner views. Scale bars: 5 mm.

pitlines and a transverse gutter often joins the pterotic edge on both sides (Fig. 11A). Ventrally, at the level of the posttemporal, the supraoccipital encloses the braincase through a semicircular vertical lamina which sutures laterally with the exoccipitals and medially with the third basidorsal of the Weberian apparatus (Fig. 11B). The posterior lateral accessory ramus of nerve VII (facial) runs in an anteroposteriorly directed canal through the lamina. On both sides of the vertical lamina, a groove allows the semicircular canal to extend outside of the braincase, between the epioccipital and the supraoccipital. All of the suture lines are interdigitated.

Some discrete characters allow us to recognize the supraoccipital of some *Synodontis* species. The pointed shape of the anterior edge of the bone in *S. sorex* is due to its insertion further anteriorly in between the frontals in that species (Fig. 11C) when compared to the others (Fig. 11D-F). In *S. clarias*, the frontal fontanel usually reaches the supraoccipital and cuts it off (Fig. 11D, see also the section The frontal, including Table 2). The sutures with the pterotic and the posttemporal are continuous except in *S. violaceus* and *S. courteti* which exhibit a concave outline due to the presence of a temporal fenestra at the junction of the three bones (Fig. 11E). In *S. nigrita* only, the articulation with the anterior nucal plate is reduced when compared to the other species (Fig. 11F). Moreover, in caudal view, the supraoccipital of *S. membranaceus* and *S. batensoda* is markedly deeper (Fig. 11E) than in the other species and it is noticeably shallower in *S. courteti*, *S. violaceus* and *S. nigrita* (Fig. 11F, G).

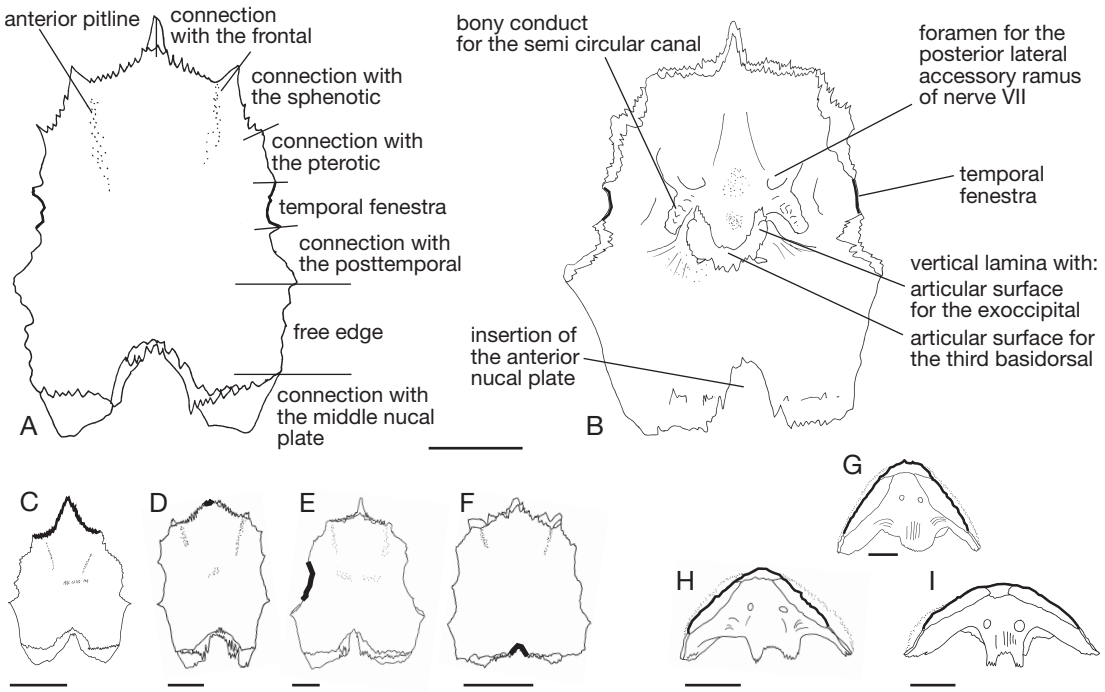

FIG. 11. — The supraoccipital of *Synodontis* Cuvier, 1816 species: **A**, **B**, main features of the bone exemplified in *S. schall* (Bloch & Schneider, 1801); **A**, dorsal view; **B**, ventral view; **C**-**I**, emphasis on the characteristics of the supraoccipital; **C**-**F**, dorsal views; **C**, *S. sorex* Günther, 1864; **D**, *S. clarias* (Linnaeus, 1758); **E**, *S. courteti* Pellegrin, 1906; **F**, *S. nigrita* Valenciennes, 1840; **G**-**I**, posterior views; **G**, *S. membranaceus* (Geoffroy Saint-Hilaire, 1809); **H**, *S. schall* (Bloch & Schneider, 1801); **I**, *S. courteti*. Scale bars: 5 mm.

To identify the supraoccipital of the several Chadian *Synodontis* species by their shape, we used seven transformed log-shape ratios (Appendix 5: variables 1-7) based on linear measurements (Fig. 12) and two log transformed variables (Appendix 5: 8, 9) based on the linear measurements compared with the bone total length. The six variables 1, 2, 4, 7, 8 and 9 are more efficient than the three remaining ones (Appendix 5). Species and species groups distinguish as follows (Appendix 5).

Synodontis membranaceus, *S. sorex*, *S. eupterus*, *S. batensoda* and *S. clarias* are alike because of their supraoccipital being narrow at its posteriormost level (Appendix 5: 8). Among them, *S. clarias* is distinguished by long posterior free edges (Appendix 5: 2), a posterior narrowing of the bone (Appendix 5: 4), and short suture lines with the anterior nucal plate (Appendix 5: 7). *Synodontis eupterus* and *S. sorex* also exhibit a narrowing at the back of their supraoccipital although not so pronounced as in *S. clarias*. At last, *S. membranaceus* is recognized thanks to its markedly long supraoccipital (Appendix 5: 1), narrow at the junction with the frontal and the sphenotic (Appendix 5: 9).

The species *Synodontis nigrita*, *S. ocellifer*, *S. schall*, *S. filamentosus*, *S. violaceus* and *S. courteti* exhibit a large supraoccipital posteriorly (Appendix 5: 8). *S. nigrita* and to a lesser extent *S. ocellifer* are distinguished by their short posterior free edges (Appendix 5: 2), and *S. nigrita* alone is characterized by the longer suture between the supraoccipital and the middle nucal plate in relation with its small anterior nucal plate, even more so than in *S. ocellifer* (Appendix 5: 4). Among the remaining species, *S. filamentosus* and *S. violaceus* are separated from *S. schall* and *S. courteti* by the larger width of their supraoccipital at the level of the junction with both the frontal and the sphenotic (Appendix 5:

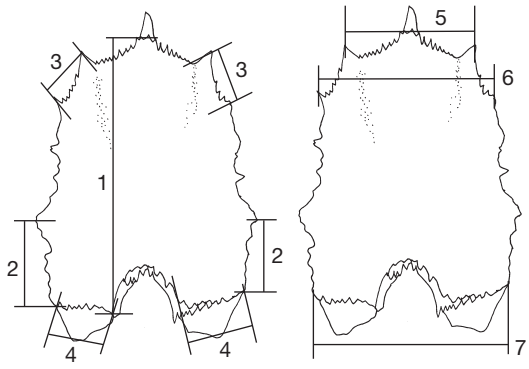

Fig. 12. — Linear and angular measurements taken on the supraoccipitals, shown in *S. schall* (Bloch & Schneider, 1801) in dorsal views: **1**, maximum length of the bone; **2**, length of the posterior free margins; **3**, length of the suture with the sphenotic; **4**, length of the suture with the middle nucal plate; **5**, width of the bone at the level of the junction frontal/supraoccipital/sphenotic; **6**, width of the bone at the level of the junction sphenotic/supraoccipital/pterotic; **7**, width of the bone at its posteriormost level.

5, 9) and also at the level of the junction with the sphenotic and the pterotic (Appendix 5: 6).

The orbitosphenoid (Figs 13, 14)

The *Synodontis* orbitosphenoid is composed of an axial median zone which lies ventrally onto the parasphenoid (Fig. 13A, B), of two lateral flanges that extend horizontally and articulate anteriorly with the lateral ethmoids through an interdigitated suture (Fig. 13A), and of two vertical laminae which join each frontal dorsally, each pterosphenoid posteriorly and the parasphenoid below the optical foramen (Fig. 13B). The axial zone and the two vertical laminae of the orbitosphenoid delimit a space which opens dorsally along the frontal fontanel. The depth of the vertical laminae varies from shallow, such as in *Synodontis violaceus*, to deep, such as in *S. batensoda* (Fig. 13C, D). The optical foramen varies in shape from fairly round in *S. filamentosus*, *S. eupterus* and *S. batensoda* (Fig. 13F) to anteriorly constricted in other species (Fig. 13E, G).

In ventral view, the lateral border of the lateral flanges is often curved and concave, giving an overall Y-shaped outline to the orbitosphenoid unit in ventral view (Figs 13A; 14A, B, D, E), except in *Synodontis membranaceus*, *S. clarias* and *S. sorex*, where the lateral border of the lateral

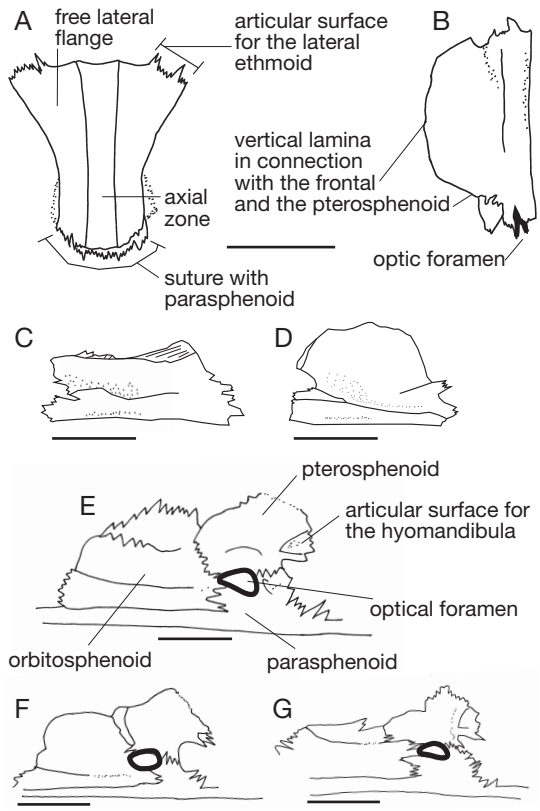

Fig. 13. — The orbitosphenoid of *Synodontis* Cuvier, 1816 species: **A**, **B**, main features of the orbitosphenoid, exemplified in *S. schall* (Bloch & Schneider, 1801); **A**, ventral view; **B**, lateral view; **C**, **D**, orbitosphenoid of two species in lateral views; **C**, *S. violaceus* Pellegrin, 1919; **D**, *S. batensoda* Rüppell, 1832; **E**-**G**, optical foramen and surrounding bones in ventral views; **E**, *S. schall*; **F**, *S. batensoda* Rüppell, 1832; **G**, *S. courteti* Pellegrin, 1906. Scale bars: 5 mm.

flanges is straight, giving the bone a V-shaped outline (Fig. 14C, F, G). Moreover in *S. batensoda*, *S. eupterus* and *S. filamentosus*, the lateral flanges do not develop all along the bone but only in its anterior part (Fig. 14A). The suture between the orbitosphenoid and the lateral ethmoid varies in orientation and in length, depending on the species. It forms an angle with the sagittal plane of the body that is smaller than 45° in *S. courteti* and *S. membranaceus* (Fig. 14B, C), about 45° in *S. violaceus*, *S. clarias*, *S. sorex*, *S. filamentosus* and *S. nigrita* (Fig. 14E-G), and larger than 45° in *S. schall* and *S. ocellifer* (Figs 13A; 14D). In

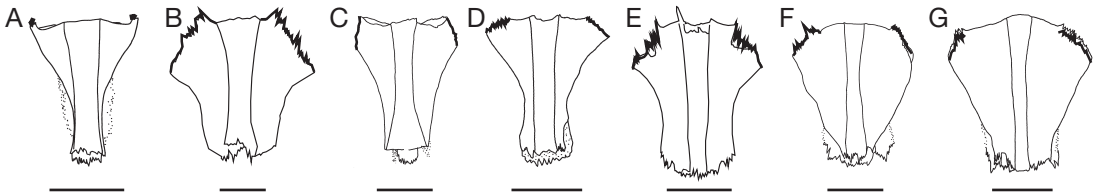

FIG. 14. — The orbitosphenoid of *Synodontis* Cuvier, 1816 species in ventral views: **A**, *S. batensoda* Rüppell, 1832; **B**, *S. courteti* Pellegrin, 1906; **C**, *S. membranaceus* (Geoffroy Saint-Hilaire, 1809); **D**, *S. ocellifer* Boulenger, 1900; **E**, *S. violaceus* Pellegrin, 1919; **F**, *S. sorex* Günther, 1864; **G**, *S. clarias* (Linnaeus, 1758). Scale bars: 5 mm.

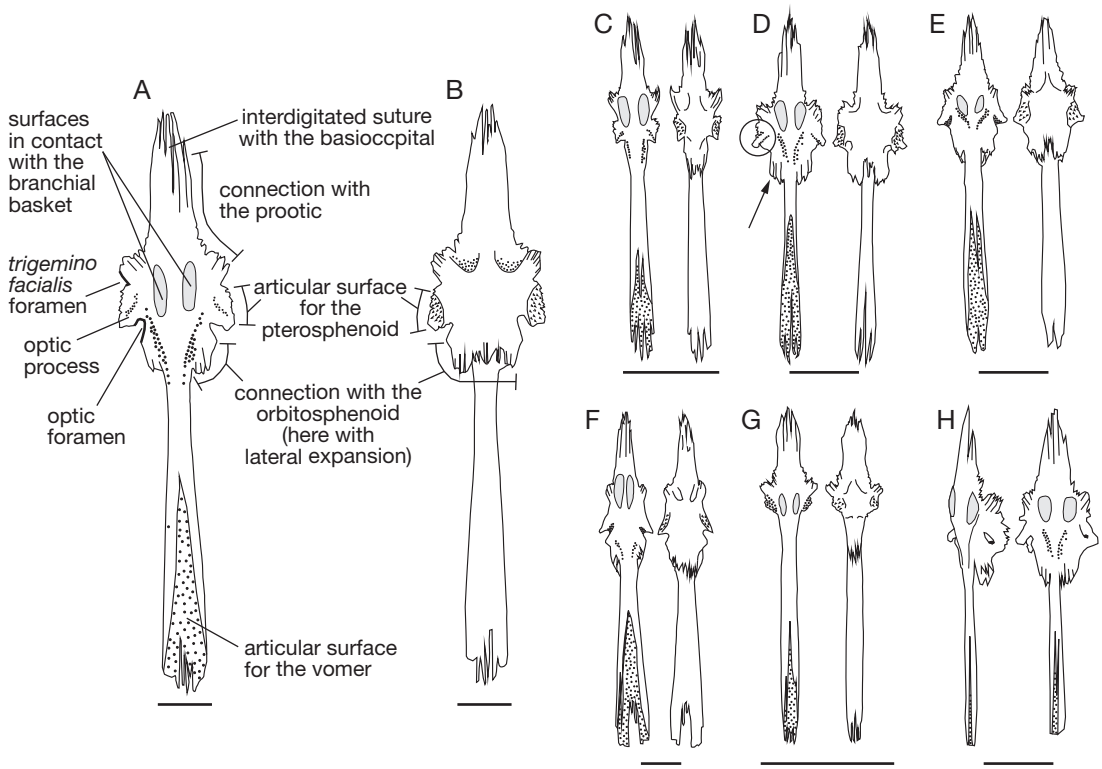

FIG. 15. — The parasphenoid of *Synodontis* Cuvier, 1816 species: **A**, **B**, main features of the parasphenoid, exemplified in *S. schall* (Bloch & Schneider, 1801); **A**, ventral view; **B**, dorsal view; **C**-**H**, the parasphenoid in ventral and dorsal views, except **H** in ventro-lateral and ventral views; **C**, *S. batensoda* Rüppell, 1832; **D**, *S. clarias* (Linnaeus, 1758); **E**, *S. sorex* Günther, 1864; **F**, *S. membranaceus* (Geoffroy Saint-Hilaire, 1809); **G**, *S. filamentosus* Boulenger, 1901; **H**, *S. clarias*. The arrow is for the lateral expansion for the orbitosphenoid. The circle is for the optic process. Scale bars: 5 mm.

S. batensoda, the angle cannot be measured because of the reduced size of the articulation (Fig. 14A). The suture line is also fairly short in *S. filamentosus*, whereas it is particularly long in *S. courteti* and *S. violaceus* (Fig. 14B, E).

THE PARASPHENOID (FIG. 15)

In *Synodontis*, the parasphenoid contacts anteriorly the vomer through a large surface and a greatly interdigitated suture (Fig. 15). Behind the level of the orbit, the parasphenoid constitutes the floor

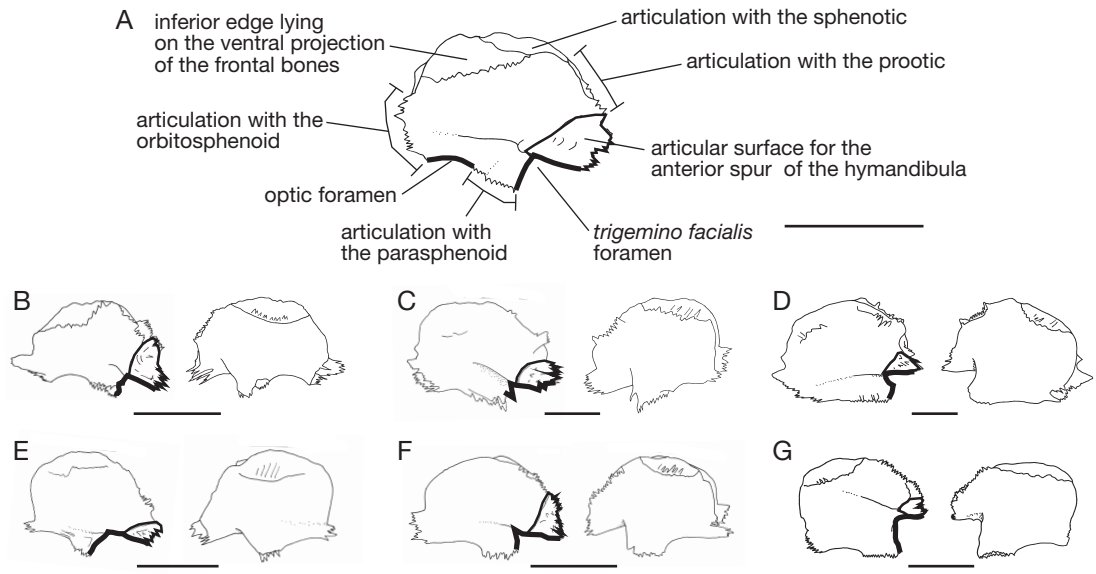

FIG. 16. — The pterosphenoid of *Synodontis* Cuvier, 1816 species: **A**, main features of the pterosphenoid, exemplified in *S. schall* (Bloch & Schneider, 1801) in outer view; **B**-**G**, the pterosphenoid in outer and inner views; **B**, *S. courteti* Pellegrin, 1906; **C**, *S. clarias* (Linnaeus, 1758); **D**, *S. sorex* Günther, 1864; **E**, *S. batensoda* Rüppell, 1832; **F**, *S. violaceus* Pellegrin, 1919; **G**, *S. filamentosus* Boulenger, 1901. Scale bars: 5 mm.

of the braincase and contributes to its lateral walls through a pair of dorsolateral expansions below the *trigemino facialis* chamber (passage of the nerves III, IV, V, VI, and VII). On both sides of the neurocranium and from anterior to posterior, this expansion sutures with the posterior tip of the orbitosphenoid, it borders the optic foramen, then it sutures the pterosphenoid, borders the *trigemino facialis* chamber and finally sutures the prootic (Fig. 15). Medially, the caudal end of the parasphenoid connects with the basioccipital. On the ventral face, at the level of the *trigemino facialis* chamber, two oval surfaces contact the branchial basket (Fig. 15A).

In *Synodontis batensoda*, *S. eupterus* and *S. filamentosus*, the parasphenoid sutures with the orbitosphenoid through the dorsal face of its axis only (Fig. 15C, G), whereas this connection extends onto the lateral expansions of the parasphenoid that exist in the other species (Fig. 15D-F, H). In all the species (Fig. 15D-F) except *S. filamentosus* and *S. eupterus* (Fig. 15C, G) an anteriorly directed process projects behind the optic foramen. Sometimes, this process joins the parasphenoid and delimits a ventral opening (Fig. 15H).

THE PTEROSPHENOID (FIG. 16)

The pterosphenoid displays a roughly rounded outline in external view. It contributes to the formation of the lateral wall of the braincase. It sutures from front to back and clockwise, with the posterior border of the vertical laminae of the orbitosphenoid, with the frontal, the sphenotic, the prootic and the parasphenoid (Fig. 16A). The optic foramen opens in front of the connection between the orbitosphenoid and the parasphenoid; the *trigemino facialis* opens posteriorly (Fig. 16A). The anterior spur of the hyomandibula, which articulates also with the sphenotic and the prootic, lies on a posterior triangular surface on the posterior edge of the pterosphenoid, dorsal to the border of the *trigemino facialis* chamber (Fig. 16A).

Depending on the specimen and the species, the outline of both the posterior triangular surface for the hyomandibula and the *trigemino facialis* chamber bordering on the pterosphenoid vary in their location and size. The surface is usually large and

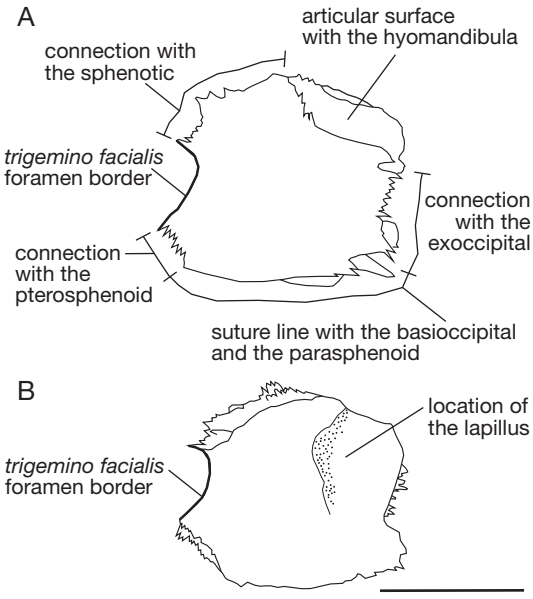

FIG. 17. — Main features of the prootic of *Synodontis* Cuvier, 1816, exemplified in *S. schall* (Bloch & Schneider, 1801) (left prootic): **A**, outer view; **B**, reverse inner view. Scale bar: 5 mm.

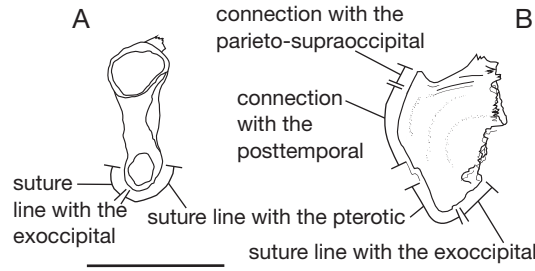

FIG. 18. — Main features of the epioccipital of *Synodontis* Cuvier, 1816, exemplified in *S. schall* (Bloch & Schneider, 1801) (left epiotic): **A**, ventral view; **B**, outer view. Scale bar: 5 mm.

in a rather posterior position above the *trigemino facialis* chamber (Fig. 16B-F) except in *Synodontis filamentosus* and *S. eupterus* where it is in a rather dorsal position (Fig. 16G). The posterior surface of the pterosphenoid for the articulation of the hyomandibula is distinctly larger in *S. courteti* (Fig. 16B).

THE PROOTIC (FIG. 17)

The prootic is the middle bone in the lateral wall of the braincase. Anteriorly, it borders the *trigemino facialis* chamber and, clockwise and from front to back, it sutures with the pterosphenoid, the sphenotic, the pterotic, the exoccipital, the basioccipital and the parasphenoid (Fig. 17A). Dorsally, it bears, together with the pterotic and the sphenotic, the elongated facet where the dorsal condyle of the hyomandibula articulates (Fig. 17A). On its internal face, the prootic bears a dorsally directed lamina which limits the *utriculus* and contains the *lapillus* (Fig. 17B).

THE EPIOCCIPITAL (FIG. 18)

The epioccipital (epiotic of some authors) of *Synodontis* fish is a bony conduit which is part of the hind margin of the neurocranium. It encloses the posterior semicircular canal of the inner ear (Fig. 18). Dorsally, it sutures with the ventral face of the posttemporal and with the supraoccipital, and on its ventral face, with the exoccipital medially and with the pterotic laterally.

THE BASIOCCIPITAL (FIG. 19)

The basioccipital forms the ventromedial wall at the back of the neurocranium of *Synodontis* fishes. The basioccipital firmly sutures with the parasphenoid and the prootics ventrally and with the Weberian apparatus posteriorly. Laterally, it articulates with the posttemporals. That gives it a cross-shape (Fig. 19A). Dorsally, the exoccipitals lie above the anterior and lateral parts of the basioccipital at its cross section (Fig. 19B, C). In dorsal view, the basioccipital also exhibits three median structures: 1) an anterior circular depression occupies almost all of the width of the anterior branch of the bone; 2) the anterior edges of the bone receive the postero-ventral corner of the prootics; and 3) behind a short and thin vertical flange, there is a posterior elongated groove, along which the exoccipitals articulate and join dorsally, constituting the *cavum* for the *sinus imparis perilymphaticus* (Fig. 19B, C). On both sides of this posterior elongated groove, the anterior part of the basioccipital holds the otoliths of the *lagena* and the *sacculus*, i.e. respectively, the *asteriscus* and the *sagitta* (Fig. 19B). Finally, a posteriorly-opening cone articulates with the first vertebral centrum above the bony interdigitated expansions that suture with the Weberian apparatus (Fig. 19C).

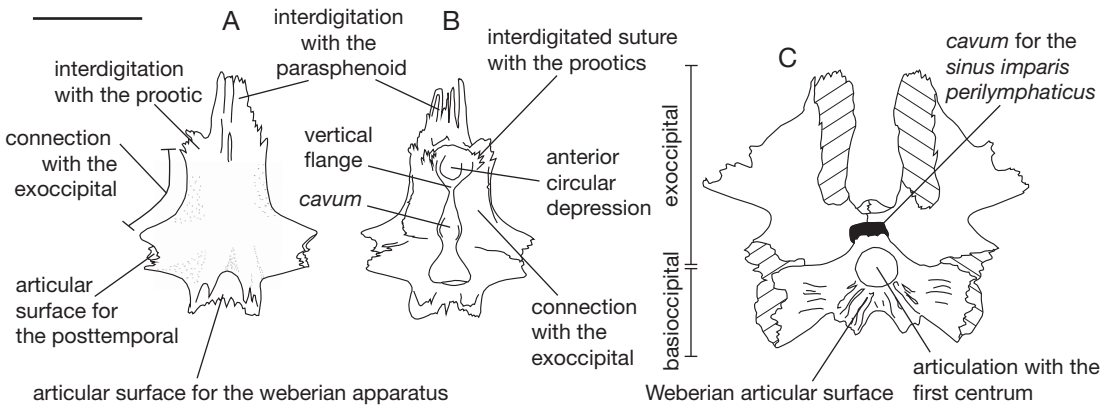

FIG. 19. — Main features of the basioccipital of *Synodontis* Cuvier, 1816, exemplified in *S. schall* (Bloch & Schneider, 1801): **A**, ventral view; **B**, dorsal view; **C**, basioccipital articulated with the exoccipitals in posterior view. Scale bar: 5 mm.

THE EXOCCIPITAL (FIGS 19C; 20)

The exoccipitals constitute the posterior part of the floor and the walls of the braincase above the basioccipital (Fig. 19C). On both sides of the braincase, the exoccipital sutures with the posterior margin of the prootic, with the basioccipital, with the median limb of the posttemporal and with the pterotic (Fig. 20). Together with the basioccipital, it encloses the *asteriscus* and the *sagitta* (Fig. 20B). The nerves IX (glossopharyngial) and X (vagus) open in a large foramen placed close in front of the small foramen for nerve XII (hypoglossal) (Fig. 20A). The posterior wall of each exoccipital sutures medially with the anterior basidorsal corresponding to the third vertebra of the Weberian apparatus. The two exoccipitals join each other medially and delimit, along with the basioccipital the *cavum* for the *sinus imparis perilymphaticus* below the foramen magnum (Fig. 19C).

GENERAL FEATURES OF THE SPLANCHNOCRANIUM (FIG. 21)

In mochokids and notably in *Synodontis* fishes, the splanchnocranium is characterized by the small size of the mouth and by the robustness of the opercular bones (Fig. 21). The upper jaw is formed by a maxilla which displays two small rounded facets carried by a bifid head (Fig. 21). It lies ventrolateral to the premaxilla anteriorly and it connects by ligamentous means with the palatine at the back. The maxilla and the palatine do not differ greatly in size from one another. The dentary bears characteristic S-shaped teeth. According to Mo (1991), the genus *Synodontis* is characterized by these distinct jaw teeth, but we observe such dental morphology in some other mochokid fishes as well. The anguloarticulo-retroarticular has a posterolateral projection which is found only in mochokids (De Pinna 1993). The coronomeckelian bone was noted present by Taverne & Aloulou-Triki (1974) but we did not observed it in any of our specimens. The horizontal branch of the meckelian cartilage only is present. The absence of the coronoid process constitutes an apomorphy of the family according to De Pinna (1993). The suspensorium does not include any ento- or ectopterygoid.

THE PREMAXILLA (FIG. 22)

The premaxilla is a small, laminar bone. Ventrally, the anterior part of the lamina displays large conical teeth, whereas the posterior part bears smaller conical teeth (Fig. 22A). The posterior part of the toothed lamina projects laterally. The pulpar cavity is toothless and placed medially behind the toothed lamina. Dorsally, the premaxilla supports the mesethmoid medially. They connect with each

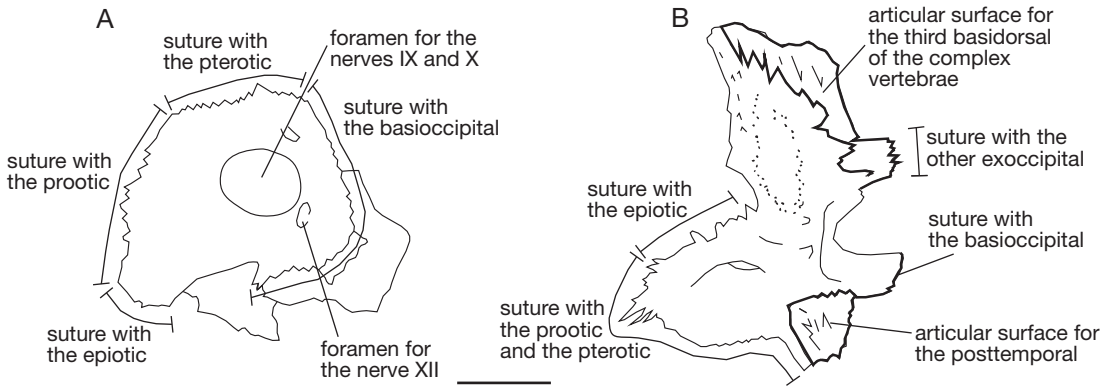

FIG. 20. — Main features of the exoccipital of *Synodontis* Cuvier, 1816, exemplified in *S. schall* (Bloch & Schneider, 1801) (right exoccipital): **A**, lateral view to show the position of the foramen for nerves IX, X and XII; **B**, ventro-lateral view. Scale bar: 5 mm.

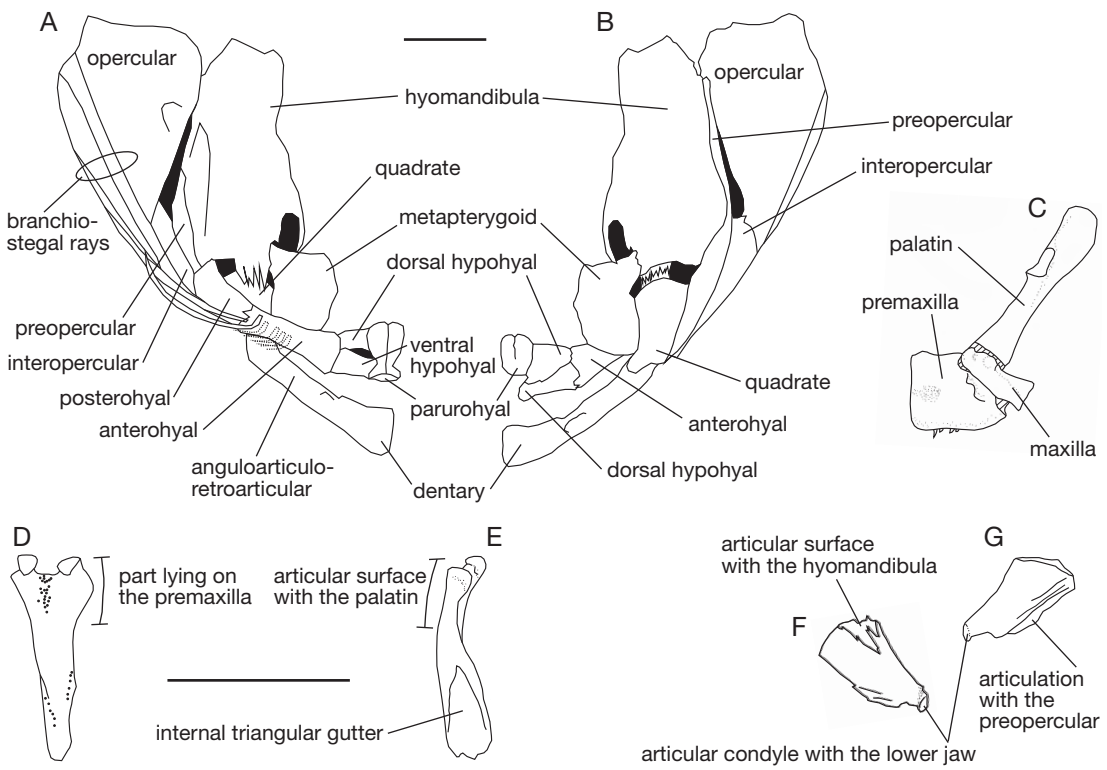

FIG. 21. — Splanchnocranium and details on certain splanchnocranial bones in *Synodontis* Cuvier, 1816 exemplified in *S. schall* (Bloch & Schneider, 1801): **A**, **B**, articulated splanchnocranial series (left series); **A**, median view; **B**, lateral view; **C**, detail of a left upper jaw, in dorsal view; **D**, **E**, main features of the maxilla (left maxilla); **D**, dorsal view; **E**, median view; **F**, **G**, main features of the quadrate (left quadrate); **F**, lateral view; **G**, median view. Scale bars: 5 mm.

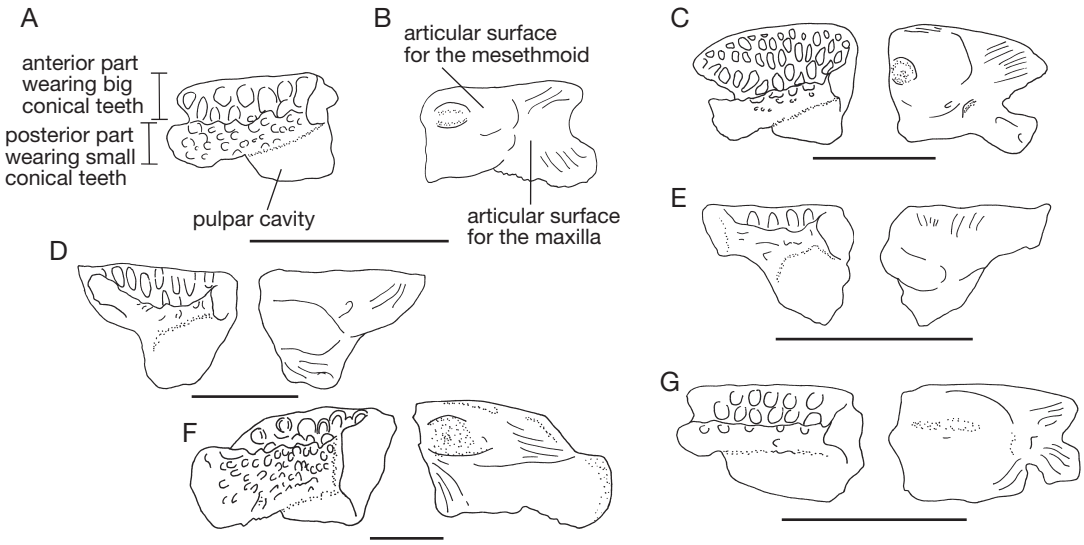

Fig. 22. — The premaxilla of *Synodontis* Cuvier, 1816 species (right premaxilla): **A**, **B**, main features of the bone, exemplified in *S. schall* (Bloch & Schneider, 1801); **A**, occlusal view; **B**, dorsal view; **C**-**G**, the premaxilla of several species; **C**, *S. courteti* Pellegrin, 1906; **D**, *S. sorex* Günther, 1864; **E**, *S. clarias* (Linnaeus, 1758); **F**, *S. violaceus* Pellegrin, 1919; **G**, *S. nigrita* Valenciennes, 1840. Scale bars: 5 mm.

other through ligaments that attach in a depression located beside the symphysis of the premaxilla. The maxilla lies on the dorsal side of the laminar lateral projection of the premaxilla.

The premaxilla usually exhibits a quadrangular outline in occlusal view (Fig. 22A-C, F), except in *Synodontis sorex* and *S. clarias* where it is triangular (Fig. 22D, E) due to the projection of the anterior part of the lamina. The proportion of the anterior part of the lamina and the number of large conical tooth ranks varies and depends on the species (Fig. 22C-G). For instance, there are at least three ranks in *S. violaceus* (Fig. 22F), whereas only one is present in *S. clarias* (Fig. 22E).

The maxilla (Fig. 21A-E)

The maxilla is a small rod-like bone which has a bifid head (Fig. 21C-E). The maxilla head lies on the premaxilla whereas its free laminar part accommodates the elastin cartilage of the maxillary barbell in an internal triangular gutter (Fig. 21E). The palatine anterior tip is connected to the dorsal side of the maxilla head by a ligament (Fig. 21D).

The dentary (Fig. 23)

The dentary has a concave lingual edge. At the symphysis, an antero-ventrally and medially opened cavity receives the mandibular teeth in alveolae that are elongated antero-posteriorly (Fig. 23A). At the back of the cavity, on the lingual face of the bone, a vertical surface allows the insertion of the horizontal branch of the Meckel's cartilage (Fig. 23B). The dentary articulates with the angulo-articulo-retroarticular bone through a stout and straight projecting process (Fig. 23A, B).

The tooth cavity varies in outline and in size. It is globulous and large when compared to the size of the posterior process in *Synodontis sorex* and *S. clarias* (Fig. 23C, D) and quadrangular in the other Chadian species. In *S. courteti* and *S. violaceus*, the cavity is large but not globulous. The latter two species differ in the relative development of the posterior process, it being large in *S. courteti* (Fig. 23G), and narrow in *S. violaceus* (Fig. 23H). In *S. membranaceus*, the dentary is rod-like and the cavity is reduced to a symphysial notch (Fig. 23I). Finally, the remaining species have a quadrangular cavity which is

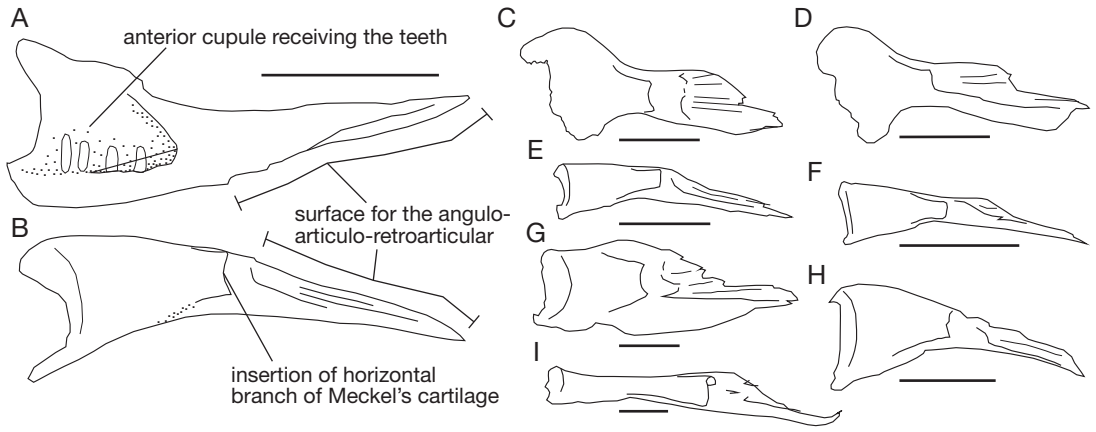

FIG. 23. — The dentary of *Synodontis* Cuvier, 1816 species (left dentary): **A**, **B**, main features of the dentary, exemplified in *S. schall* (Bloch & Schneider, 1801); **A**, occlusal view; **B**, postero-dorsal view; **C**-**I**, shape of the dentary in postero-dorsal views; **C**, *S. clarias* (Linnaeus, 1758); **D**, *S. sorex* Günther, 1864; **E**, *S. ocellifer* Boulenger, 1900; **F**, *S. batensoda* Rüppell, 1832; **G**, *S. courteti* Pellegrin, 1906; **H**, *S. violaceus* Pellegrin, 1919; **I**, *S. membranaceus* (Geoffroy Saint-Hilaire, 1809). Scale bars: 2 mm.

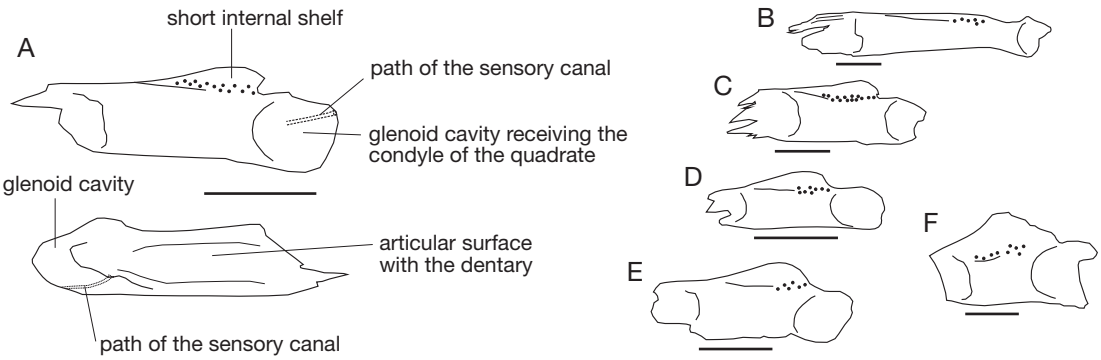

FIG. 24. — The anguloarticulo-retroarticular of *Synodontis* Cuvier, 1816 species: **A**, main features, exemplified in *S. schall* (Bloch & Schneider, 1801) in dorsal and median views; **B**-**F**, shape of the anguloarticulo-retroarticular in several species; **B**, *S. membranaceus* (Geoffroy Saint-Hilaire, 1809); **C**, *S. courteti* Pellegrin, 1906; **D**, *S. ocellifer* Boulenger, 1900; **E**, *S. filamentosus* Boulenger, 1901; **F**, *S. sorex* Günther, 1864. Scale bars: 5 mm.

less than two times the width of the posterior process (Fig. 23E, F).

The dentary teeth are usually S-shaped in *Synodontis* fishes. Their number and their shape have been described and figured by Poll (1971) and the tooth formulae of the West African species have been reviewed by Paugy & Roberts (1992). The tooth formula varies from about ten elongated teeth (*S. sorex*) to about fifty smaller teeth (*S. batensoda*). As previously noticed by Paugy & Roberts (1992), *S. sorex* and *S. clarias* are easily identified by their long teeth which never exceed ten in number.

THE ANGULOARTICULO-RETROARTICULAR (FIG. 24)

The rod-like anguloarticulo-retroarticular antero-laterally sutures with the dentary along almost all of its length and the horizontal branch of the Meckel's cartilage firmly joins its proximal end to the dentary (Fig. 24A, B). The glenoid cavity opens caudally and dorsally and articulates with the globular articular condyle of the quadrate. A short

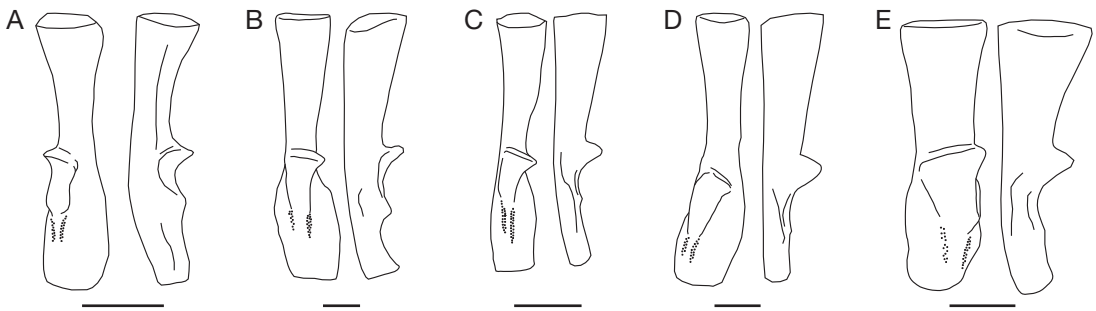

FIG. 25. — The palatine of *Synodontis* Cuvier, 1816 species in dorsal and median views: **A**, *S. schall* (Bloch & Schneider, 1801); **B**, *S. membranaceus* (Geoffroy Saint-Hilaire, 1809); **C**, *S. clarias* (Linnaeus, 1758); **D**, *S. sorex* Günther, 1864; **E**, *S. courteti* Pellegrin, 1906. Scale bars: 5 mm.

internal shelf develops medially in most species (Fig. 24A, C-F), except *Synodontis batensoda* and *S. membranaceus* which have slender jaw bones (Fig. 24B). The anguloarticulo-retroarticular is the widest in *S. sorex* (Fig. 24F) and *S. clarias* which both exhibit very bulky jaws. The mandibular sensory canal extends along the dentary and through the anguloarticulo-retroarticular in a bony tube below the glenoid cavity length (Fig. 24A).

THE PALATINE (FIG. 25)

The palatine is a rod-like bone. At its anterior tip, the palatine attaches through ligaments to the bifid head of the maxilla, and just behind, the lacrymal bone lies on the lateral face of the palatine. In its posterior half a dorsal articular facet connects with the lateral ethmoid. Anterior to this facet, the palatine has a rounded section, whereas posteriorly it is dorso-ventrally flattened but not laminar. The palatine of *Synodontis courteti* is notably bulkier (Fig. 25E) than all of the others (Fig. 25A-D).

THE HYOMANDIBULA (FIG. 26)

The hyomandibula is a laminar bone roughly rectangular in outline, with a dorsal edge devoted to the articulation with the neurocranium, through an anterodorsal spur, a condylar dorsal facet and a posterior articular facet (Fig. 26A-D). They articulate respectively with a deep triangular fossa formed by the sphenotic and pterosphenoid, with an elongated shallow fossa formed by the sphenotic, the pterotic and the prootic, and with the pterotic spine (Fig. 26E). Also, the opercular articulates on the hyomandibula through a bulky condyle located on its posterior edge, below the articular surface for the pterotic, and above the lateral surface where the preopercular lies (Fig. 26A, B). Ventrally on the internal face of the hyomandibula, the distal end of the posterior ceratohyal of the hyoid arch contacts the postero-ventral corner of the bone, and the whole surface of the ventral process sutures with the quadrate. In front of this process, the metapterygoid lies on the anterior border of the hyomandibula. At last, the hyomandibula exhibits an anteriorly directed process located on its anteromedial edge.

In *Synodontis membranaceus* and *S. batensoda*, the hyomandibula is more slender than in the other Chadian species with a clearly marked antero-dorsal spur (Fig. 26F, G). Moreover, the process of the anteromedial edge is markedly short (Fig. 26F, G), whereas it is a thin, long and often bent rod in the other species (Fig. 26H-K). It is located ventrally in most species (Fig. 26F-I) and in a proximal position in *S. sorex*, *S. clarias* and *S. courteti* (Fig. 26J, K).

The dorsal articular surface exhibits an antero-posteriorly elongated outline in *Synodontis eupterus*, *S. batensoda*, *S. ocellifer*, *S. nigrita*, *S. violaceus* and *S. schall* (Fig. 26D, G, H), which is even more so in *S. membranaceus* (Fig. 26F). On the contrary, the dorsal articular surface is roughly rounded in *S. clarias* and *S. filamentosus* (Fig. 26I, J) and shows latero-medially directed elongation in *S. courteti* and *S. sorex* (Fig. 26K, L).

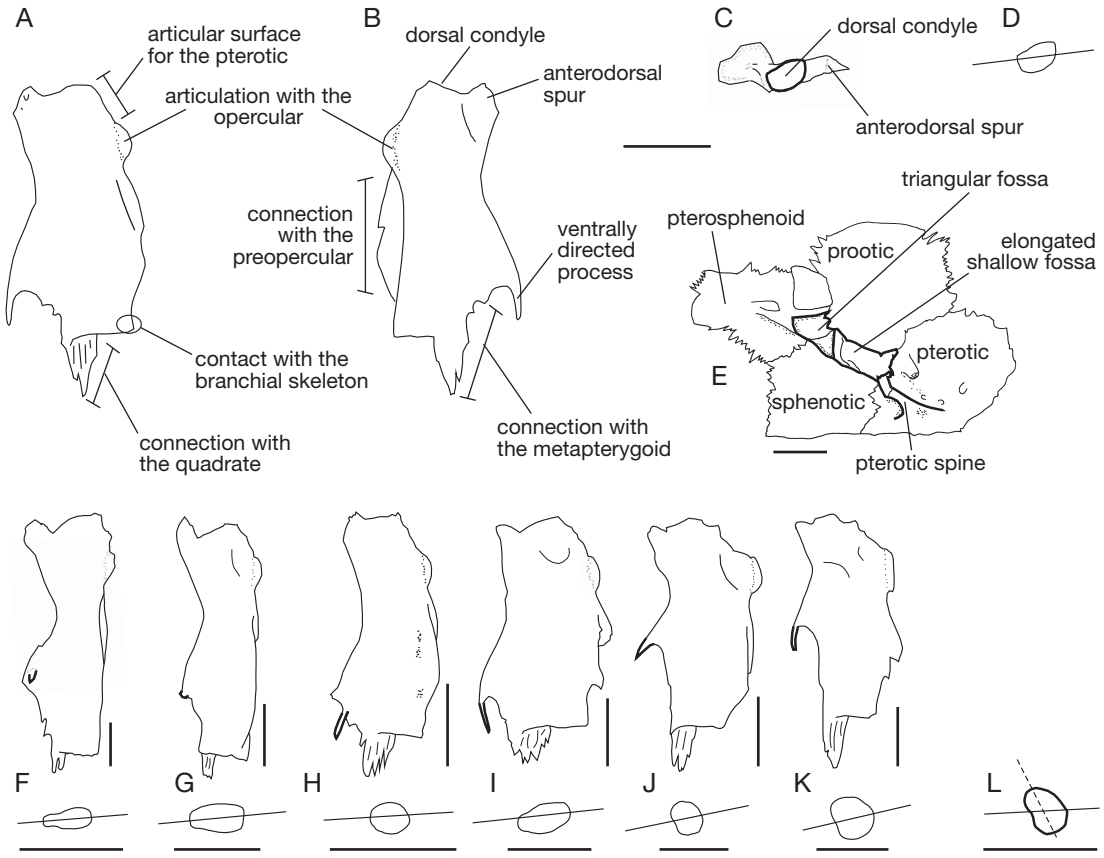

Fig. 26. — The hyomandibula of *Synodontis* Cuvier, 1816 species: **A**-**D**, main features exemplified in *S. schall* (Bloch & Schneider, 1801) (right hyomandibula); **A**, inner view; **B**, outer view; **C**, proximal view; **D**, schematic representation of the outline of the dorsal condyle in proximal view; **E**, lateral view of the articular counterpart of the hyomandibula on the neurocranium in the same species; **F**-**L**, the hyomandibula of several species in outer views (top) with a schematic representation of the dorsal condyle outline (bottom); **F**, *S. membranaceus* (Geoffroy Saint-Hilaire, 1809); **G**, *S. batensoda* Rüppell, 1832; **H**, *S. filamentosus* Boulenger, 1901; **I**, *S. ocellifer* Boulenger, 1900; **J**, *S. clarias* (Linnaeus, 1758); **K**, *S. sorex* Günther, 1864; **L**, *S. courteti* Pellegrin, 1906. Scale bars: 5 mm.

The quadrate (Fig. 21A, B, F, G)

The quadrate is subtriangular. It articulates with the anguloarticulo-retroarticular glenoid cavity through its globular condyle and with the preopercular all along its postero-ventral edge (Fig. 21F, G). The surface that connects with the hyomandibula through an interdigitated suture is located on its internal face (Fig. 21F). The metapterygoid lies along the dorsal edge of the quadrate (Fig. 21A, B).

The pterygoid series (Fig. 21A, B)

The pterygoid series is reduced to the metapterygoid only and neither the entopterygoid nor the ectopterygoid have been observed in any of the studied specimens. The absence of the entopterygoid is noted by Taverne & Aloulou-Triki (1974) who also noted the reduction of the ectopterygoid located just behind. The metapterygoid is somewhat quadrangular in outline. It connects with the anteroventral part of the hyomandibula; ventrally it lies all along the dorsal edge of the quadrate (Fig. 21A, B).

Nasal bone and infraorbital series

In *Synodontis* fishes, the minute nasal bone is reduced to a bony tube around the anterior part of the supraorbital branch of the sensory canal. It lies on

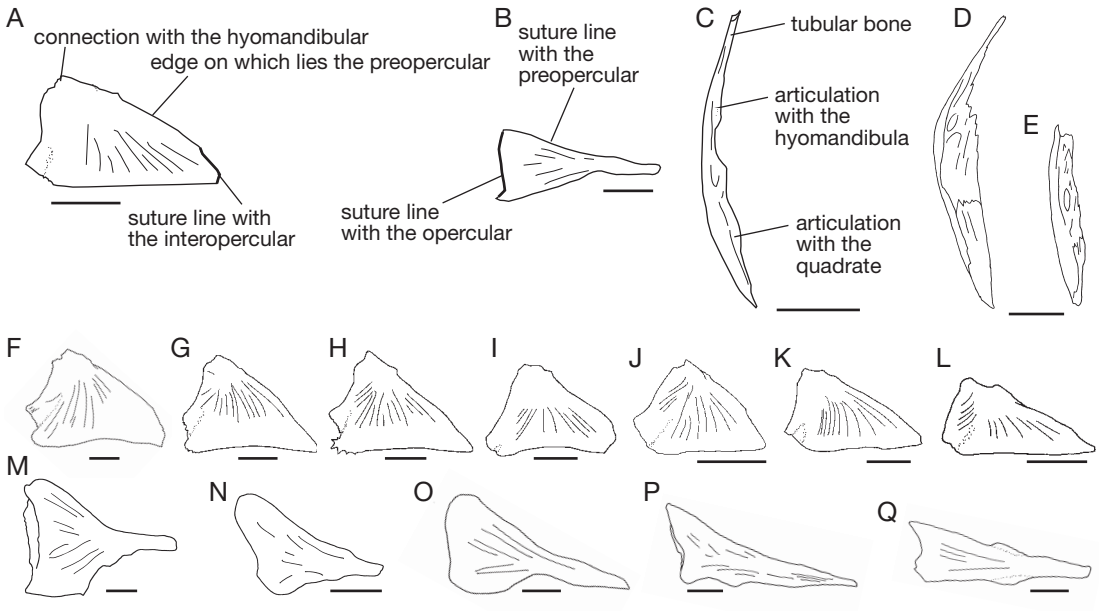

Fig. 27. — The bones of the opercular series of *Synodontis* Cuvier, 1816 species: **A**-**C**, main features of the bones in lateral views, exemplified in *S. schall* (Bloch & Schneider, 1801) (right bones); **A**, opercular; **B**, interopercular; **C**, preopercular; **D**-**Q**, outline of the bones, in lateral views (right bones); **D**, **E**, preoperculars; **D**, *S. courteti* Pellegrin, 1906; **E**, *S. sorex* Günther, 1864; **F**-**L**, operculars; **F**, *S. membranaceus* (Geoffroy Saint-Hilaire, 1809); **G**, **H**, *S. batensoda* Rüppell, 1832; **I**, *S. sorex*; **J**, *S. nigrita* Valenciennes, 1840; **K**, *S. violaceus* Pellegrin, 1919; **L**, *S. filamentosus* Boulenger, 1901; **M**-**Q**, interopercular; **M**, *S. membranaceus*; **N**, *S. batensoda*; **O**, *S. ocellifer* Boulenger, 1900; **P**, *S. courteti*; **Q**, *S. sorex*. Scale bars: 5 mm.

the lateral ethmoid in front of the anterior opening for the sensory canal. The infraorbital series is composed of four laterally flattened bones. The anteriormost infraorbital bone, i.e. the lacrymal, is clearly distinguished by a median pointed expansion. It joins anteriorly with the maxilla, covers the palatine all along its length, and it connects posteriorly with the anterior tip of the lateral ethmoid. The second infraorbital bone is fairly straight and bracketed along its total length by the lateral ethmoid. The curved third and fourth infraorbitals ventrally border the orbit. The anterior half of the third infraorbital lies along the posterior part of the lateral ethmoid and its posterior half is free. The fourth infraorbital is free and joins the sphenotic at the back.

The opercular series (Fig. 27)

The opercular series of *Synodontis* fishes is composed of three bones, and as in all catfishes, lacks the subopercular (Fig. 27A-C). The preopercular is an elongated and slender bone whose anterior border firmly connects with the posterior margin of both the hyomandibula dorsally and the quadrate ventrally (Fig. 27C). Dorsally the preopercular covers the articulation between the hyomandibula and the opercular. The sensory canal runs in a bony tube, except in the dorsalmost part. The dorsal tubular part is long (Fig. 27A, D), except in *S. sorex* (Fig. 27E).

The opercular exhibits a triangular shape in outline and articulates with the hyomandibula through its dorsal corner whereas its anterior corner supports the interopercular (Fig. 27B). The branchiostegal rays lie ventrally on its internal face.

The opercular height depends on the species; the bone is deep in *Synodontis batensoda*, *S. membranaceus*, *S. nigrita* and *S. sorex* (Fig. 27F-J) and shallow in *S. filamentosus*, *S. eupterus* and *S. violaceus* (Fig. 27K, L). The anterior corner is pointed in all the species except in *S. sorex* where it is trun-

cated (Fig. 27I). The posterior corner exhibits a marked notch in S. *membranaceus* and *S. batensoda* (Fig. 27F-H). Moreover, in *S. batensoda*, and sometimes in *S. membranaceus*, the posterior corner is denticulated (Fig. 27F-H). In the studied specimens the denticulations are much less developed than those figured and described by Taverne & Aloulou-Triki (1974).

The interopercular is a stout rod which is widened posteriorly. In *Synodontis membranaceus*, *S. batensoda* and *S. ocellifer* it is deeper posteriorly (Fig. 27M-O) than in the other species (Fig. 27P, Q). Moreover, in the former species, it has a peculiar paddle-like shape whereas it is roughly triangular in the others.

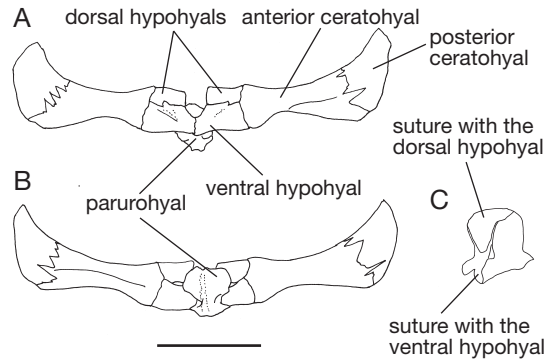

FIG. 28. — Main features of the hyoid arch of *Synodontis* Cuvier, 1816, exemplified in *S. schall* (Bloch & Schneider, 1801): **A**, anterior view of the paired bones; **B**, posterior view of the paired bones; **C**, lateral view of a parurohyal. Scale bar: 5 mm.

THE HYOID ARCH (FIG. 28)

The ventral hypohyal exhibits a conical shape. The anterior ceratohyal is a rod-like bone enlarged on both extremities (Fig. 28A, B). The posterior section of the bone is antero-posteriorly flattened and the anterior section is ovoid. The anterior ceratohyal proximally connects with both dorsal and ventral hypohyals (Fig. 28A, B); in its proximal half it contacts the anguloarticulo-retroarticular with which it is united by ligaments (Fig. 21A). The posterior ceratohyal exhibits a triangular shape. Anteriorly, it articulates with the anterior ceratohyal by strong interdigitations (Fig. 28A, B). The dorsolateral edge of the anterior ceratohyal lies on the quadrate, whereas the posterior ceratohyal lies on the interopercular. The posterior corner of the posterior ceratohyal contacts the hyomandibula and the preopercular. The anterior and the posterior ceratohyals bear respectively four or five and two branchiostegal rays. The medial parurohyal is reduced to the anterior articular head (Fig. 28C) and lacks a posterior portion, which constitutes an apomorphy of the family Mochokidae (Mo 1991).

PECTORAL GIRDLE AND FINS

The pectoral girdle is a paired structure that comprises the posttemporal firmly linked on both sides to the neurocranium, the cleithra which exhibit well-developed humeral plates and articulate with the pectoral spines and the pectoral radials, and the scapulo-coracoids that connect with each other ventrally. The cleithra and the scapulo-coracoids are intimately linked. The pectoral radials are represented by a series of three radials that insert in between each pair of hemi-lepidotriches. As detailed by Taverne & Aloulou-Triki (1974) the pectoral fins are characterized by the presence of the spine followed by 5 to 7 soft rays.

THE POSTTEMPORAL (FIG. 29)

In *Synodontis* fishes, the posttemporal is firmly sutured to the neurocranium. The sensory canal runs from the pterotic across this bone and gives off a branch in the middle of the bone where a pore is observed (Fig. 29A). The posttemporal is part of the skull roof. Its dermal ossification is great and shows the typical tuberculated ornamentation. Dorsally, the posttemporal connects with the pterotic anteriorly, with the supraoccipital dorso-medially, and the posterodorsal corner of the inner face of the bone receives the epioccipital (Fig. 29B). Also, the posttemporal has a postero-ventral limb (Fig. 29A). A stout median limb which corresponds to the ossified transcapular ligament projects medially from the roof of the bone towards the otic region of the neurocranium (Fig. 29B). It sutures with the exoccipital dorsally but principally with the basioccipital ventrally. It bears an excavation on its ventral edge and a ventromedial projection (Fig. 29B). The first dorsal process of the cleithrum lies on the limb in front of this excavation. The postero-ventral limb of the posttemporal roof covers the horseshoe-shaped

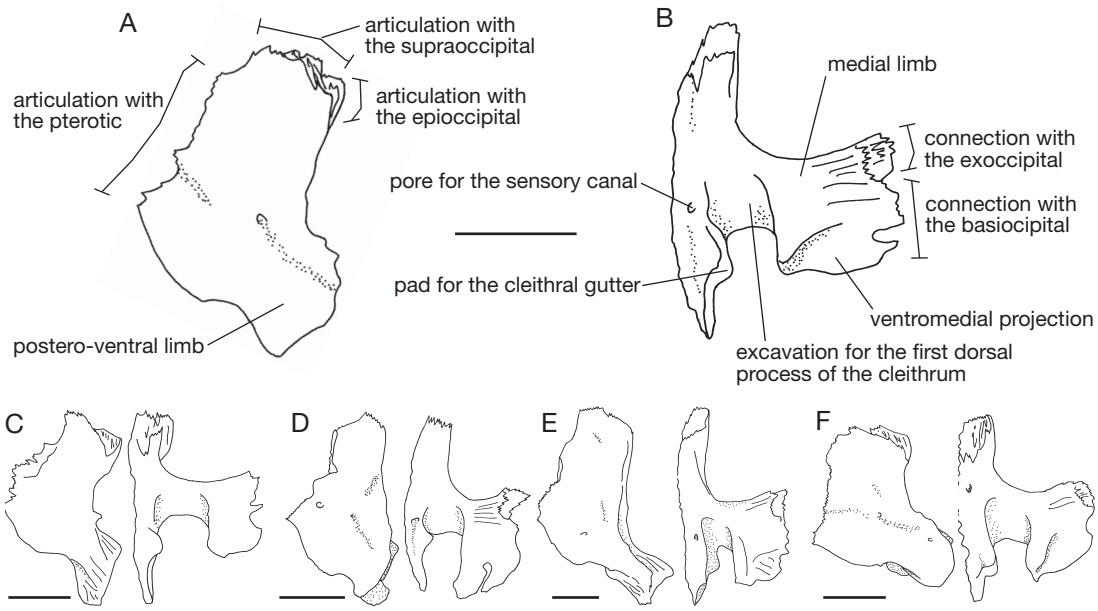

FIG. 29. — The left posttemporal of *Synodontis* Cuvier, 1816 species, in lateral view (right) and caudal view (left): **A**, **B**, main features exemplified in *S. schall* (Bloch & Schneider, 1801); **C**-**F**, shape of the bone in several species; **C**, *S. courteti* Pellegrin, 1906; **D**, *S. clarias* (Linnaeus, 1758); **E**, *S. membranaceus* (Geoffroy Saint-Hilaire, 1809); **F**, *S. ocellifer* Boulenger, 1900. Scale bars: 5 mm.

notch and the two dorsal processes of the cleithrum. Moreover, on the inner face of the postero-ventral limb there is a lower pad which slides within a vertical gutter that develops along the first dorsal process of the cleithrum.

Depending on the species, the postero-ventral limb varies in its development. It is narrow and extended in *Synodontis courteti*, *S. membranaceus* and *S. violaceus* (Fig. 29C, E), very short in *S. clarias* (Fig. 29D), and of intermediate length in the other Chadian species where it is wider than in S. *membranaceus*, *S. courteti* or *S. violaceus* (Fig. 29F).

The species also differ from each other by the shape of the medial limb, notably by the width of the excavation and by the height of the ventromedial projection. The ventromedial projection is the longest in *Synodontis membranaceus* (Fig. 29E) and it is the shortest in *S. courteti* (Fig. 29C). In *S. clarias*, the ventromedial projection is at least as deep as the inferior limb is high (Fig. 29D).

Finally, a temporal fenestra may be present at the junction of the posttemporal, the supraoccipital and the pterotic. Compared with the other Chadian species, the fenestra is well developped in *Synodontis courteti* and *S. violaceus* and it is closed in all the studied *S. nigrita* specimens and in most *S. schall*.

THE CLEITHRUM (FIGS 30-32; APPENDIX 6)

The first (anteriormost) dorsal process of the cleithrum lies in front of the excavation of the posttemporal medial limb (Fig. 30A). It has a gutter in which slides the posterior process of the posttemporal lower limb (Fig. 30B). Between the two dorsal processes of the cleithrum, a deep horseshoe-shaped notch accommodates the lower limb of the posttemporal (Fig. 30A). Laterally on the cleithrum, a large lateral triangular humeral plate extends between the second dorsal process, which is postero-dorsally directed, and the humeral process, which points posteriorly (Fig. 30B). In front of the humeral process, the cleithrum receives the articular surface of the pectoral spine in a deep crescentic medially-faced gutter on its internal face (Fig. 30B). Laterally it corresponds to a raised area, from which the stout ventral limb develops anteriorly in a laminar plate that joins its couterpart

medially. Internally, an inner laminar plate extends up to the mid height of the first dorsal process. The scapulo-coracoid lies on and sutures with the cleithrum at the posterior face of the inner plate, all along the length of the posterior edge of the ventral limb (Fig. 30C), and also by two distinct surfaces in front of and above the gutter for the articulation of the pectoral spine (Fig. 30B). The cleithrum, and in particular the humeral plate, has been considered as a key-structure to identify *Synodontis* taxa by Poll (1971), Taverne & Aloulou-Triki (1974), Paugy & Roberts (1992). The humeral characters they observed concern the outline of the posterior corner, the presence of spines at the ventral edge of the plate, and the presence or absence of a stout ventral crest. Taverne & Aloulou-Triki (1974) also distinguished a different type of anterior dorsal process. For the Chadian species we agree with their remarks and emphasize the following features.

In *Synodontis membranaceus* and *S. batensoda* only, the humeral plate is deep, and the length of the humeral process is larger in front of the second dorsal process than behind it (Fig. 31A, B). The humeral plate is longer than high in all of the other species (see e.g., Fig. 31G). Moreover, it exhibits a posterior corner that is rounded in outline in *S. sorex* and *S. filamentosus* (Fig. 31C, K) whereas it is pointed in the other species. Finally, *S. violaceus* exhibits a prominent first dorsal process (Fig. 31J). Moreover, the outline of the ventral edge of the humeral plate varies depending on the species, from straight in *S. batensoda* (Fig. 31B) to curve in *S. clarias* (Fig. 31D).

To enhance the recognition of the cleithra according to the shape, and to quantify the differences observed among the species, we used 6 linear measurements on the humeral plates (Fig. 32A) transformed into log-shape ratios, together with 2 angular measurements (Fig. 32B) and 2 ratios. Among variables that allow statistical distinction of mono- and poly-specific groups (Appendix 6), the most evident are explained as follows.

Synodontis membranaceus (Fig. 31A) is characterized by δ clearly more acute than γ, by an extremely short postero-ventral edge (Appendix 6: variable 5), by a relatively long antero-ventral edge as in *S. batensoda* only (Fig. 31B; Appendix 6: 4), and the total

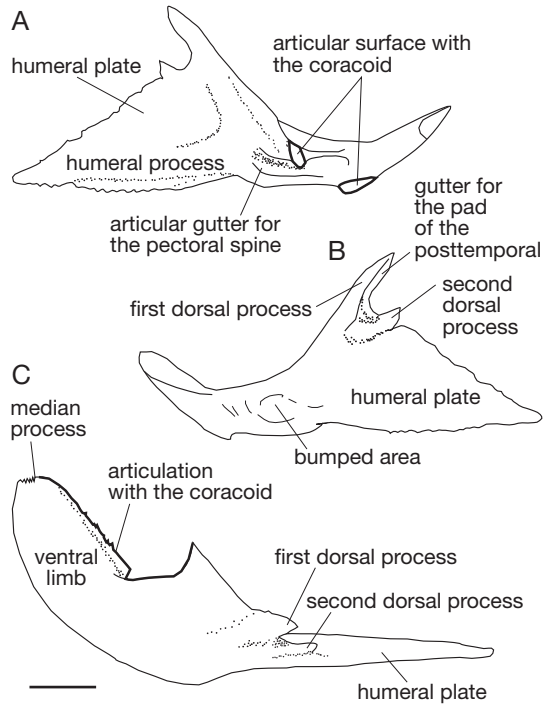

FIG. 30. — Main features of the cleithrum of *Synodontis* Cuvier, 1816, exemplified in *S. schall* (Bloch & Schneider, 1801) (left cleithrum): **A**, lateral view; **B**, median view; **C**, dorsal view. Scale bar: 5 mm.

height of the bone is very great when compared with the total length (Appendix 6: 8).

In *Synodontis batensoda*, *S. clarias* and *S. sorex*, δ is slightly more acute than γ. For the three species, the total height of the bone is much greater than the total length (Appendix 6: 8). As previously noticed in *S. batensoda*, the antero-ventral edge is short (Fig. 31C; Appendix 6: 4). Moreover, the ventral edge of the bone is straight, whereas it is curved in *S. sorex* and *S. clarias* (Fig. 31B-D). On the other hand, *S. sorex* and *S. filamentosus* resemble each other by the rounded posterior corner of the humeral plate (Fig. 31C, K) and differ from each other by the length of the postero-ventral edge (Appendix 6: 5) and by angles δ and γ. Also, the cleithrum is shallower in *S. filamentosus* than in *S. sorex* (Fig. 31C, K; Appendix 6: 1).

In *Synodontis nigrita*, *S. eupterus* and *S. ocellifer*, both the postero-ventral and the dorsal edges are

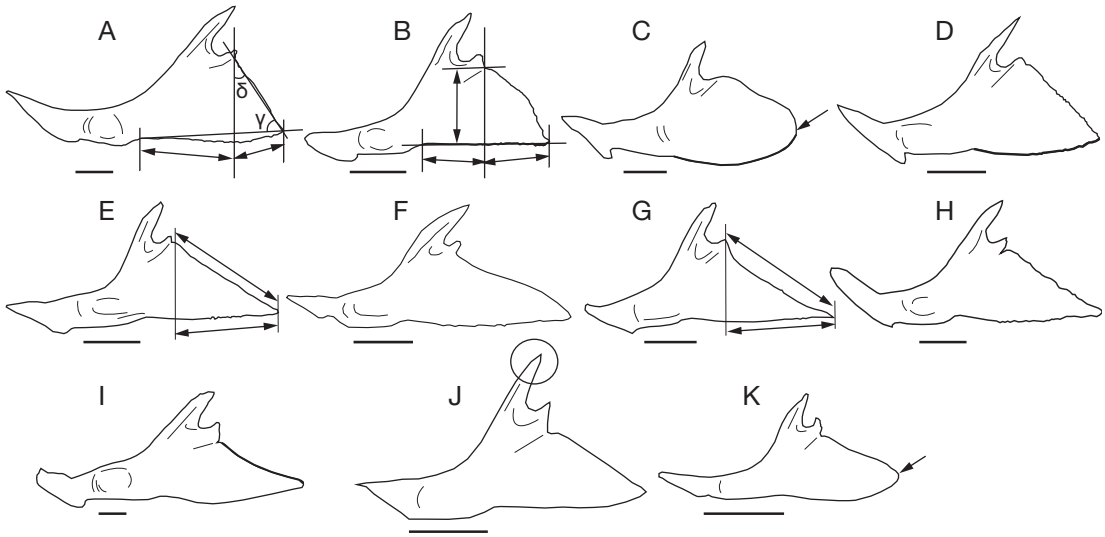

Fig. 31. — Left cleithrum of *Synodontis* Cuvier, 1816 species, in lateral views: **A**, *S. membranaceus* (Geoffroy Saint-Hilaire, 1809); **B**, *S. batensoda* Rüppell, 1832; **C**, *S. sorex* Günther, 1864; **D**, *S. clarias* (Linnaeus, 1758); **E**, *S. ocellifer* Boulenger, 1900; **F**, *S. eupterus* Boulenger, 1901; **G**, *S. nigrita* Valenciennes, 1840; **H**, *S. schall* (Bloch & Schneider, 1801); **I**, *S. courteti* Pellegrin, 1906; **J**, *S. violaceus* Pellegrin, 1919; **K**, *S. filamentosus* Boulenger, 1901. The double arrows are for the dimensions of the humeral process. The single arrows are for the rounded outline of the posterior corner of the humeral plate. The circle is for the prominent first dorsal process. The black lines underline the characteristics in the shape of the ventral and postero-dorsal borders outline of the humeral plates. Scale bars: 5 mm.

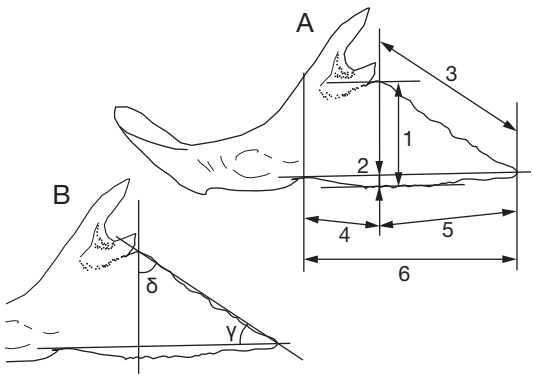

Fig. 32. — Linear and angular measurements taken on the cleithra, shown in *Synodontis schall* (Bloch & Schneider, 1801) (left cleithrum in lateral views): **A**, linear measurements; **1**, total height of the humeral plate; **2**, height of its lower part; **3**, length of the dorsal edge; **4**, length of the antero-ventral edge; **5**, length of the postero-ventral edge; **6**, total length of the humeral plate; **B**, angular measurements; **γ**, formed by the dorsal edge and the ventral line of the humeral plate, i.e. the line passing by the ventral inflection point behind the articular gutter for the pectoral spine and the posteriormost point of the posterior corner; **δ**, formed by the dorsal edge and the vertical line at the level of the first dorsal process.

elongated (Fig. 31E-G). They share with *S. schall*, *S. violaceus*, *S. courteti* and *S. filamentosus* a δ angle frankly more open than the angle γ (Appendix 6).

The cleithra of *Synodontis courteti*, *S. schall* and *S. violaceus* (Fig. 31H-J) resemble to each other by the shape of the humeral process and are distinguished from those of the other species by the length of their postero-ventral edge (Appendix 6: 5) which is intermediate between *S. membranaceus* and *S. ocellifer* + *S. nigrita*. Their humeral plate is also markedly shallow (Appendix 6: 1) which thus distinguishes them from *S. membranaceus*, *S. batensoda*, *S. ocellifer*, *S. nigrita* and *S. clarias* (Fig. 31A, B, D, E, G). They differ from each other by the outline of the dorsal edge of the humeral plate which is always slightly concave in *S. courteti* (Fig. 31I), sometimes in *S. schall*, but never in *S. violaceus* (Fig. 31J).

The coracoid (Fig. 33)

The two laminae that constitute the coracoid describe a right angle. The ventral (horizontal)

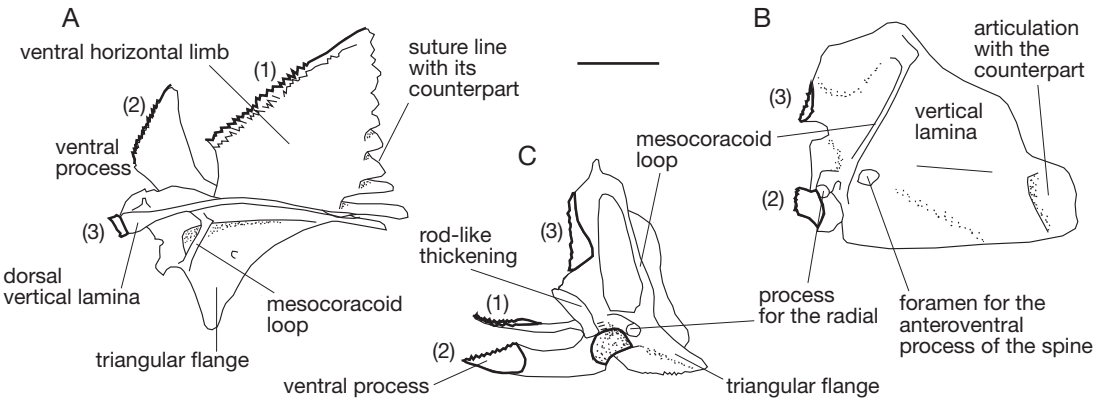

FIG. 33. — Main features of the coracoid in *Synodontis* Cuvier, 1816, exemplified in *S. schall* (Bloch & Schneider, 1801) (left coracoid): **A**, dorsal view; **B**, posterior view; **C**, lateral view. The black lines underline the suture lines and the articular surfaces which are numbered. Scale bar: 5 mm.

lamina sutures anteriorly with the ventral limb of the cleithrum. The dorsal (vertical) lamina lies on the posterior face of the inner laminar plate of the cleithrum. Both lamina of the coracoid suture with their counterpart medially through strongly interdigitated sutures located postero-ventrally (Fig. 33A). The other parts of the coracoid of *Synodontis* fishes are the ventral process that projects anteriorly and sutures with the cleithrum in front of the deep crescentic gutter for the pectoral spine, and the triangular flange that extends posteriorly and laterally from the hinge between the two laminae (Fig. 33A). Furthermore, a thin bony bridge, called the mesocoracoid loop, develops from the triangular flange, sub-vertically to the latero-dorsal edge of the dorsal (vertical) lamina of the coracoid (Fig. 33). Close to the ventral end of the mesocoracoid loop, a short process contacts the pectoral radial which accommodates the inner fossa of the pectoral spine (Fig. 33B, C). In this area, there are three openings: the large foramen that receives the proximal ventral process of the pectoral spine in total abduction (Fig. 33B), and also two small pores that allow the passage of nerves and vessels. Moreover, the articular groove of the pectoral spine rotates around a rod-like thickening of the bone (Fig. 33C), and, in total abduction, the distal ventral process of the spine lies in a circular depression located ventrally.

THE PECTORAL FIN (FIGS 34-36; APPENDIX 7)

The pectoral spine articulates with both the cleithrum and the coracoid. The articular groove of the spine, which starts at the dorsal process (Fig. 34A), rotates around the rod-like thickening of the scapulo-coracoid and the articular plateau (Fig. 34B) slides against the deep crescentic gutter of the cleithrum (see above). The proximal and the distal ventral processes of the pectoral spine (Fig. 34C) are blocked against the coracoid in total abduction: the distal ventral process lies in a circular depression located ventrally whereas the other process lodges in a foramen located near the base of the mesocoracoid loop. The body of the spine is dorsoventrally flattened, with the two faces ornamented by longitudinal linear striae, an inner edge always coarsely serrated, and the outer edge often finely serrated. The first radial carries the first pair of hemilepidotrichs (Fig. 34D). Its small outer end articulates (Fig. 34D) in the inner fossa of the pectoral spine (Fig. 34A). The second radial is rod-like and exhibits a small triangular flange at its proximal end which contacts the third and last radial (Fig. 34D). The pectoral spine contains all the characters that allow the pectoral fins to be distinguished according to species.

A preliminary study, using ratios of five linear and angular measurements and one discrete character, allows us to distinguish four modern Chadian *Synodontis* species (Pinton *et al.* 2006). The

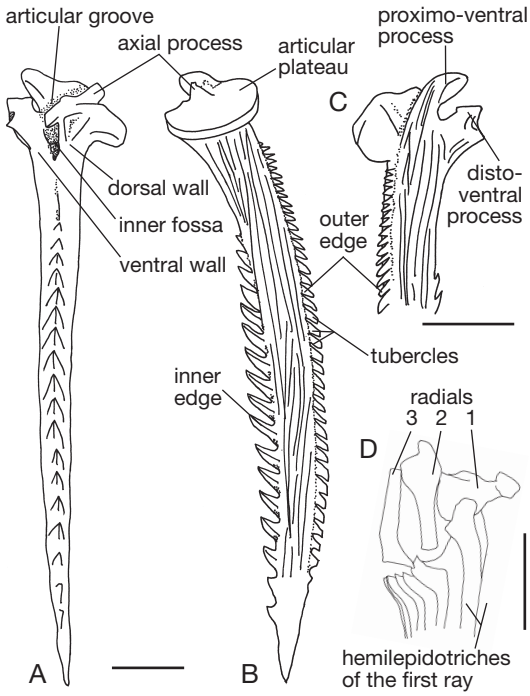

FIG. 34. — Main features of the pectoral radials and spine in *Synodontis* Cuvier, 1816, exemplified in *S. schall* (Bloch & Schneider, 1801) (right fin): **A**-**C**, pectoral spine; **A**, inner view; **B**, dorsal view; **C**, ventral view; **D**, series of the pectoral radials, in dorsal view. Scale bars: 5 mm.

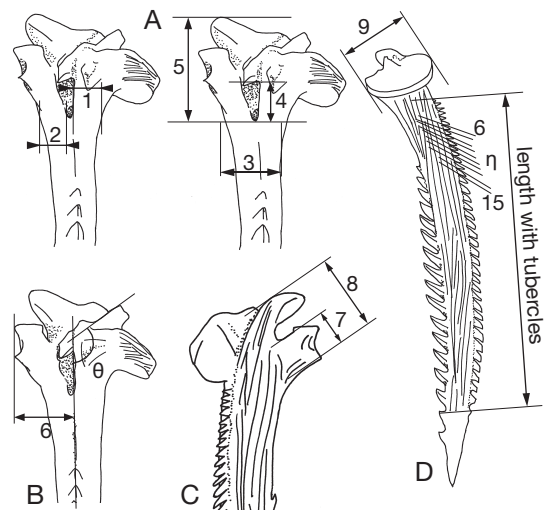

FIG. 35. — Linear and angular measurements taken on the pectoral spines, shown in *S. schall* (Bloch & Schneider, 1801): **A**, linear measurements taken looking at the inner fossa of the spine; **B**, linear and angular measurements taken looking at the inner edge of the spine; **C**, **D**, linear and angular measurements are taken looking at the ventral face of the body of the spine. Measurements: **1**, minimum width of the dorsal wall of the inner fossa; **2**, minimum width of the ventral wall; **3**, width of the spine at the base of the inner fossa; **4**, maximum height of the inner fossa; **5**, distance between the dorsal edge of the inner fossa and the tip of the distal ventral process; **6**, minimum height of the distal ventral process; **7**, maximum width of the articular plateau; **8**, maximum length between the outer edge of the distal ventral and proximal ventral processes; **9**, maximum height of the head of the spine taken between the base of the fossa and the proximal ventral process; length with tubercles, linear length where tubercles are present on the outer edge; **θ**, angle between the axial process and the line formed by the tubercles of the inner edge; **η**, average angle between the proximal edge of the outer 6th to 15th tubercles and the tangent to the edge of the spine. The measurements are taken on stereomicroscope photographs (1-8, angles), or with a digital calliper (9, "length with tubercles").

measurements are used here together with complementary ones. The discrete character "presence of a crest along the outer edge" is also included. The complex morphology of the articular head of the spine (Fig. 34A-C) makes it necessary to define very accurately the position of the spine, either to take measurements (Fig. 35A-C) or to compare the morphology of the head between different species (Fig. 36A-D). To describe the modern *Synodontis* species of the Chadian basin, we also use the ornamentation of the outer and the inner edge of the spine (Fig. 36E-J) together with linear, angular and density measurements. The measurements are taken on spines with an articular plateau (Fig. 35C: variable 8) larger than 5 mm because the morphological traits are poorly marked on smaller specimens. For that reason, the species *S. nigrita* is not included in our quantitative study. As a first point, we note that the spines show great intraspecific morphological variations which often overlap between species. However, the following morphological tendencies were found (Appendix 7; Fig. 36).

In *Synodontis courteti*, *S. violaceus* and *S. filamentosus*, the pectoral spine presents a relatively thin dorsal wall (Appendix 7: 1) and a narrow base at the level of the inner fossa (Appendix 7: 3). *Synodontis courteti* exhibits a very deep fossa (Appendix 7: 4) and can also be clearly identified by evaluating the angle between the 6th to 15th tubercles and the edge of the spine (Fig. 36D). *Synodontis violaceus* is distinguished from *S. courteti*, *S. filamentosus* and from all the other Chadian species by its distal ventral

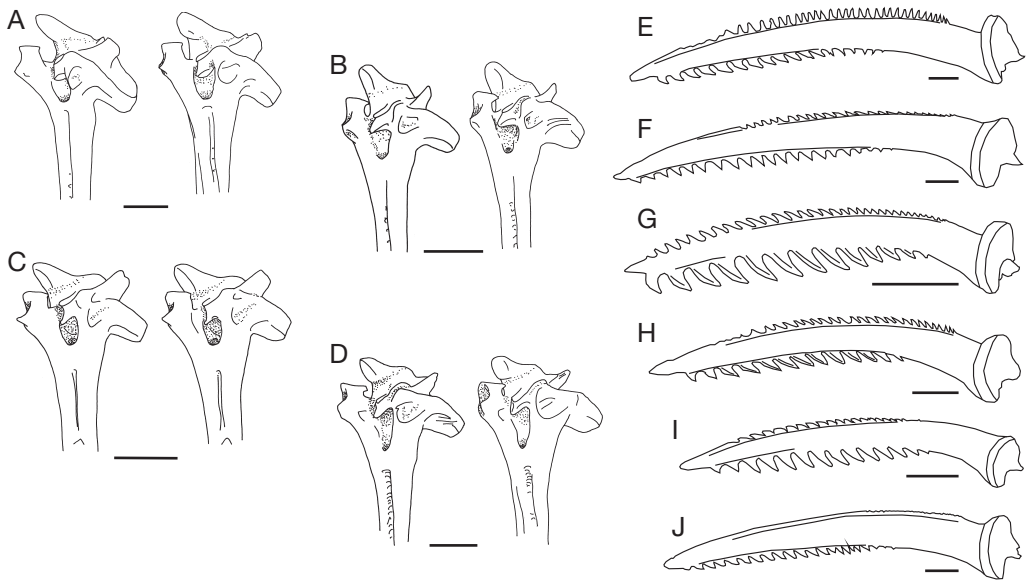

FIG. 36. — Head and body outline of the left pectoral spine of *Synodontis* Cuvier, 1816 species: **A**-**D**, head of the spine in inner views, looking at the inner edge of the spine (left) and the inner fossa (right); **A**, *S. membranaceus* (Geoffroy Saint-Hilaire, 1809); **B**, *S. violaceus* Pellegrin, 1919; **C**, *S. clarias* (Linnaeus, 1758); **D**, *S. courteti* Pellegrin, 1906; **E**-**J**, body of the spines in dorsal views; **E**, *S. courteti*; **F**, *S. membranaceus*; **G**, *S. filamentosus* Boulenger, 1901; **H**, *S. violaceus*; **I**, *S. batensoda* Rüppell, 1832; **J**, *S. sorex* Günther, 1864. Scale bars: 5 mm.

process which projects more posteriorly (Appendix 7: 4, 8; Fig. 36B). Compared with *S. courteti*, *S. violaceus*, the pectoral spine of *S. filamentosus* is characterized by a large articular plateau when compared to the width of the spine at the base of the fossa (Appendix 7: 11); moreover, the tubercles developed on its inner edge are larger than those of the outer edge (Fig. 36G).

The head of the spine of *Synodontis clarias* or *S. ocellifer* is compact with a distal ventral process which does not project posteriorly (Fig. 36C). The pectoral spine of *S. sorex* is distinguished by unique features of its outer edge. First, a crest links the tubercles (Fig. 36J). Second, density of the tubercles on the outer edge is the highest of all the species. *S. membranaceus* is recognized by the length between the dorsal edge of the fossa and the most exterior point of the distal ventral process which is high, and by the fact that this latter process is very extended (Appendix 7: 6, 7; Fig. 36A). This species also exhibits the lowest density of tubercles along the outer edge of the spine (Fig. 36F). Together with *S. batensoda* only, they present the lowest values for the angles η and θ.

THE PELVIC FIN

Each pelvic bone is composed of a pair of spiny pads and a median plate that contacts medially with its counterpart. The pelvic fin has 6 or 7 rays depending on the species and the individual (Poll 1971).

WEBERIAN APPARATUS (FIG. 37)

The Weberian apparatus *sensu lato* consists of the modified anteriormost centra, neural arches, supraneurals and pleural ribs (Fig. 37). The Weberian ossicles, i.e. the tripus, the scaphium, the intercalarium and the suspensorium, connect the gas bladder with the inner ear. They are associated with the complex centrum, which is a very solid unit formed by the fusion of the second to the fourth centra (Fig. 37B). The complex centrum itself develops in close relationships with the first, fifth and sixth centra. Altogether, they form the complex vertebra (Fig. 37B-D).

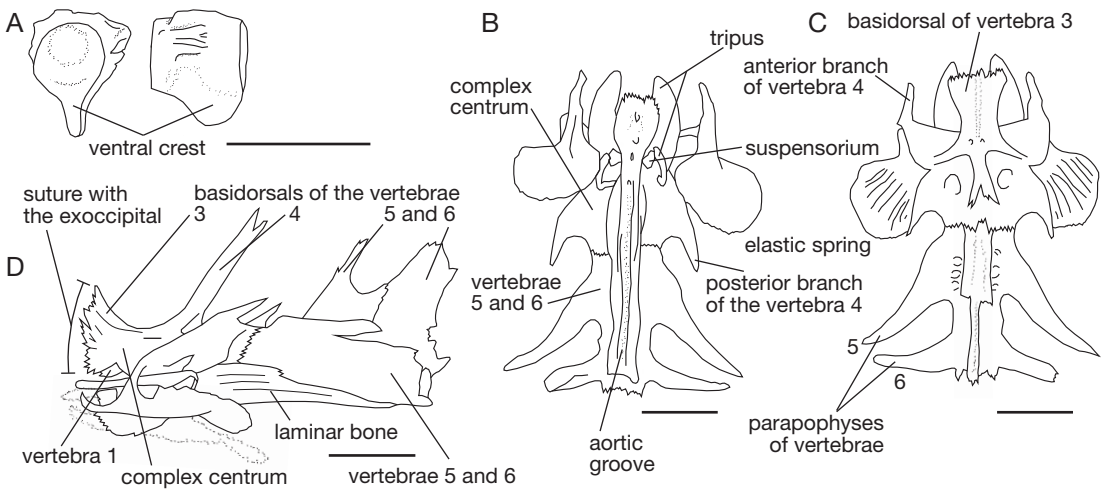

FIG. 37. — Main features of the complex vertebra of *Synodontis* Cuvier, 1816, exemplified in *S. schall* (Bloch & Schneider, 1801): **A**, first centrum in successively anterior and lateral views; **B**-**D**, Weberian apparatus; **B**, ventral view; **C**, dorsal view; **D**, lateral view. Scale bars: 5 mm.

The first centrum is slightly dorso-ventrally compressed and exhibits an axial ventral crest (Fig. 37A). It is attached to the posterior opening cone of the basioccipital and is completely included in the complex centrum. Both the basioccipital and complex centrum are strongly united with one another through interdigitated sutures. They insulate the first vertebra which supports the Weberian ossicles. According to Chardon *et al.* (2003) this provides an advantage by preserving the ossicles from mechanical perturbations and uninformative stimuli. The aortic groove opens ventrally from the basioccipital to the sixth vertebra (Fig. 37B). On each side, the complex centrum is flanked by superficial laminar ossifications which ventrally contribute to protect the aortic groove laterally, and extend posteriorly onto the fifth and sixth fused centra. Dorsally, the fused neural arches cover the pathway of the spinal cord (Fig. 37C). The basidorsals of the first and second vertebrae are lacking, whereas the basidorsals of the third through the sixth vertebrae are well developed (Fig. 37D). The third basidorsal projects dorsally, joining the supraoccipital and thus forming part of the posterior wall of the braincase (Fig. 37D). The following two basidorsals project postero-dorsally; the anterior one is a pillar that connects with the anterior nucal plate; the posterior one connects with the posterior nucal plate. The basidorsal of the sixth vertebra sutures with the first proximal radial dorsally and the neural spine of the seventh vertebra posteriorly. All along the complex vertebra axial laminar bone develops between the pillars, notably between the fifth and the sixth basidorsals (Fig. 37D).

On both sides of the complex vertebra, the parapophyses of the fourth to sixth vertebrae are well developed and extend laterally. The sixth vertebra bears the anteriormost pair of ribs. The parapophyses of the fifth vertebra are expanded in triangular horizontal laminae which are postero-laterally directed. Anteriorly, the parapophyses of the fourth vertebra are divided into a posterior branch and an anterior one which is called the Müllerian process and bears the elastic spring apparatus (Fig. 37C). The latter consists of a discoid spring that attaches to the swim bladder (Fig. 37B, C). The posterior branch of the parapophyses of the fourth vertebra is a triangular plate pointing backwards (Fig. 37B, C). Ventrally, beneath the anterior branch of the fourth vertebral parapophyses, the ossa suspensoria and the triangular tripus connect the complex vertebra (Fig. 37B). Posteriorly, the tripus has a

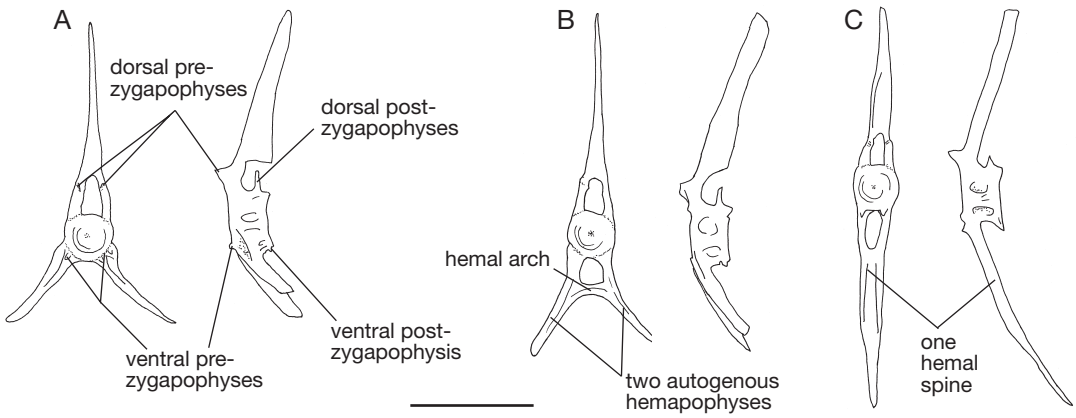

FIG. 38. — The three different types of free vertebrae observed along the vertebral column in *Synodontis* Cuvier, 1816, exemplified in *S. schall* (Bloch & Schneider, 1801), in anterior (left) and lateral (right) views: **A**, 3rd free vertebra; **B**, 14th free vertebra; **C**, 1st post-abdominal vertebra. Scale bar: 5 mm.

crescentic projection which lies on the superficial laminar ossifications and turns around the ossa suspensoria (Fig. 37B). The anterior tip of the tripus ends below the basioccipital and is medially linked to the reduced intercalarium, which is also connected to the rounded conchae scaphii of the scaphium. The claustrum has not been observed in any of the specimens.

VERTEBRAE (FIG. 38; TABLE 3)

The axial skeleton is made up of 36 to 41 vertebrae including the six anteriormost that participate in the Weberian apparatus, and 12 to 18 abdominal vertebrae. These counts vary depending on the species and also within a species (Table 3). For instance, *Synodontis violaceus* exhibits 40 to 41 vertebrae and *S. batensoda* exhibits 36 to 37 vertebrae. Taverne & Aloulou-Triki (1974) described several features of the vertebral skeleton of the genus *Synodontis*. Here, we clarify the range of inter- and intraspecific variation.

In the Chadian species, the morphology of the free vertebrae varies along the axial skeleton. Behind the Weberian apparatus, each of the 7th to 10/14th anteriormost free abdominal vertebrae displays a neural spine and stout autogenous parapophyses (Fig. 38A; Table 3). From front to back the parapophyses project more and more ventrally. The neural arches of the 7th and 8th vertebrae are robust, laterally flattened and antero-posteriorly enlarged (Fig. 38A). Only the 7th and sometimes the 8th neural spine articulate with the dorsal proximal radials. A hemal bridge is present on the 11/15th vertebra up to the 13/18th posteriormost abdominal vertebrae (Fig. 38B; Table 3). Each of the post-abdominal vertebrae, except the ural centrum, bears a hemal spine (Fig. 38C). The 1st hemal spine supports the first anal pterygiophore (Fig. 38C), and the anteriormost following ones only support further pterygiophores of the anal fin. Anterior and posterior to the neural and the hemal spines, the centra bear small zygapophyses (Fig. 38A). The ventral zygapophyses are increasingly more developed on posteriormost vertebrae whereas the dorsal zygapophyses are more reduced. Moreover, the post-zygapophyses fuse with their respective spine in the posteriormost vertebrae. Except for the variation observed in the vertebral formulae in our specimens and in the study by Taverne & Aloulou-Triki (1974), no remarkable features characterize the different species.

CAUDAL FIN SKELETON (FIG. 39; TABLE 4)

The caudal fin is supported by the fourth preural centrum and the following vertebrae. The third and fourth preural centra and their neural and hemal spines are autogenous and not modified. As previously described by Taverne & Aloulou-Triki

TABLE 3. — Vertebral formula of the studied specimens of *Synodontis* Cuvier, 1816: **A**, abdominal vertebrae with a neural spine; **B**, abdominal vertebrae with a hemal bridge; **C**, post-abdominal vertebrae; **D**, total number of vertebrae.

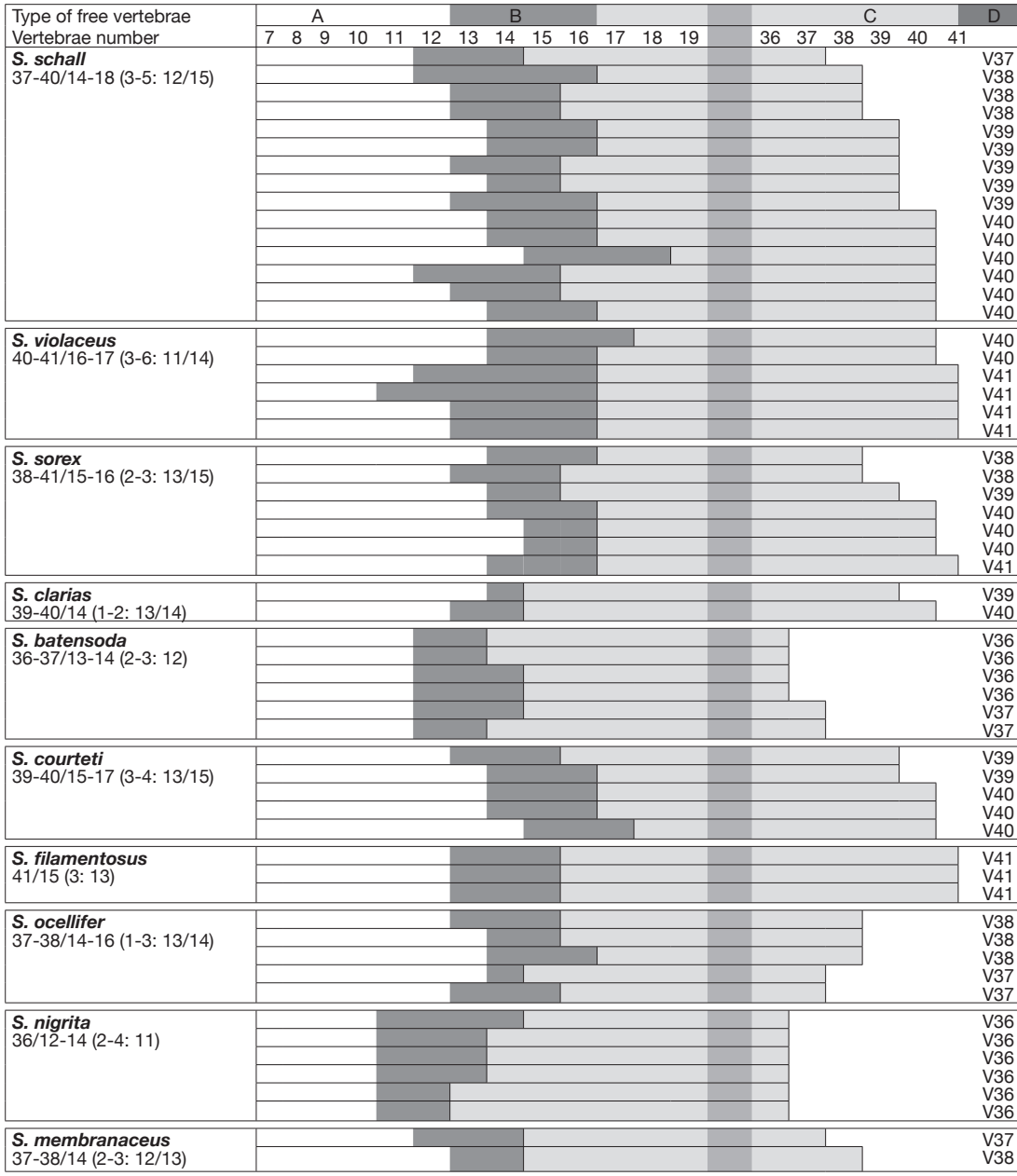

(1974), we observed two different types of caudal skeleton of *Synodontis* fishes, depending on the morphology of the second preural centrum which exhibits either a reduced neural spine (Fig. 39A, B) or a complete one (Fig. 39C). The two types may be observed in the same species (Table 4). Thirteen of

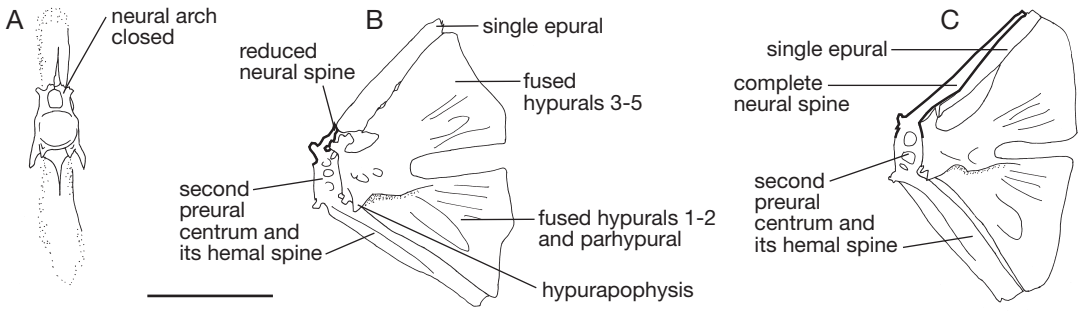

FIG. 39. — The two types of caudal skeleton observed in *Synodontis* Cuvier, 1816, exemplified in *S. schall* (Bloch & Schneider, 1801): **A**, **B**, first type; **A**, anterior view; **B**, lateral view; **C**, second type in lateral view. Scale bar: 5 mm.

the 15 specimens of *S. schall* and four of the seven specimens of *S. sorex* examined have a reduced neural spine (Table 4). When the neural spine is reduced, the single epural is enlarged. In anterior view, the neural arch of preural centrum 1 is closed (Fig. 39A). It does not bear any neural spine but is associated with a single epural (Fig. 39B, C). The first preural and first ural centra form the compound centrum which is fused ventrally with the parhypural and hypurals 1 and 2, and dorsally with the hypurals 3 to 5 (Fig. 39B, C). The so-constituted dorsal lobe is generally more developed than the ventral one. Also, on each side the compound centrum, ventrally there is a hypurapophysis with a foramen for the dorsal branch of the caudal artery at its base (Fig. 39B). The number of caudal fin rays varies from 15 to 18 dorsally and from 16 to 20 ventrally.

TABLE 4. — Distribution of the two types of the caudal skeleton of *Synodontis* Cuvier, 1816 shown in Figure 39 and described in the text.

Species (number of specimens)	second preural centrum with a reduced neural spine	second preural centrum with a complete neural spine
S. membranaceus (5)	5	0
S. sorex (7)	4	3
S. batensoda (6)	6	0
S. nigrita (7)	6	1
S. clarias (2)	2	0
S. schall (15)	13	2
S. filamentosus (6)	5	1
S. courteti (3)	2	1
S. violaceus (6)	6	0
S. ocellifer (5)	4	1
S. eupterus (1)	1	0

MAIN FEATURES OF THE DORSAL FIN SKELETON (FIGS 40; 41)

The dorsal fin skeleton of *Synodontis* fishes (Fig. 40) consists of two anterior rays modified into a spinelet and a spine followed by a variable number of bifurcated rays, from 6 to 8 (Poll 1971; Taverne & Aloulou-Triki 1974; Paugy & Roberts 1992). The anterior spinelet is small and smooth, whereas the dorsal spine is stout and often tuberculated at its anterior and posterior edge (Fig. 40). The three anteriormost pterygiophores are modified and are part of the nucal shield. The dorsal spinelet and the spine articulate with the second and third modified pterygiophores respectively, within the middle and posterior nucal plates (Fig. 40). The following pterygiophores are serially associated with unmodified rays (Fig. 40). The inner part of the pterygiophore is composed of a laminar process which connects with the preceding and following pterygiophores, and which is reinforced by a stout pad on its axis (Figs 40; 41).

The following pterygiophores consist of two autogenous elements, i.e. a large proximal radial and a small distal radial. The axis of the proximal radial is laminar and two lateral wings develop dorsally except on the last one (Fig. 41A). From front to back, the proximal radials and their wings are progressively more reduced in size, and the anterior

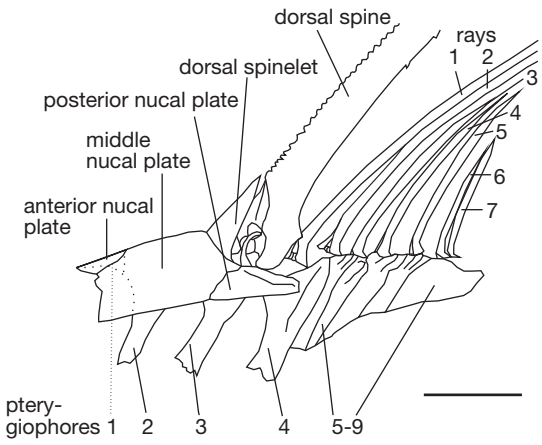

FIG. 40. — Main features of the dorsal fin skeleton of *Synodontis* Cuvier, 1816, exemplified in *S. schall* (Bloch & Schneider, 1801), in lateral view. Scale bar: 20 mm.

ones only articulate with the successive neural spines. The posteriormost proximal radial exhibits a peculiar ovoid outline in lateral view. Each distal radial corresponds with a pair of rounded elements that are synchondrally joined with each other. Each pair lies on a circular surface on the serially associated proximal radial, except the posteriormost one which supports two distal radials. The count of dorsal pterygiophores varies in relation to the count of fin rays.

The anal fin numbers 3 to 6 simple rays followed by 7 to 10 bifurcated rays supported by pterygiophores, depending on both the species and on the specimens (Poll 1971). The anal pterygiophores are composed of two autogenous radials, the proximal and the distal ones. They present the same morphology as the dorsal ones (Fig. 41), with drastic reduction in their dimension and characteristics toward the back of the fin. The first pterygiophore is stouter and articulates with the hemal spine of the first post-abdominal vertebra, the following ones do not contact the following spines. Except for the meristematic characters, the only median fin elements exhibiting characters that vary according to the species are the shape of the nucal shield plates and the dorsal spine morphology. We focus on these in the next two points.

THE NUCAL SHIELD (FIGS 40; 42-45; APPENDIX 8) From anterior to posterior, the *Synodontis* shield includes an anterior, a middle and a posterior nucal plates (Fig. 40). All three are supported by a median process projecting antero-ventrally which may correspond to the modification of the three anteriormost pterygiophores (Fig. 40). The anterior nucal plate inserts dorsally between the supraoccipital at the front and the middle nucal plate at the back (Fig. 40). Its outline varies from oval to circular. Its median process is reduced to a shallow lamina which lies along the front of the anterior edge of the following (second) pterygiophore (Fig. 40). In dorsal view, the middle nucal plate anteriorly connects with the anterior nucal plate medially and with the supraoccipital laterally, and it also sutures posteriorly with the posterior nucal plate on both sides of the dorsal spine (Fig. 42A, B). This gives the middle nucal plate a typical quadrangular shape with one anterior and one posterior notch in dorsal view (Fig. 42A). The middle nucal plate is folded medially (Fig. 42A). The antero-ventrally projecting median pterygiophore process of the middle nucal plate (Fig. 42) sutures with the process of the anterior nucal plate anteriorly, with the basidorsal of the fourth vertebra of the Weberian apparatus ventrally, and with the third pterygiophore posteriorly (Fig. 40). Dorsally, a projecting conical process supports the spinelet (Fig. 42). The posterior nucal plate is made up of the second laminar pterygiophore process and two lateral dermal plates that articulate anteriorly with the middle nucal plate. The pterygiophore process of the posterior nucal plate articulates with the second spine thanks to a median ring that passes through the dorsal spine foramen, and also via two surfaces that receive the lateral articular surfaces of the head of the spine. Moreover, it connects ventrally with the second pterygiophore at the front, with the basidorsal of the fifth vertebra, and with the following pterygiophore at the back (Fig. 40).

The axial fold of the nucal shield, which is more or less acute according to the species, is particularly marked on the middle nucal plate (Fig. 43A-C). For instance, it is deeper than wide in *Synodontis membranaceus* (Fig. 43A), whereas it is wider than deep in *S. courteti* (Fig. 43C), and roughly as deep as wide in *S. schall* (Fig. 43B). Moreover, the mid-

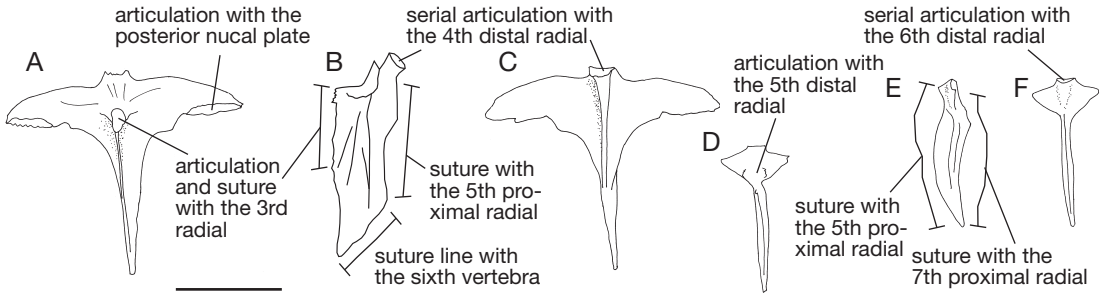

FIG. 41. — Main features of the fourth and fifth pterygiophores of *Synodontis* Cuvier, 1816, exemplified in *S. schall* (Bloch & Schneider, 1801): **A**-**C**, fourth pterygiophore; **A**, anterior view; **B**, lateral view; **C**, posterior view; **D**-**F**, fifth pterygiophore; **D**, anterior view; **E**, lateral view; **F**, posterior view. Scale bar: 5 mm.

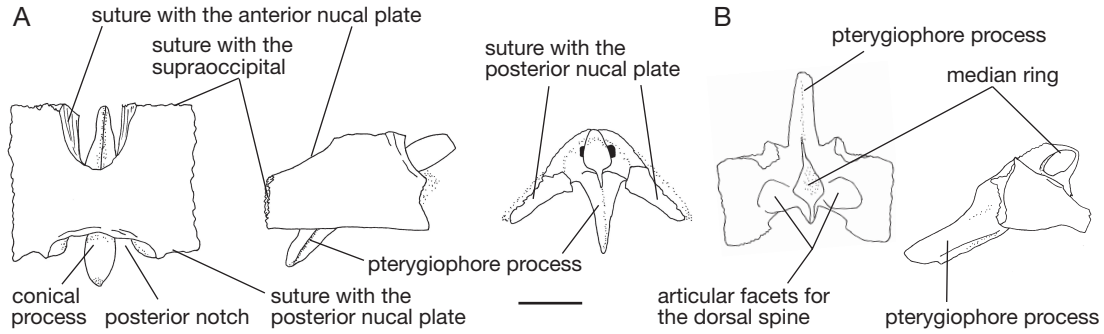

FIG. 42. — Main features of the middle and posterior plates of the nucal shield of *Synodontis* Cuvier, 1816, exemplified in *S. schall* (Bloch & Schneider, 1801): **A**, middle nucal plate in dorsal, lateral and posterior views; **B**, posterior nucal plate in dorsal view and lateral views. Scale bar: 5 mm.

dle nucal plate varies in its shape in dorsal view, partly because of the folding, but not only. Notably, the middle plate has a parallel lateral border or is enlarged posteriorly (trapezoidal versus rectangular shape), and the notch for the anterior nucal plate is more or less developed (Fig. 43D-I).

We used linear measurements (Fig. 44) transformed in six log-shape ratios and one ratio to recognize middle nucal plates of extant species or groups of species (Appendix 8). For instance, we can statistically differentiate species and groups of species on the following characters (Appendix 8).

Synodontis membranaceus differs from the other species for all of the log-shape ratios except those related to the length of the lateral edge (Appendix 8: variable 1) and with the anterior width of the bone (Appendix 8: 3). Its middle nucal plate is very high (Appendix 8: 6) with a long articular surface for the posterior nucal plate (Appendix 8: 2) and a narrow posterior notch (Appendix 8: 5; Fig. 43A, D). *Synodontis batensoda* resembles *S. membranaceus*, by similar morphological trends, but the features are less pronounced, notably the posterior notch (Appendix 8: 5) which is larger than in *S. membranaceus*, but still narrower than in all of the other Chadian species.

Synodontis courteti and *S. violaceus* exhibit a markedly shallow middle nucal plate (Appendix 8: 6; Fig. 43C). Moreover, the plate is anteriorly and posteriorly wide with a large posterior notch and a small articular surface for the posterior nucal plate (Appendix 8: 2-5; Fig. 43C, I). They differ from each other by the outline of the plate in dorsal view being trapezoidal in *S. violaceus* and rectangular in *S. courteti* (Appendix 8: 7). As observed in *S. courteti* and *S. violaceus*, the anterior nucal plate of *S. nigrita*

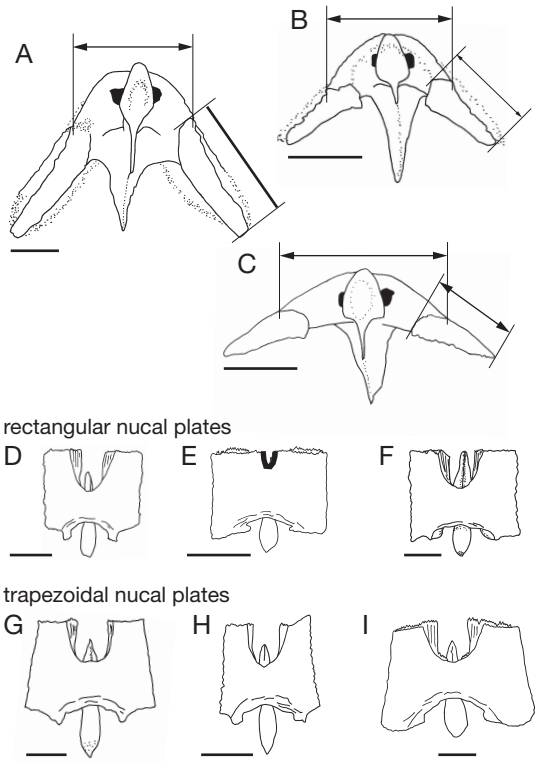

FIG. 43. — The middle nucal plate of several *Synodontis* Cuvier, 1816 species: **A**-**C**, posterior views; **A**, *S. membranaceus* (Geoffroy Saint-Hilaire, 1809); **B**, *S. schall* (Bloch & Schneider, 1801); **C**, *S. courteti* Pellegrin, 1906; **D**-**I**, dorsal views; **D**, *S. membranaceus*; **E**, *S. nigrita* Valenciennes, 1840; **F**, *S. schall*; **G**, *S. sorex* Günther, 1864; **H**, *S. clarias* (Linnaeus, 1758); **I**, *S. violaceus* Pellegrin, 1919. Scale bars: 5 mm.

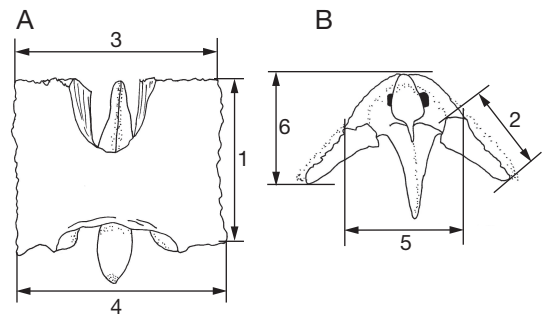

FIG. 44. — Linear measurements taken on the middle nucal plate, shown in *S. schall* (Bloch & Schneider, 1801): **A**, dorsal view; **B**, posterior view. Measurements: **1**, length of the lateral edge; **2**, length of the suture with the posterior nucal plate; **3**, anterior width of the nucal complex; **4**, posterior width of the nucal complex; **5**, maximum width of the posterior notch; **6**, maximum depth of the plate.

and *S. filamentosus* presents a large posterior notch (Appendix 8: 5), but they differ from the former species notably by a deeper middle plate (Appendix 8: 6). Finally, the two species are distinguished from one another by the outline of the middle plate in dorsal view (Appendix 8: 7): it is rectangular with a small anterior notch in *S. nigrita* (Fig. 43E) and posteriorly enlarged in *S. filamentosus*.

In *Synodontis sorex* and *S. clarias*, the middle nucal plate is trapezoidal in dorsal view, with an anterior border much narrower than in any other *Synodontis* exhibiting this shape (Appendix 8: 7; Fig. 43G, H). *Synodontis sorex* differs by the length of the suture with the posterior nucal plate which is larger than in *S. clarias* (Appendix 8: 2).

The two specimens of *Synodontis eupterus* present values in the same range of variation as *S. batensoda* for the maximum height of the bone (Appendix 8: 6) and the length of the suture with the posterior nucal plate (Appendix 8: 2). They exhibit a trapezoidal anterior plate as in *S. sorex* and *S. clarias*.

Finally, *Synodontis schall* and *S. ocellifer* present intermediate values for all of the log-shape ratios, which correlates with a "mean-shape" of the bone when compared with the other Chadian species (Fig. 43B, F).

Four types of posterior nucal plates are recognized. In *Synodontis membranaceus* and *S. batensoda* only the posterior nucal plate is deep with a convex free edge (Fig. 45A). In *S. nigrita*, the posterior nucal plate is always shallow with a pointed posterior free corner and a free edge longer than the suture with the middle plate (Fig. 45B).

In *Synodontis sorex*, the posterior nucal plate is deep, with a pointed posterior free corner, and a free edge as long as the suture with the anterior plate (Fig. 45C). In *S. courteti* and *S. violaceus*, the posterior nucal plate is rectangular in lateral view (Fig. 45D). The intraspecific variation of the shape of the plate depends on the species, with a minimum range observed in *S. membranaceus* and a maximum one in *S. schall*. In the latter species several types (the three last ones) are observed.

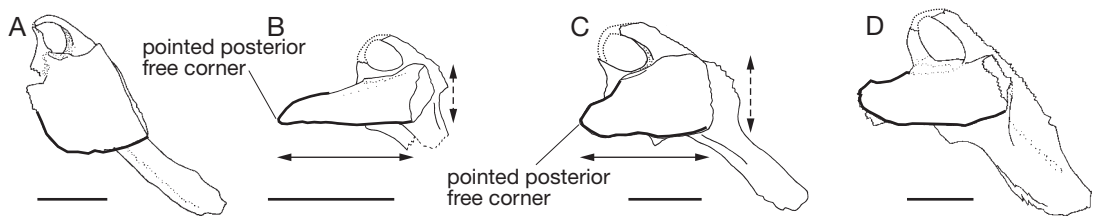

FIG. 45. — The posterior nucal plate of *Synodontis* Cuvier, 1816 species in lateral views: **A**, *S. membranaceus* (Geoffroy Saint-Hilaire, 1809); **B**, *S. nigrita* Valenciennes, 1840; **C**, *S. sorex* Günther, 1864; **D**, *S. violaceus* Pellegrin, 1919. The plain line arrows are for the free edge length, whereas the dotted line arrows are for the suture with the middle plate length. Scale bars: 5 mm.

THE DORSAL SPINE (FIGS 46-48; APPENDIX 9)

The dorsal spine is positioned behind the spinelet and articulates ventrally with the posterior nucal plate (including the modified pterygiophore). It presents a symmetric morphology and has several characters of the articular head and along its body (Fig. 46).

Depending on the species, the dorsal spine varies in shape and ornamentation. A preliminary study, using ratios of four linear and angular measurements and two discrete characters, allowed us to distinguish the dorsal spines of four modern Chadian species (Pinton *et al*. 2006). The three linear measurements are employed here again together with complementary ones. Here, we did not use the angular measurement, because it is redundant with the other data. The two discrete characters (ornamentation of the crest along the anterior edge; curvature of the body of the spine) are included. So, to describe the dorsal spines of the different Chadian species we use both qualitative characters and log transformed variables based on linear measurements (Fig. 47, Appendix 9). The species can be differentiated as follows.

Synodontis membranaceus and *S. batensoda* dorsal spines have a straight body with a well developed smooth anterior median crest and poorly marked tubercles at the posterior edge (Fig. 48A, B). The head of the spine is notably narrow in the two species (Appendix 9: variable 1; Fig. 48A, B) and *S. membranaceus* is distinguished by the articular foramen which is the narrowest observed, even more so than in *S. sorex* (Appendix 9: 6).

In *Synodontis courteti*, *S. filamentosus*, *S. nigrita* and *S. violaceus*, the head of the spine is large (Appendix 9: 1; Fig. 48C-E). *Synodontis courteti* and *S. violaceus* are recognized by their low articular process (Appendix 9: 5), and *S. nigrita* by the smooth and weakly developed anterior crest which is tuberculated in the three other species (Fig. 48C-E).

Finally, the remaining species can be easily recognized. *Synodontis sorex* has a distinctly bent dorsal spine with a narrow base of the head (Appendix 9: 2; Fig. 48F). *Synodontis clarias* presents a unique feature among the Chadian species with the anterior edge of the spine very strongly tuberculated (Fig. 48G). We have not observed this character in any *Synodontis* species outside Chad, and Paugy & Roberts (1992) used it to identify *S. clarias* in their identification key of the Western African species. *Synodontis ocellifer* exhibits a dorsal spine with a large base of the head and with tubercles on the anterior edge feebly developed (Appendix 9: 2; Fig. 48H).

RESULTS

Through the study of the comparative anatomy of Chadian *Synodontis* skeletons, qualitative characters have been established for most of the bones when any difference between the species was observed. When pertinent, we also established quantitative characters based on shape that complements the qualitative observations and provides accurate systematic information particularly for the bones that preserve well in fossils.

As a first result, the Chadian *Synodontis* species can be recognized on the basis of bony characters. As a second result, we are also able to

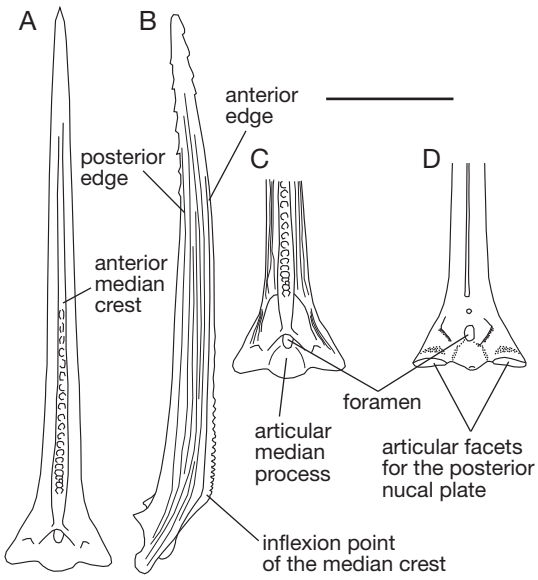

FIG. 46. — Main features of the dorsal spines of *Synodontis* Cuvier, 1816, exemplified in *S. schall* (Bloch & Schneider, 1801): **A**, anterior view of the spine; **B**, lateral view of the spine; **C**, posterior view of the head of the spine; **D**, anterior view of the head of the spine. Scale bar: 5 mm.

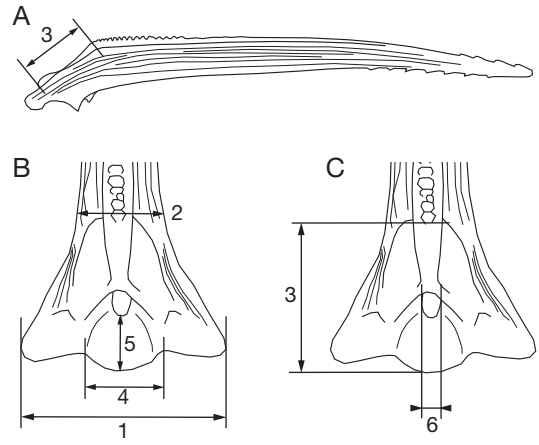

FIG. 47. — Linear measurements taken on the dorsal spines, shown in *S. schall* (Bloch & Schneider, 1801): **A**, lateral view of the whole spine; **B**, anterior view of the head of the spine. Measurements: **1**, width of the head of the spine; **2**, width at the base of the body of the spine (i.e. at the point of inflexion of the anterior median crest); **3**, distance between the inflexion point of the anterior median crest and the most ventral point of articular median process; **4**, width of the articular median process; **5**, depth of the articular median process; **6**, width of the foramen. The measurements are taken with a digital calliper (1-4) or on stereomicroscope photographs (5-6).

TABLE 5. — Contribution of each bone on the three axis of principal component analysis (Fig. 49).

	Axis 1 (%)	Axis 2 (%)	Axis 3 (%)
Nucal plate	34.9	10.6	2.7
Mesethmoid	6.0	36.2	21.8
Frontal	6.5	20.9	14.7
Parieto-supraoccipital	16.7	15.4	3.3
Cleithrum	28.4	15.9	13.5
Lateral ethmoid	7.5	1.1	44.0

assign isolated bones to nominative species or to a group of species, which was the main aim of the study.

To complete the bone by bone quantitative analysis we explored the relative weight of each bone in the variation of shape among the *Synodontis* Chadian species. We thus completed a principal component analysis on the 46 log-shape ratios established on the following bones: mesethmoid, frontals, middle nucal plate, lateral ethmoids, supraoccipital and cleithra. This analysis is based on a correlation matrix. The first and the second axes consist respectively of 27.71% and 20.54% of the total variability whereas the third axis represents 15.21% of the variability (Fig. 49).

Synodontis membranaceus and *S. batensoda* are distinguished from *S. nigrita*, *S. courteti*, *S. schall*, *S. filamentosus*, *S.ocellifer* and *S. violaceus* based on the first axis (Fig. 49). On this axis, the contribution of the variables dealing with the anterior nucal plate and the cleithrum is the most important (Table 5). More particularly, the great height of the anterior nucal plate and the highly developed suture with the posterior nucal plate are two of the striking morphological features present in *S. membranaceus* and *S. batensoda*. With the latter two characters, *S. membranaceus* and *S. batensoda* are easily recognized by their deep cleithra which exhibit a long antero-ventral edge with respect to the postero-ventral one.

Synodontis sorex and *S. clarias* are easily distinguished from all of the other *Synodontis* species based on the second axis (Fig. 49). Log-shape ratios established on the mesethmoid and on the

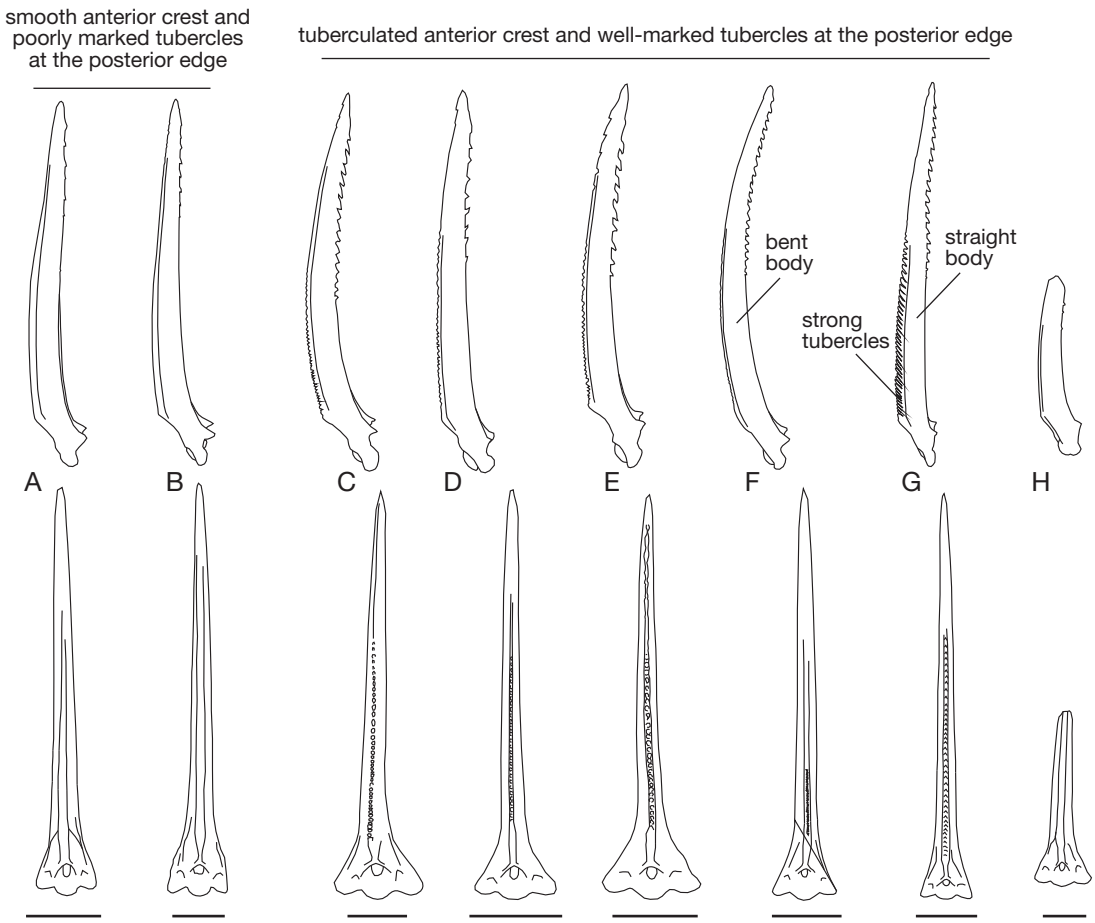

FIG. 48. — The dorsal spine of several *Synodontis* Cuvier, 1816 species in left lateral views (top) and anterior views (bottom): **A**, *S. batensoda* Rüppell, 1832; **B**, *S. membranaceus* (Geoffroy Saint-Hilaire, 1809); **C**, *S. courteti* Pellegrin, 1906; **D**, *S. filamentosus* Boulenger, 1901; **E**, *S. violaceus* Pellegrin, 1919; **F**, *S. sorex* Günther, 1864; **G**, *S. clarias* (Linnaeus, 1758); **H**, *S. ocellifer* Boulenger, 1900. Scale bars: 5 mm.

frontal contribute half of the variability observed on this axis (Table 5). Notably, a large mesethmoid exhibiting a trapezoidal shape with a reduced anterior edge and an important suture with the frontal bones are notable characters observed in *S. sorex* and *S. clarias*. The large inter-orbital width and the large preorbital width of the frontal, as well as the angle formed between the sutures of the frontal/supraoccipital on one hand and frontal/sphenotic on the other hand are the three characters which contribute largely to the weight of the frontal bone on axis 2 (Table 5).

The third axis allows us to distinguish *Synodontis courteti*, *S. violaceus*, *S. filamentous*, *S. nigrita*, *S. ocellifer* and *S. schall* (Fig. 49). The lateral ethmoids contribute nearly half of the variability of the third axis and the mesethmoid to about a fifth (Table 5). Indeed, in *S. courteti* and *S. violaceus*, the lateral ethmoid is noticeably extended antero-posteriorly, whereas it is fairly large in the other species. Their mesethmoid is strikingly long and narrow with a posterior position of the insertion of the lateral wings contrasting with that of *S. nigrita*, *S. schall*, *S. ocellifer* and *S. filamentosus* which is short and large.

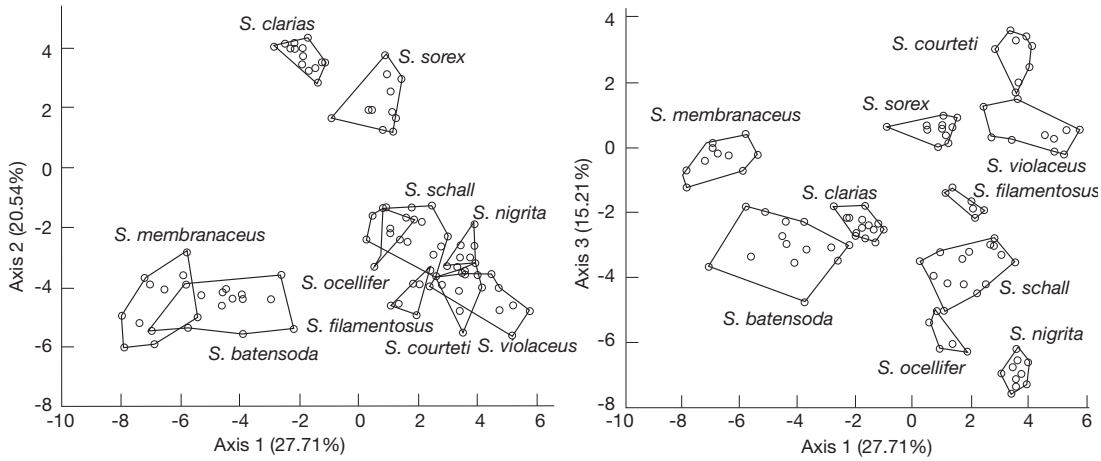

FIG. 49. — Distribution of the Chadian *Synodontis* Cuvier, 1816 specimens on the first three factorial axis of a principal component analysis obtained from the correlation matrix of 46 log-shape ratios calculated on the following bones: mesethmoid, lateral ethmoid, frontals, supraoccipital and middle nucal plate

DISCUSSION

A recent osteological study demonstrated the monophyly of the family Mochokidae and of the genus *Synodontis* (Vigliotta 2008). Whenever generic and familiar osteological differences are sometimes studied, the osteological variability among catfishes remains unexplored, at inter-specific and intra-specific levels. Our extensive osteological study of the Chadian *Synodontis* species reveals important osteological variation as well qualitatively as quantitatively and we demonstrate that osteological characters are sufficient to define and recognize species, which is essential for further paleontogical studies of mochokids.

The study presented here accurately explored the inter-specific morphological variation among about 10% of the genus by considering only certain Nilo-Sudanese species. Besides the definition of qualitative characters, our study notably permits us to quantify the global morphological distance between species of *Synodontis*, by using the squared Euclidean distance based on the 46 metric characters. The largest distance observed among all of the Chadian *Synodontis* species is between *S. courteti* and *S. membranaceus* (Table 6). The morphotypes they represent (*S. membranaceus* "narrow skull" and *S. courteti* "flat skull") are the poles of a continuous variation between the species. The smallest average distance calculated is the one between *S. schall* and the other *Synodontis* species, which reflects its median morphological features as noted previously. The continuous pattern of the variation in the morphology of the species between two poles provides new original information on the genus diversity that might be explored further. We have to confirm this pattern more widely in the genus and over all we have to explore the morphological diversity pattern among catfish. The interest of such quantification of the morphological variation between species is evident notably when considering the systematic. As a case study, our results provide new elements for the debate on the attribution of *S. membranaceus* and *S. batensoda* to the genus *Synodontis* together with the review of the qualitative morphological characters used.

Some authors consider that these two species should be attributed to two different genera, as *Hemisynodontis membranaceus* and *Brachysynodontis batensoda* (Geoffroy Saint-Hilaire 1809; Poll 1971; Taverne & Aloulou-Triki 1974; Gosse 1986; Burgess 1989; Paugy & Roberts 1992). They have been differentiated from *Synodontis* on both soft (Poll 1971) and osteological characters (Taverne &

TABLE 6. — Squared Euclidean distance values calculated on the 46 log-shape ratios established on the five following bones: mesethmoid, lateral ethmoid, frontal, supraoccipital and middle nucal plate.

	S. sorex	*S. nigrita*	*S. clarias*	*S. schall*	*S. filamentosus*	*S. courteti*	*S. violaceus*	*S. ocellifer*	*S. membranaceus*	*S. batensoda*
S. membranaceus	7.4	11.3	7.0	8.7	9.1	15.7	8.5	10.4	1.1	3.4
S. batensoda	7.5	6.6	5.1	5.6	5.7	15.1	6.7	6.1	3.4	1.2
S. sorex	0.6	7.4	2.7	3.7	4.5	7.3	3.6	6.8		
S. nigrita	7.4	0.9	6.5	2.4	4.9	11.6	4.5	1.8		
S. clarias	2.7	6.5	0.6	3.5	4.1	12.9	5.8	5.4		
S. schall	3.7	2.4	3.5	0.9	2.1	9.3	2.5	2.1		
S. filamentosus	4.5	4.9	4.1	2.1	0.5	12.4	3.3	3.9		
S. courteti	7.3	11.6	12.9	9.3	12.4	1.0	5.8	13.8		
S. violaceus	3.6	4.5	5.8	2.5	3.3	5.8	1.2	4.9		
S. ocellifer	6.8	1.8	5.4	2.1	3.9	13.8	4.9	1.0		
Mean	5.1	5.6	5.9	3.6	5.0	10.4	4.3	5.5		

Aloulou-Triki 1974) most of them being located in the opercular region and the gill basket. We find it interesting to discuss the osteological characters that have been used to justify the genera and the morphological distance of the species *S. membranaceus* and *S. batensoda* with each other and with the other *Synodontis* species. According to Taverne & Aloulou-Triki (1974), *Hemisynodontis* differs from the *Synodontis sensu stricto* by 1) the strong development of the humeral plate, 2) a denticulate opercular, 3) a long and narrow dentary, 4) a hyomandibula without anteriorly directed expansion, 5) a strong development of the conical process of the middle nucal plate, and finally 6) a median ring of the posterior nucal plate particularly developed. The same authors recognize *Brachysynodontis* by the presence of the characters 1-4 but in a less pronounced state. Regarding the humeral plate (1), we observe that it is always well developed and varies in shape (deep or elongated) rather than in "strength". The denticulation at the opercular posterior corner (2) exists in some specimens of *Synodontis membranaceus* and of *S. batensoda*, but always much less pronounced than figured by Taverne & Aloulou-Triki (1974), and it is absent in smaller specimens. We agree that the dentary (3) of *S. membranaceus* clearly differs because of the poorly delineated anterior cavity (Fig. 23I), but disagree concerning the dentary of *S. batensoda* (Fig. 23F) which does not differ significantly from that observed in other *Synodontis*, notably *S. ocellifer* (Fig. 23E). Therefore, *S. membranaceus* only appears to be an extreme case of reduction of the cavity, which is observed in diverse stages within the genus depending on the species. We disagree with character 4 because we observe an anteriorly directed expansion on the hyomandibula although it is extremely reduced (Fig. 26F, G). Finally, from our observations, a strong development of the conical process of the middle nucal plate (5), and the presence of a median ring of the posterior nucal plate particularly developed (6) do not exist in different states between *S. membranaceus* on one hand (Figs 43D; 45A) and other *Synodontis* species on the other hand. Together with the discussion on the diagnostic characters used to erect the two genera, we also consider the global morphological distance between the species, by using the squared Euclidean distance based on the 46 metric characters. The distance of *S. membranaceus* and *S. batensoda* from the other *Synodontis* species except *S. courteti* (Table 6: 5.7 to 11.3) does not exceed the maximum values observed between the other couples of *Synodontis* species (Table 6: 13.8 between *S. courteti* and *S. ocellifer*). This supports the hypothesis that

S. membranaceus and *S. batensoda* belong to the genus *Synodontis*. To conclude on this point, neither the characters established here to identify the species, nor the morphological distances support a separate generic designation. Complementary phylogenetic information is compulsory to further discuss the systematic status. Finally, one notes marked characters on some morphological trends (narrow and deep body). *Synodontis membranaceus* and *S. batensoda* also have modifications of their branchial apparatus (elongated branchiospines) which are directly correlated to their ecology, as they are both filter zoo-planctonophagous which is unique in the genus (Lauzanne 1988). Indeed, we may also assign their body shape to their ecological preferences. Their high and laterally compressed bodies (see nucal plates and cleithrum) clearly represent unique features among the *Synodontis* species in Chad and also in Africa (AP, pers. obs.). We can reasonably hypothesize that the depth and shortness of the cleithrum and the opercular, and the laterally compressed nucal shield are linked to an adaptation to their feeding mode by contributing to an important flux of water.

Finally, another point that rises in our morphometrical study is that the intra-specific variation does not show any significant differences between the species of *Synodontis* . This provides important information to delimitate characters in the fossil. However, this point should be explored further, by including several populations of geographically spread species, and through the study of other *Synodontis* species including those that inhabit restricted area in relation with peculiar ecological habits.

CONCLUSION

The bony anatomy of *Synodontis* species that inhabit Chad today has been accurately described and illustrated. Moreover, this study has revealed new osteological characters as far today unused in Siluriformes phylogeny. Except for the basicranium, isolated neurocranial bones carry accurate diagnostic information, together with the jaw bones, the cleithra, the nucal shield and the pectoral and dorsal fin spines. The osteological variability of the genus, within and among species, has been quantified for the most diagnostic bones. We are confident that this type of laborious anatomical study opens interesting perspectives. As a first step, this will allow the identification of the numerous *Synodontis* fossils collected in Chad. The identification of fossil fish from other Nilo-Sudanese sub-basins will only require completing the study with a few additional taxa. For instance, further descriptions of four complementary species (*S. frontosus* Vaillant, 1895, *S. serratus* Rüppell, 1829, *S. khartoumensis* Gideiri, 1967 and *S. caudovittatus* Boulenger, 1901) will allow us to study the Nile River drainage past diversity.

The emergence of the genus *Synodontis* is at least 18 Myr based on its first occurrence in the fossil record of Chalouf, Egypt (Priem 1920) and aged at about 35 Myr (23-40 Myr) based on a previous molecular study (Koblmüller *et al*. 2006). It thus mainly diversified in the Neogene of Africa (23-2.5 Myr), a period of climate change and drastic modification of the African geology that are both thought to have strongly influenced faunal distribution and evolution by reshuffling ecological barriers. Thus, reconstructing the history of *Synodontis* may provide a first order frame within which the evolution of past biodiversity could be drawn. This study will constitute, without doubt, an important cornerstone for resolving the evolution of the genus both by a taxonomic and a phylogenetic point of view.

Acknowledgements
We thank Didier Paugy (Institut de Recherche pour le Développement – IRD, Muséum national d'Histoire naturelle, Paris – MNHN) for discussions; the IRD Bamako, notably Gilles Fédière, Bruno Sicard and Yacouba Traore for hosting and assistance in Mali; Fabrice Lihoreau, Andossa Likius and Mahamat Adoum for hosting and assistance in Chad (Ministère des Affaires étrangères, France; Université de N'Djaména and Centre national d'Appui à la Recherche, Chad); Patrick Campbell and Oliver Crimmen for access to the ichthyological collections at the Natural History Museum (London); Jos Snoecks and Emmanuel Vreven for access to

the ichthyological collection of the Musée royal de l'Afrique Centrale (Tervuren); Wim Van Neer for access to his collection of dry skeletons (Institut royal des Sciences naturelles, Brussels); to Patrice Pruvost and Zora Gabsi for access to the ichthyological collections and X-ray facilities at the MNHN. We extend gratitude to the Centre de Valorisation des Collections de l'Université de Poitiers that hosts the material collection. The research was supported by Agence nationale de la Recherche (Projet ANR 05-BLAN-0235) and National Science Foundation (Revealing Hominid Origins Initiative). Finally, we greatly thank Alison Murray for all her comments and the two reviewers, Louis Taverne and François Meunier, for their helpful advises. The English was extensively reviewed by L. Foley-Ducrocq. Drawings by A. Pinton.

REFERENCES

BLACHE J. 1964. — *Les poissons du bassin du Tchad et du bassin adjacent du Mayo Kébi. Étude systématique et biologique.* Mémoires Orstom 4, 483 p.

BRUNET M., BEAUVILAIN A., BILLIOU D., BOCHERENS H., BOISSERIE J.-R., DE BONIS L., BRANGER P., BRUNET A., COPPENS Y., DAAMS R., DEJAX J., DENYS C., DURINGER P., EISENMANN V., FANONÉ F., FRONTY P., GAYET M., GERAADS D., GUY F., KASSER M., KOUFOS G., LIKIUS A., LOPEZ-MARTINEZ N., LOUCHART A., MACLATCHY L., MACKAYE H. T., MARANDAT B., MOUCHELIN G., MOURER-CHAUVIRÉ C., OTERO O., PEIGNÉ S., PELAEZ CAMPOMANES P., PILBEAM D., RAGE J.-C., DE RUITTER D., SCHUSTER M., SUDRE J., TASSY P., VIGNAUD P., VIRIOT L. & ZAZZO A. 2000. — Chad: discovery of a vertebrate fauna close to the Mio-Pliocene boundary. *Journal of Vertebrate Paleontology* 1: 205-209.

BURGESS W. E. 1989. — *An Atlas of Freshwater and Marine Catfishes: a Preliminary Study of the Siluriforms*. TFH publications, Neptun City, New Jersey, 784 p.

CHARDON M., PARMENTIER E. & VANDEWALLE P. 2003. — Morphology, development and evolution of the weberian apparatus in catfish, *in* ARRATIA G., KAPOOR B. G., CHARDON M. & DIOGO R. (eds), *Catfishes*. Science Publishers, Enfield, NH: 71-120.

DE PINNA M. C. C. 1993. — *Higher-Level Phylogeny of Siluriformes, with a New Classification of the Order (Teleostei, Ostariophysi)*. Thesis, University of New York, USA, 482 p.

GAUDANT J. 1987. — A preliminary report on the osteichthyan fish-fauna from the Upper Neogene of Sahabi, Libya, *in* BOAZ N. T., EL-ARNAUTI A., GAZIRY A. W., HEINZELIN J. DE & BOAZ D. D. (eds), *Neogene Paleontology and Geology of Sahabi*. Alan Liss, New York: 91-100.

GEOFFROY SAINT-HILAIRE É. 1809. — Poissons du Nil, de la mer Rouge et de la Méditerranée, *in Description de l'Égypte, histoire naturelle*. Paris: 1-52.

GOSSE J. P. 1986. — Mochokidae, *in* DAGET J., GOSSE J. P. & THYS VAN DEN AUDENAERDE D. F. E. (eds), *Check-List of the Freshwater Fish of Africa.* Volume 2. Musée royal de l'Afrique Centrale, Tervuren: 105-152.

GREENWOOD P. H. 1951. — Fish remains from Miocene deposits of Rusinga Island and Kavirondo Province, Kenya. *Annals and Magazine of Natural History* 12 (4): 1192-1201.

GREENWOOD P. H. 1972. — New fish fossils from the Pliocene of Wadi Natrum, Egypt. *Journal of Zoology* 168: 503-519.

GREENWOOD P. H. 1973. — Fish fossils from the Late Miocene of Tunisia. *Notes du Service géologique de Tunisie* 37: 41-72.

GREENWOOD P. H. & HOWES G. J. 1975. — Neogene fossil fishes from the Lake Albert-Lake Edward rift (Zaire). *Bulletin of the Bristish Museum of Natural History*, Geology, 26 (3): 69-126.

KOBLMÜLLER S., STRURMBAUER C., VERHEYEN E., MEYER A. & SALZBURGER A. 2006. — Mitochondrial phylogeny and phylogeography of East African squeaker catfishes (Siluriformes: *Synodontis*). *BMC Evolutionary Biology* 6: 49.

LAUZANNE L. 1988. — Biologie et écologie des poissons d'eau douce africains, *in* LÉVÊQUE C., BRUTON M. N. & SSENTONGO G. W. (eds), *Les habitudes alimentaires des poissons d'eau douce africains.* Orstom, Bondy: 221-242.

MO T. 1991. — *Anatomy, Relationships and Systematics of the Bagridae (Teleostei, Siluroidei), with a Hypothesis of Siluroid Phylogeny*. Koeltz Scientific Books, Koenigstein, 216 p.

MOSIMANN J. E. 1970. — Size allometry: size and shape variables with characterizations of the lognormal and generalized gamma distributions. *Journal of American Statistician Association* 65: 930-945.

OTERO O., PINTON A., MACKAYE H. T., LIKIUS A., VIGNAUD P. & BRUNET M. 2009. — First description of a Pliocene ichthyofauna from Central Africa (site KL2, Kolle area, Eastern Djurab, Chad): what do we learn? *African Journal of Earth Science* 54: 62-74.

OTERO O., PINTON A., MACKAYE H. T., LIKIUS A., VIGNAUD P. & BRUNET M. in press. — The fish assemblage associated with the Late Miocene Chadian hominid (site TM266, Toros-Menalla, Western Djurab), and its palaeoenvironmental signification. *Paleontographica Acta*.

PAUGY D. & ROBERTS T. 1992. — Mochokidae, *in* LÉVÊQUE C., PAUGY D. & TEUGELS G. G. (eds),

Faune des poissons d'eaux douces et saumâtres d'Afrique de l'Ouest. Volume 2. MRAC, Tervuren; Orstom, Paris, collection faune tropicale: 500-563.

PINTON A., FARA E. & OTERO O. 2006. — Spine anatomy reveals the diversity of catfish through time: a case study of the genus *Synodontis* (Ostariophysi, Siluriformes). *Naturwissenschaften* 93 (1): 22-26.

POLL M. 1971. — Révision des *Synodontis* africains (famille Mochokidae). *Annales du Musée royal d'Afrique Centrale (Zoologie)*, Tervuren, 497 p.

PRIEM R. 1920. — Poissons fossiles du Miocène d'Égypte (Burdigalien de Moghara, « Désert lybique »), *in* FOURTAU R. (ed.), *Contribution à l'étude des Vertébrés miocènes de l'Égypte*. Government Press, Cairo: 8-15.

SCHWARTZ H. L. 1983. — *Paleoecology of Late Cenozoic Fish from the Turkana Basin, Northern Kenya*. Thesis, University of California, Santa Cruz, USA, 291 p.

STEWART K. M. 1990. — Fossil fish remains from the Lusso Formation, *in* BOAZ N.T. (ed.), Evolution of Environments and Hominidae in the African Western Rift Valley. *Virginia Museum of Natural History Memoirs* 1: 141-163.

STEWART K. M. 2003a. — Fossils fish remains from Mio-Pliocene deposits at Lothagam, Kenya, *in* LEAKEY M. G. & HARRIS J. H. (eds), *Lothagam, the Dawn of Humanity in Eastern Africa*. Columbia University Press, New York: 79-111.

STEWART K. M. 2003b. — Fossils fish remains from the Pliocene Kanapoi site, Kenya, *in* HARRIS J. H. & LEAKEY M. G. (eds), Geology and vertebrate paleontology of the Early Pliocene site of Kanapoi, Northern Kenya. *Contributions in Science, Natural History Museum of Los Angeles County* 498: 21-38.

TAVERNE L. & ALOULOU-TRIKI A. 1974. — Étude anatomique, myologique et ostéologique du genre *Synodontis* Cuvier (Pisces: Siluriformes, Mochocidae). *Annales du Musée royal d'Afrique Centrale (Zoologie)*, Tervuren, 69 p.

VAN COUVERING J. A. H. 1977. — Early record of freshwater fishes in Africa. *Copeia* 1: 163-166.

VAN NEER W. 1992. — New Late Tertiary fish fossils from the Sinda Region, eastern Zaire. *African Study Monographs*, *supplementary issue* 17: 27-47.

VAN NEER W. 1994. — Cenozoic fish fossil from the Albertine Rift Valley in Uganda, *in* SENUT B. & PICKFORD M. (eds), *Geology and Palaeobiology of the Albertine Rift Valley, Uganda-Zaire*, II: *Palaeobiology*. CIFEG occasional publications, Orléans: 89-127.

VIGLIOTTA T. 2008. — A phylogenetic study of the African catfish family Mochokidae (Osteichthyes, Ostariophysi, Siluriformes), with a key to genera. *Proceedings of the Academy of Natural Sciences, Philadelphia* 157: 73-136.

VIGNAUD P., DURINGER P., MACKAYE H.T., LIKIUS A., BLONDEL C., BOISSERIE J.-R., DE BONIS L., EISENMANN V., GERAADS D., GUY F., LEHMANN T., LIHOREAU F., LOPEZ-MARTINEZ N., MOURER-CHAUVIRÉ C., OTERO O., RAGE J.-C., SCHUSTER M., VIRIOT L., ZAZZO A. & BRUNET M. 2002. — Geology and palaeontology of the Upper Miocene Toros-Menalla fossiliferous area, Djurab Desert, Northern Chad. *Nature* 418 (6894): 152-155.

Submitted on 22 December 2008;
accepted on 1st October 2009.

APPENDIX 1

Values of variables that allow distinguishing the mesethmoids of *Synodontis* Cuvier, 1816 species: **1**-**6**, log-shape ratios obtained from linear dimensions on the mesethmoid; **7**, log transformed variable. The measurements taken to calculate the variables are shown in Figure 3 and described in the figure caption. Abbreviation: **sd**, standard deviation.

Variable used for the log-shape ratio	**1 – maximum length of the bone**				**2 – maximum width of the bone**				**3 – width of the lateral wings**				**4 – width of the anterior edge of the bone**			
Species (no. of specimens)	**min**	**mean**	**max**	**sd**	**min**	**mean**	**max**	**sd**	**min**	**mean**	**max**	**sd**	**min**	**mean**	**max**	**sd**
S. membranaceus (13)	0.80	**0.86**	0.90	0.03	-0.37	**-0.28**	-0.16	0.06	0.14	**0.20**	0.28	0.04	-0.19	**-0.06**	0.00	0.05
S. sorex (13)	0.69	**0.75**	0.81	0.05	-0.14	**-0.04**	0.08	0.06	-0.29	**-0.20**	-0.13	0.05	-0.52	**-0.43**	-0.35	0.05
S. batensoda (16)	0.84	**0.91**	0.95	0.04	-0.16	**-0.10**	-0.04	0.04	-0.06	**0.04**	0.13	0.05	-0.40	**-0.34**	-0.28	0.04
S. nigrita (12)	0.47	**0.58**	0.71	0.07	-0.17	**-0.06**	0.04	0.07	-0.03	**0.02**	0.07	0.03	-0.40	**-0.29**	-0.20	0.07
S. clarias (17)	0.73	**0.78**	0.82	0.02	0.01	**0.09**	0.14	0.03	-0.11	**-0.03**	0.05	0.05	-0.88	**-0.73**	-0.55	0.08
S. schall (25)	0.56	**0.77**	0.85	0.06	-0.14	**-0.05**	0.07	0.05	-0.10	**-0.05**	0.03	0.04	-0.32	**-0.20**	-0.10	0.05
S. filamentosus (7)	0.87	**0.95**	1.01	0.05	-0.30	**-0.23**	-0.15	0.05	-0.14	**-0.12**	-0.09	0.02	-0.34	**-0.29**	-0.24	0.03
S. courteti (9)	0.84	**0.97**	1.02	0.06	-0.35	**-0.30**	-0.22	0.04	-0.37	**-0.24**	-0.18	0.06	-0.32	**-0.21**	-0.13	0.06
S. violaceus (10)	0.86	**0.92**	0.96	0.03	-0.36	**-0.30**	-0.24	0.04	-0.27	**-0.17**	-0.08	0.06	-0.16	**-0.06**	0.00	0.05
S. ocellifer (5)	0.69	**0.73**	0.77	0.03	-0.10	**-0.07**	-0.03	0.03	-0.12	**-0.09**	-0.06	0.03	-0.16	**-0.13**	-0.11	0.02
S. eupterus (1)	0.76				-0.11				0.07				-0.14			

Variable used for the log-shape ratio	**5 – width of the bone at the suture with the frontals**				**6 – length from the anterior edge of the mesethmoid to the level of the maximum width of the lateral wings**				**7 – log "(4)/(2)"**			
Species (no. of specimens)	**min**	**mean**	**max**	**sd**	**min**	**mean**	**max**	**sd**	**min**	**mean**	**max**	**sd**
S. membranaceus (13)	-0.53	**-0.41**	-0.28	0.07	-0.47	**-0.32**	-0.16	0.09	-0.03	**0.21**	0.34	0.10
S. sorex (13)	-0.17	**-0.06**	0.03	0.07	-0.25	**-0.12**	-0.03	0.05	-0.53	**-0.39**	-0.27	0.07
S. batensoda (16)	-0.35	**-0.21**	-0.08	0.08	-0.42	**-0.30**	-0.21	0.06	-0.32	**-0.24**	-0.12	0.05
S. nigrita (12)	-0.12	**-0.03**	0.03	0.05	-0.50	**-0.43**	-0.29	0.05	-0.27	**-0.23**	-0.16	0.03
S. clarias (17)	-0.02	**0.05**	0.14	0.04	-0.25	**-0.17**	-0.11	0.04	-1.00	**-0.82**	-0.56	0.10
S. schall (25)	-0.25	**-0.10**	0.02	0.06	-0.54	**-0.39**	-0.28	0.06	-0.30	**-0.15**	0.01	0.09
S. filamentosus (7)	-0.31	**-0.23**	-0.15	0.06	-0.18	**-0.15**	-0.13	0.02	-0.16	**-0.06**	0.02	0.07
S. courteti (9)	-0.38	**-0.29**	-0.22	0.05	-0.03	**0.02**	0.08	0.04	-0.05	**0.08**	0.22	0.07
S. violaceus (10)	-0.50	**-0.31**	-0.24	0.08	-0.14	**-0.08**	-0.03	0.03	0.11	**0.24**	0.35	0.07
S. ocellifer (5)	-0.14	**-0.07**	-0.03	0.04	-0.49	**-0.37**	-0.31	0.08	-0.09	**-0.06**	-0.04	0.03
S. eupterus (1)	-0.13				-0.45				-0.03			

APPENDIX 2

Values of the log transformed variable that allow distinguishing the lateral ethmoids of *Synodontis* Cuvier, 1816 species. The measurements taken to calculate the variable are shown in Figure 5H and described in the figure caption. Abbreviation: **sd**, standard deviation.

Species (number of specimens)	left lateral ethmoid			
	min	**mean**	**max**	**sd**
S. membranaceus (13)	-1.05	**-0.96**	-0.83	0.07
S. sorex (13)	-1.43	**-1.31**	-1.22	0.07
S. batensoda (16)	-0.89	**-0.71**	-0.60	0.07
S. nigrita (12)	-1.10	**-0.82**	-0.58	0.15
S. clarias (17)	-0.91	**-0.74**	-0.58	0.10
S. schall (25)	-1.17	**-0.84**	-0.44	0.17
S. filamentosus (7)	-0.68	**-0.58**	-0.50	0.06
S. courteti (9)	-2.82	**-2.64**	-2.34	0.16
S. violaceus (10)	-1.50	**-1.29**	-0.98	0.15
S. ocellifer (5)	-0.60	**-0.42**	-0.26	0.14
S. eupterus (2)	-0.29		-0.25	

APPENDIX 3

Variations in the proportions of the *Synodontis* Cuvier, 1816 frontals: **A**, relative part of the ante-orbital (Fig. 7: dimension 2), of the orbital (Fig. 7: dimension 1-[2+4]) and of the post-orbital length (Fig. 7: dimension 4) compared with the total length of the frontal (Fig. 7: 1), in percent; **B**, values of the angles respectively made by the frontal/supraoccipital suture line (**α**) and by the frontal/sphenotic (**β**), both with the symmetry plan of the body (Fig. 7B). Abbreviation: **sd**, standard deviation.

Species (no. of specimens)	A – position and size of the orbit			B – position of the suture line relatively to the body symmetry plan							
	ante-orbital length	orbital length	post-orbital length	α – suture line with the parieto-supraoccipital				β – suture line with the sphenotic			
	mean (sd)	**mean (sd)**	**mean (sd)**	**min**	**mean**	**max**	**sd**	**min**	**mean**	**max**	**sd**
S. membranaceus (12)	35 (2.41)	35 (3.14)	30 (1.15)	22	**25.7**	31	2.2	107	**113.8**	120	3.7
S. sorex (13)	**47 (2.57)**	32 (3.66)	21 (1.80)	41	**45.1**	51	3.1	127	**133.6**	142	5.0
S. batensoda (16)	29 (2.18)	**43 (4.75)**	27 (2.86)	23.5	**26.7**	34	3.2	92	**102.6**	115	6.3
S. nigrita (12)	28 (1.88)	**39 (3.55)**	33 (2.59)	34.5	**40.4**	45.5	2.8	103	**113.9**	126	5.0
S. clarias (17)	32 (3.23)	33 (3.88)	35 (2.13)	37	**41.8**	44.5	1.7	101	**106.9**	116	3.4
S. schall (20)	30 (3.28)	**40 (3.79)**	30 (4.07)	36	**36.5**	44	3.0	105	**113.4**	121	4.2
S. filamentosus (7)	25 (2.37)	**50 (1.03)**	25 (2.36)	24	**27.8**	33.5	3.0	111.5	**119.2**	128	4.7
S. courteti (9)	**44 (2.09)**	30 (3.40)	26 (2.65)	24	**30.5**	39	4.4	99	**104.5**	111	4.4
S. violaceus (10)	**43 (1.77)**	35 (1.68)	22 (2.66)	29	**36.6**	47.5	4.6	108	**112.3**	125	3.7
S. ocellifer (5)	27 (0.76)	**41 (3.42)**	32 (2.90)	32	**38.6**	44	3.3	103	**111.0**	117.5	3.7
S. eupterus (2)	29	**40**	31	25		32		110		118	

APPENDIX 4

Values of log-shape ratios that allow distinguishing the frontals of *Synodontis* Cuvier, 1816 species. The measurements taken to calculate the variables are shown in Figure 7 and described in the figure caption. Abbreviation: **sd**, standard deviation.

Variable used for the log-shape ratio	1 – total length				2 – ante-orbital length				3 – orbital distance				4 – post-orbital length			
Species (no. of specimens)	**min**	**mean**	**max**	**sd**	**min**	**mean**	**max**	**sd**	**min**	**mean**	**max**	**sd**	**min**	**mean**	**max**	**sd**
S. membranaceus (12)	1.24	**1.29**	1.33	0.03	0.10	**0.25**	0.40	0.09	0.19	**0.29**	0.40	0.08	0.01	**0.09**	0.17	0.05
S. sorex (13)	1.12	**1.18**	1.25	0.03	0.34	**0.43**	0.53	0.05	-0.07	**0.06**	0.20	0.08	-0.51	**-0.41**	-0.26	0.09
S. batensoda (16)	1.23	**1.27**	1.32	0.03	-0.15	**0.05**	0.19	0.09	0.26	**0.44**	0.62	0.09	-0.21	**-0.04**	0.14	0.11
S. nigrita (12)	0.97	**1.04**	1.07	0.04	-0.35	**-0.23**	-0.16	0.06	-0.01	**0.16**	0.28	0.09	-0.23	**-0.11**	-0.02	0.08
S. clarias (20)	1.06	**1.10**	1.16	0.02	-0.38	**-0.03**	0.13	0.12	-0.03	**0.12**	0.27	0.07	-0.10	**0.01**	0.18	0.07
S. schall (28)	1.08	**1.15**	1.21	0.03	-0.33	**-0.03**	0.24	0.14	0.05	**0.22**	0.38	0.08	-0.27	**-0.06**	0.16	0.13
S. filamentosus (7)	1.20	**1.25**	1.29	0.03	-0.20	**-0.11**	-0.01	0.08	0.49	**0.56**	0.61	0.04	-0.42	**-0.19**	-0.07	0.14
S. courteti (9)	1.27	**1.34**	1.39	0.03	0.46	**0.53**	0.62	0.06	-0.02	**0.13**	0.33	0.11	-0.19	**-0.03**	0.07	0.09
S. violaceus (10)	1.24	**1.28**	1.33	0.04	0.37	**0.45**	0.53	0.04	0.13	**0.24**	0.34	0.08	-0.42	**-0.27**	-0.06	0.12
S. ocellifer (5)	1.08	**1.13**	1.17	0.04	-0.21	**-0.19**	-0.15	0.03	0.16	**0.25**	0.31	0.07	-0.13	**-0.02**	0.09	0.08
S. eupterus (2)	1.10		1.11		-0.18		-0.08		0.19		0.35		-0.08		-0.01	

Variable used for the log-shape ratio	5 – ante-orbital width				6 – orbital width				7 – post-orbital width				8 – depth of the orbital edge			
Species (no. of specimens)	**min**	**mean**	**max**	**sd**	**min**	**mean**	**max**	**sd**	**min**	**mean**	**max**	**sd**	**min**	**mean**	**max**	**sd**
S. membranaceus (12)	-0.10	**-0.03**	0.06	0.04	-0.29	**-0.21**	-0.13	0.05	-0.04	**0.03**	0.11	0.04	-1.65	**-1.39**	-1.12	0.18
S. sorex (13)	0.18	**0.23**	0.27	0.03	-0.02	**0.11**	0.20	0.07	0.17	**0.29**	0.39	0.07	-2.04	**-1.72**	-1.43	0.20
S. batensoda (16)	-0.21	**-0.16**	-0.07	0.04	-0.53	**-0.40**	-0.33	0.06	-0.01	**0.09**	0.19	0.06	-1.16	**-0.95**	-0.73	0.10
S. nigrita (12)	-0.01	**0.05**	0.12	0.04	0.05	**0.12**	0.21	0.05	0.33	**0.41**	0.47	0.04	-1.69	**-1.38**	-1.16	0.15
S. clarias (20)	0.08	**0.15**	0.25	0.05	-0.01	**0.08**	0.18	0.06	0.24	**0.31**	0.37	0.04	-1.90	**-1.50**	-1.18	0.20
S. schall (28)	-0.05	**0.05**	0.16	0.06	-0.14	**0.00**	0.15	0.07	0.25	**0.35**	0.44	0.04	-1.89	**-1.56**	-1.12	0.19
S. filamentosus (7)	-0.33	**-0.24**	-0.15	0.06	-0.60	**-0.50**	-0.41	0.06	0.17	**0.26**	0.31	0.05	-1.20	**-0.95**	-0.72	0.16
S. courteti (9)	-0.02	**0.09**	0.14	0.06	-0.16	**0.00**	0.09	0.08	0.12	**0.20**	0.26	0.04	-2.11	**-1.94**	-1.70	0.15
S. violaceus (10)	-0.01	**0.04**	0.13	0.05	-0.24	**-0.13**	0.00	0.08	0.16	**0.24**	0.31	0.05	-1.58	**-1.49**	-1.35	0.09
S. ocellifer (5)	0.00	**0.01**	0.02	0.01	-0.05	**-0.01**	0.02	0.04	0.38	**0.41**	0.44	0.02	-1.59	**-1.49**	-1.36	0.10
S. eupterus (2)	-0.10		0.04		-0.20		-0.01		0.22		0.27		-1.30		-1.04	

Variable used for the log-shape ratio	9 – length of the supraoccipital suture line				10 – length of the frontal suture line			
Species (no. of specimens)	**min**	**mean**	**max**	**sd**	**min**	**mean**	**max**	**sd**
S. membranaceus (12)	-0.60	**-0.38**	-0.25	0.09	-0.03	**0.06**	0.18	0.07
S. sorex (13)	-0.32	**-0.19**	-0.06	0.08	-0.08	**0.02**	0.14	0.08
S. batensoda (16)	-0.45	**-0.28**	-0.07	0.09	-0.21	**-0.03**	0.06	0.07
S. nigrita (12)	-0.44	**-0.30**	-0.22	0.06	0.17	**0.24**	0.30	0.04
S. clarias (20)	-0.54	**-0.42**	-0.29	0.06	0.10	**0.19**	0.33	0.07
S. schall (28)	-0.48	**-0.29**	-0.09	0.10	-0.01	**0.17**	0.35	0.09
S. filamentosus (7)	-0.19	**-0.07**	0.05	0.10	-0.15	**-0.01**	0.10	0.09
S. courteti (9)	-0.53	**-0.42**	-0.26	0.08	0.00	**0.08**	0.18	0.07
S. violaceus (10)	-0.52	**-0.32**	-0.17	0.11	-0.17	**-0.04**	0.05	0.10
S. ocellifer (5)	-0.43	**-0.33**	-0.22	0.08	0.20	**0.25**	0.33	0.05
S. eupterus (2)	-0.19		-0.07		-0.07		0.05	

APPENDIX 5

Values of variables that allow us to distinguish the supraoccipitals of *Synodontis* Cuvier, 1816 species: **1**-**7**, log-shape ratios obtained from linear dimensions on the supraoccipitals; **8**, **9**, log transformed variables. The measurements taken to calculate the variables are shown in Figure 12 and described in the figure caption. Abbreviation: **sd**, standard deviation.

Variable used for the log-shape ratio	**1 – maximum length of the bone**				**2 – length of the posterior free margins**				**3 – length of the suture with the sphenotic**			
Species (no. of specimens)	**min**	**mean**	**max**	**sd**	**min**	**mean**	**max**	**sd**	**min**	**mean**	**max**	**sd**
S. membranaceus (12)	0.84	**0.97**	1.02	0.01	-0.81	**-0.60**	-0.33	0.04	-1.22	**-0.97**	-0.71	0.04
S. sorex (13)	0.77	**0.82**	0.92	0.01	-0.85	**-0.51**	-0.22	0.04	-0.99	**-0.81**	-0.67	0.03
S. batensoda (16)	0.77	**0.85**	0.92	0.01	-0.81	**-0.57**	-0.37	0.04	-1.17	**-0.97**	-0.75	0.03
S. nigrita (12)	0.73	**0.78**	0.84	0.01	-1.44	**-1.11**	-0.93	0.04	-0.98	**-0.87**	-0.78	0.02
S. clarias (20)	0.78	**0.86**	0.92	0.01	-0.26	**-0.17**	-0.06	0.02	-0.99	**-0.82**	-0.70	0.02
S. schall (28)	0.63	**0.77**	0.84	0.01	-0.87	**-0.54**	-0.22	0.04	-1.24	**-0.94**	-0.64	0.04
S. filamentosus (7)	0.66	**0.71**	0.81	0.02	-0.80	**-0.55**	-0.46	0.05	-1.06	**-0.93**	-0.79	0.04
S. courteti (9)	0.74	**0.79**	0.87	0.01	-0.69	**-0.58**	-0.46	0.03	-1.18	**-0.90**	-0.72	0.05
S. violaceus (10)	0.62	**0.70**	0.77	0.01	-0.77	**-0.66**	-0.48	0.03	-1.15	**-0.85**	-0.68	0.04
S. ocellifer (5)	0.79	**0.83**	0.87	0.01	-1.14	**-0.95**	-0.66	0.09	-0.83	**-0.78**	-0.74	0.02
S. eupterus (2)	0.86		0.92		-0.80		-0.65		-1.09		-0.99	

Variable used for the log-shape ratio	**4 – length of the suture with the anterior nucal plate**				**5 – width at the level of the junction with the frontal and the sphenotic**				**6 – width at the level of the junction with the sphenotic and the pterotic**			
Species (no. of specimens)	**min**	**mean**	**max**	**sd**	**min**	**mean**	**max**	**sd**	**min**	**mean**	**max**	**sd**
S. membranaceus (12)	-0.56	**-0.28**	-0.05	0.04	-0.16	**0.05**	0.17	0.03	0.30	**0.38**	0.49	0.01
S. sorex (13)	-0.67	**-0.51**	-0.43	0.02	0.02	**0.13**	0.22	0.02	0.43	**0.48**	0.56	0.01
S. batensoda (16)	-0.61	**-0.43**	-0.26	0.03	-0.04	**0.17**	0.38	0.03	0.36	**0.48**	0.59	0.02
S. nigrita (12)	-0.12	**-0.08**	-0.03	0.01	0.06	**0.17**	0.27	0.02	0.45	**0.50**	0.56	0.01
S. clarias (20)	-0.98	**-0.74**	-0.63	0.03	-0.01	**0.11**	0.22	0.02	0.42	**0.47**	0.56	0.01
S. schall (28)	-0.51	**-0.32**	-0.18	0.02	-0.07	**0.07**	0.37	0.03	0.27	**0.42**	0.53	0.01
S. filamentosus (7)	-0.56	**-0.41**	-0.29	0.04	0.10	**0.19**	0.32	0.04	0.44	**0.49**	0.54	0.02
S. courteti (9)	-0.45	**-0.29**	-0.19	0.03	-0.10	**0.01**	0.24	0.04	0.35	**0.40**	0.51	0.02
S. violaceus (10)	-0.58	**-0.45**	-0.31	0.03	-0.05	**0.15**	0.40	0.04	0.45	**0.53**	0.61	0.02
S. ocellifer (5)	-0.26	**-0.23**	-0.19	0.01	-0.03	**0.07**	0.13	0.03	0.33	**0.43**	0.48	0.03
S. eupterus (2)	-0.29		-0.23		0.23		0.26		0.48		0.53	

Variable used for the log-shape ratio	**7 – width of the bone at its posteriormost level**				**8 – log "(7)/(1)"**				**9 – log "(5)/(1)"**			
Species (no. of specimens)	**min**	**mean**	**max**	**sd**	**min**	**mean**	**max**	**sd**	**min**	**mean**	**max**	**sd**
S. membranaceus (12)	0.32	**0.44**	0.54	0.02	-0.67	**-0.52**	-0.32	0.02	-0.70	**-0.58**	-0.51	0.02
S. sorex (13)	0.35	**0.40**	0.45	0.01	-0.57	**-0.43**	-0.32	0.02	-0.42	**-0.34**	-0.25	0.01
S. batensoda (16)	0.38	**0.46**	0.55	0.02	-0.51	**-0.38**	-0.22	0.02	-0.53	**-0.36**	-0.18	0.03
S. nigrita (12)	0.52	**0.60**	0.67	0.01	-0.24	**-0.18**	-0.11	0.01	-0.38	**-0.28**	-0.22	0.02
S. clarias (20)	0.21	**0.28**	0.38	0.01	-0.68	**-0.58**	-0.48	0.02	-0.49	**-0.39**	-0.23	0.02
S. schall (28)	0.46	**0.53**	0.60	0.01	-0.36	**-0.24**	-0.08	0.02	-0.56	**-0.35**	-0.16	0.02
S. filamentosus (7)	0.43	**0.50**	0.54	0.02	-0.38	**-0.20**	-0.14	0.03	-0.26	**-0.22**	-0.19	0.01
S. courteti (9)	0.49	**0.56**	0.61	0.01	-0.33	**-0.23**	-0.17	0.02	-0.44	**-0.39**	-0.34	0.01
S. violaceus (10)	0.51	**0.57**	0.64	0.01	-0.19	**-0.12**	-0.04	0.02	-0.32	**-0.16**	-0.09	0.02
S. ocellifer (5)	0.53	**0.62**	0.69	0.03	-0.26	**-0.20**	-0.16	0.02	-0.48	**-0.39**	-0.33	0.03
S. eupterus (2)	0.33		0.45		-0.59		-0.41		-0.39		-0.38	

APPENDIX 6

Values of variables that allow distinguishing the cleithra of *Synodontis* Cuvier, 1816 species: **1**-**6**, log-shape ratios obtained from linear dimension of the humeral plate of the cleithra; **7**, **8**, log transformed variables; **δ**, **γ**, angle values. The measurements taken to calculate the variables are shown in Figure 32 and described in the figure caption. Abbreviation: **sd**, standard deviation.

Variable used for the log-shape ratio	**1 – total height of the humeral plate**				**2 – height of the lower part**				**3 – length of the dorsal edge**				**4 – length of the antero-ventral edge**			
Species (no. of specimens)	**min**	**mean**	**max**	**sd**	**min**	**mean**	**max**	**sd**	**min**	**mean**	**max**	**sd**	**min**	**mean**	**max**	**sd**
S. membranaceus (13)	0.30	**0.37**	0.51	0.02	-3.12	**-2.20**	-1.75	0.13	0.37	**0.45**	0.63	0.02	0.37	**0.59**	0.80	0.05
S. sorex (13)	0.12	**0.23**	0.32	0.02	-1.10	**-0.87**	-0.59	0.05	0.12	**0.25**	0.37	0.02	-0.44	**-0.25**	-0.08	0.03
S. batensoda (16)	0.21	**0.39**	0.59	0.03	-3.57	**-2.57**	-1.84	0.13	0.50	**0.62**	0.82	0.03	0.04	**0.34**	0.63	0.04
S. nigrita (12)	0.16	**0.22**	0.32	0.01	-2.83	**-2.28**	-1.56	0.10	0.67	**0.82**	0.93	0.02	-0.67	**-0.41**	-0.19	0.05
S. clarias (17)	0.21	**0.28**	0.36	0.01	-1.63	**-1.27**	-0.94	0.05	0.30	**0.39**	0.47	0.01	-0.34	**-0.16**	0.03	0.03
S. schall (25)	0.01	**0.11**	0.25	0.01	-2.01	**-1.52**	-1.24	0.04	0.41	**0.56**	0.68	0.02	-0.67	**-0.36**	-0.16	0.03
S. filamentosus (7)	0.06	**0.10**	0.12	0.01	-1.23	**-1.06**	-0.96	0.04	0.30	**0.36**	0.41	0.02	-0.39	**-0.30**	-0.17	0.04
S. courteti (9)	-0.06	**0.04**	0.17	0.02	-1.80	**-1.38**	-1.12	0.08	0.35	**0.47**	0.66	0.03	-0.44	**-0.27**	-0.10	0.04
S. violaceus (10)	-0.09	**0.09**	0.25	0.03	-1.78	**-1.51**	-1.20	0.05	0.40	**0.51**	0.59	0.02	-0.43	**-0.23**	0.14	0.05
S. ocellifer (5)	0.18	**0.31**	0.40	0.04	-2.27	**-1.97**	-1.69	0.10	0.67	**0.78**	0.89	0.05	-1.03	**-0.60**	-0.27	0.14
S. eupterus (2)	0.13		0.16		-2.35		-2.05		0.69		0.78		-0.28		-0.25	

Variable used for the log-shape ratio and angles measured	**5 – length of the postero-ventral edge**				**6 – total length of the humeral plate**				**7 – log "(4)/(5)"**				**8 – log "(1)/(6)"**			
Species (no. of specimens)	**min**	**mean**	**max**	**sd**	**min**	**mean**	**max**	**sd**	**min**	**mean**	**max**	**sd**	**min**	**mean**	**max**	**sd**
S. membranaceus (13)	-0.26	**-0.16**	0.00	0.02	0.82	**0.96**	1.18	0.04	0.54	**0.75**	0.94	0.04	-0.75	**-0.59**	-0.43	0.03
S. sorex (13)	**-0.03**	**0.07**	**0.15**	**0.01**	0.49	**0.56**	0.63	0.01	-0.59	**-0.32**	-0.05	0.04	-0.50	**-0.34**	-0.19	0.03
S. batensoda (16)	0.10	**0.23**	0.42	0.03	0.84	**0.98**	1.19	0.03	-0.21	**0.11**	0.34	0.03	-0.71	**-0.59**	-0.49	0.02
S. nigrita (12)	0.51	**0.67**	0.81	0.03	0.79	**0.97**	1.11	0.02	-1.44	**-1.08**	-0.82	0.06	-0.88	**-0.75**	-0.59	0.02
S. clarias (17)	-0.02	**0.10**	0.19	0.02	0.54	**0.65**	0.73	0.01	-0.50	**-0.26**	-0.02	0.05	-0.50	**-0.36**	-0.22	0.02
S. schall (25)	0.27	**0.42**	0.53	0.01	0.73	**0.80**	0.89	0.01	-1.15	**-0.78**	-0.50	0.04	-0.82	**-0.69**	-0.59	0.01
S. filamentosus (7)	**0.15**	**0.23**	**0.30**	**0.02**	0.64	**0.67**	0.71	0.01	-0.67	**-0.53**	-0.32	0.06	-0.61	**-0.57**	-0.51	0.01
S. courteti (9)	0.28	**0.36**	0.56	0.03	0.70	**0.77**	0.90	0.02	-0.92	**-0.63**	-0.38	0.07	-0.86	**-0.73**	-0.63	0.03
S. violaceus (10)	0.09	**0.34**	0.47	0.03	0.73	**0.79**	0.83	0.01	-0.88	**-0.57**	0.05	0.08	-0.86	**-0.70**	-0.48	0.04
S. ocellifer (5)	0.49	**0.59**	0.71	0.05	0.83	**0.88**	0.95	0.02	-1.71	**-1.19**	-0.77	0.18	-0.70	**-0.57**	-0.47	0.04
S. eupterus (2)	0.56		0.69		0.92		1.00		-0.97		-0.80		-0.84		-0.79	

Variable used for the log-shape ratio and angles measured	**δ – formed by the dorsal edge and the ventral line of the humeral plate**				**γ – formed by the dorsal edge and the vertical line at the level of the first dorsal process**			
Species (no. of specimens)	**min**	**mean**	**max**	**sd**	**min**	**mean**	**max**	**sd**
S. membranaceus (13)	29.81	**32.59**	34.48	0.47	58.55	**60.07**	63.10	0.46
S. sorex (13)	43.06	**49.91**	55.32	1.09	44.33	**50.45**	58.45	1.03
S. batensoda (16)	38.17	**42.27**	50.76	0.90	42.15	**48.98**	52.68	0.76
S. nigrita (12)	56.05	**59.87**	64.95	0.67	26.39	**31.47**	35.59	0.72
S. clarias (17)	42.68	**46.05**	50.45	0.57	46.81	**49.66**	54.66	0.60
S. schall (25)	53.75	**59.59**	62.61	0.45	31.17	**34.19**	39.51	0.37
S. filamentosus (7)	55.34	**58.21**	61.01	0.77	37.30	**39.07**	41.91	0.75
S. courteti (9)	53.16	**60.90**	64.89	1.31	30.28	**33.75**	38.97	1.01
S. violaceus (10)	47.30	**57.83**	68.53	2.00	29.02	**36.75**	44.39	1.71
S. ocellifer (5)	52.21	**56.31**	58.36	1.07	34.64	**36.34**	38.93	0.75
S. eupterus (2)	63.82		66.85		29.88		30.68	

APPENDIX 7

Values of variables that allow distinguishing the pectoral spines of *Synodontis* Cuvier, 1816 species: **1**-**9**, log-shape ratios obtained from linear dimensions on the head of the pectoral spine; **10**, **11**, log transformed variables; **θ**, **η**, angle values; **density**, ratio "number of tubercles along the outer edge of the spine/ total length where tubercles are present". The measurements taken to calculate the variables are shown in Figure 35 and described in the figure caption. Abbreviation: **sd**, standard deviation.

Variable used for the log-shape ratio	**1 – minimum width of the dorsal wall of the inner fossa**				**2 – minimum width of the ventral wall**				**3 – width of the spine at the base of the inner fossa**			
Species (no. of specimens)	**min**	**mean**	**max**	**sd**	**min**	**mean**	**max**	**sd**	**min**	**mean**	**max**	**sd**
S. membranaceus (12)	-0.52	**-0.39**	-0.27	0.02	-1.00	**-0.86**	-0.68	0.03	0.22	**0.31**	0.41	0.01
S. sorex (13)	-0.52	**-0.44**	-0.33	0.02	-0.97	**-0.83**	-0.59	0.03	0.14	**0.26**	0.34	0.02
S. batensoda (16)	-0.44	**-0.33**	-0.25	0.02	-1.00	**-0.85**	-0.76	0.02	0.25	**0.30**	0.36	0.01
S. clarias (20)	-0.45	**-0.33**	-0.24	0.02	-0.88	**-0.71**	-0.52	0.03	0.26	**0.34**	0.47	0.02
S. schall (28)	-0.51	**-0.44**	-0.35	0.01	-0.86	**-0.70**	-0.53	0.02	0.19	**0.27**	0.35	0.01
S. filamentosus (7)	-0.59	**-0.48**	-0.36	0.03	-1.01	**-0.87**	-0.76	0.04	0.16	**0.19**	0.24	0.01
S. courteti (9)	-0.60	**-0.50**	-0.43	0.02	-0.92	**-0.85**	-0.79	0.02	0.13	**0.17**	0.23	0.01
S. violaceus (10)	-0.68	**-0.53**	-0.44	0.03	-0.98	**-0.84**	-0.72	0.03	0.13	**0.18**	0.24	0.01
S. ocellifer (5)	-0.47	**-0.41**	-0.34	0.02	-0.71	**-0.63**	-0.48	0.04	0.27	**0.33**	0.41	0.03
S. eupterus (2)	-0.45		-0.23		-0.85		-0.53		0.18		0.39	

Variable used for the log-shape ratio	**6 – minimum height of the posteroventral process**				**7 – maximum width of the articular plateau**				**8 – maximum length between the postero- and anteroventral processes**			
Species (no. of specimens)	**min**	**mean**	**max**	**sd**	**min**	**mean**	**max**	**sd**	**min**	**mean**	**max**	**sd**
S. membranaceus (12)	-0.67	**-0.51**	-0.42	0.02	0.62	**0.70**	0.76	0.01	0.22	**0.30**	0.34	0.01
S. sorex (13)	-0.44	**-0.36**	-0.20	0.02	0.55	**0.62**	0.69	0.01	0.27	**0.33**	0.41	0.01
S. batensoda (16)	-0.53	**-0.38**	-0.11	0.04	0.55	**0.62**	0.67	0.01	0.24	**0.31**	0.40	0.01
S. clarias (20)	-0.67	**-0.43**	-0.33	0.02	0.60	**0.68**	0.75	0.01	0.22	**0.30**	0.39	0.01
S. schall (28)	-0.54	**-0.35**	-0.20	0.02	0.57	**0.67**	0.74	0.01	0.25	**0.34**	0.43	0.01
S. filamentosus (7)	-0.51	**-0.38**	-0.29	0.03	0.67	**0.75**	0.79	0.02	0.31	**0.35**	0.38	0.01
S. courteti (9)	-0.44	**-0.32**	-0.22	0.02	0.52	**0.57**	0.60	0.01	0.26	**0.29**	0.35	0.01
S. violaceus (10)	-0.39	**-0.31**	-0.12	0.02	0.56	**0.63**	0.68	0.01	0.37	**0.40**	0.44	0.01
S. ocellifer (5)	-0.40	**-0.33**	-0.27	0.02	0.58	**0.63**	0.67	0.01	0.27	**0.29**	0.34	0.01
S. eupterus (2)	-0.41		-0.28		0.67		0.79		0.25		0.40	

Variable used for the log-shape ratio, and other variables	**11 – log "(9)/(3)"**				**θ – angle between the axial process and the line formed by the inner tubercles**				**η – average angle of the proximal edge of the outer 6th to 15th tubercles with the edge of the spine**			
Species (no. of specimens)	**min**	**mean**	**max**	**sd**	**min**	**mean**	**max**	**sd**	**min**	**mean**	**max**	**sd**
S. membranaceus (12)	0.07	**0.26**	0.44	0.03	116	**121.3**	129	1.12	27	**37.0**	51	2.55
S. sorex (13)	0.19	**0.31**	0.56	0.03	120	**126.4**	133	1.54				
S. batensoda (16)	0.15	**0.26**	0.36	0.02	112	**121.3**	130	2.02	21	**30.3**	41	2.06
S. clarias (20)	-0.08	**0.14**	0.30	0.03	120	**126.2**	132	0.97	31	**38.6**	45	1.27
S. schall (28)	0.05	**0.26**	0.35	0.02	113	**127.8**	138	1.93	36	**49.7**	60	1.77
S. filamentosus (7)	0.24	**0.45**	0.54	0.04	126	**132.3**	138	1.74	37	**45.3**	52	2.57
S. courteti (9)	0.28	**0.40**	0.46	0.03	123	**126.8**	134	1.34	76	**79.3**	89	1.63
S. violaceus (10)	0.39	**0.49**	0.60	0.02	120	**130.1**	138	2.37	44	**50.6**	61	1.56
S. ocellifer (5)	0.03	**0.13**	0.23	0.03	125	**129.2**	132	1.32	45	**49.0**	51	1.41
S. eupterus (2)	0.24		0.39		127		134		34		45	

APPENDIX 7

Continuation.

Variable used for the log-shape ratio	4 – maximum height of the inner fossa				5 – distance between the dorsal edge of the inner fossa and the tip of the posteroventral process			
Species (no. of specimens)	**min**	**mean**	**max**	**sd**	**min**	**mean**	**max**	**sd**
S. membranaceus (12)	-0.65	**-0.41**	-0.17	0.04	0.25	**0.31**	0.35	0.01
S. sorex (13)	-0.52	**-0.37**	-0.20	0.03	0.02	**0.24**	0.35	0.03
S. batensoda (16)	-0.55	**-0.45**	-0.33	0.02	0.09	**0.23**	0.38	0.02
S. clarias (20)	-0.70	**-0.57**	-0.43	0.02	0.14	**0.23**	0.35	0.02
S. schall (28)	-0.59	**-0.41**	-0.26	0.02	-0.01	**0.11**	0.28	0.02
S. filamentosus (7)	-0.40	**-0.28**	-0.22	0.03	-0.01	**0.09**	0.20	0.03
S. courteti (9)	-0.21	**-0.12**	-0.02	0.02	0.12	**0.18**	0.25	0.02
S. violaceus (10)	-0.45	**-0.29**	-0.20	0.02	-0.09	**0.13**	0.29	0.04
S. ocellifer (5)	-0.60	**-0.47**	-0.39	0.04	0.05	**0.13**	0.27	0.04
S. eupterus (2)	-0.54		-0.26		0.03		0.30	

Variable used for the log-shape ratio	9 – maximum height of the head of the spine				10 – log «(7)/(3)»			
Species (no. of specimens)	**min**	**mean**	**max**	**sd**	**min**	**mean**	**max**	**sd**
S. membranaceus (12)	0.47	**0.57**	0.70	0.02	0.28	**0.39**	0.51	0.02
S. sorex (13)	0.50	**0.57**	0.71	0.02	0.24	**0.36**	0.48	0.02
S. batensoda (16)	0.47	**0.56**	0.65	0.02	0.22	**0.32**	0.42	0.02
S. clarias (20)	0.34	**0.48**	0.57	0.02	0.16	**0.34**	0.49	0.03
S. schall (28)	0.40	**0.53**	0.61	0.01	0.30	**0.40**	0.55	0.02
S. filamentosus (7)	0.48	**0.64**	0.71	0.03	0.43	**0.56**	0.63	0.03
S. courteti (9)	0.51	**0.57**	0.63	0.02	0.29	**0.40**	0.46	0.02
S. violaceus (10)	0.58	**0.67**	0.73	0.01	0.37	**0.45**	0.54	0.01
S. ocellifer (5)	0.43	**0.46**	0.50	0.01	0.21	**0.30**	0.35	0.02
S. eupterus (2)	0.53		0.66		0.39		0.49	

Variable used for the log-shape ratio, and other variables	density – density of tubercles on the outer edge of the spine			
Species (no. of specimens)	**min**	**mean**	**max**	**sd**
S. membranaceus (12)	0.78	**1.03**	1.39	0.05
S. sorex (13)	1.87	**2.03**	2.24	0.03
S. batensoda (16)	1.00	**1.16**	1.34	0.03
S. clarias (20)	1.12	**1.26**	1.37	0.02
S. schall (28)	1.19	**1.32**	1.47	0.02
S. filamentosus (7)	1.39	**1.51**	1.68	0.04
S. courteti (9)	0.96	**1.12**	1.23	0.03
S. violaceus (10)	1.37	**1.60**	1.81	0.04
S. ocellifer (5)	1.27	**1.51**	2.05	0.14
S. eupterus (2)	1.16		1.72	

APPENDIX 8

Values of variables that allow distinguishing the middle nucal plate of *Synodontis* Cuvier, 1816 species: **1**-**6**, log-shape ratios obtained from linear dimensions; **7**, log transformed variable. The measurements taken to calculate the variables are shown in Figure 44 and described in the figure caption. Abbreviation: **sd**, standard deviation.

Variable used for the log-shape ratio	**1 – length of the lateral edge of the middle nucal plate**				**2 – length of the suture with the posterior nucal plate**				**3 – anterior width of the nucal complex**				**4 – posterior width of the nucal complex**			
Species (no. of specimens)	**min**	**mean**	**max**	**sd**	**min**	**mean**	**max**	**sd**	**min**	**mean**	**max**	**sd**	**min**	**mean**	**max**	**sd**
S. membranaceus (13)	-0.15	**0.01**	0.08	0.05	-0.27	**-0.20**	-0.11	0.05	0.20	**0.24**	0.27	0.02	0.10	**0.21**	0.31	0.07
S. sorex (13)	-0.07	**0.03**	0.12	0.06	-0.54	**-0.42**	-0.33	0.06	0.20	**0.27**	0.30	0.03	0.39	**0.43**	0.48	0.03
S. batensoda (16)	0.03	**0.12**	0.20	0.04	-0.43	**-0.36**	-0.27	0.04	0.22	**0.26**	0.33	0.03	0.21	**0.26**	0.31	0.03
S. nigrita (12)	-0.15	**-0.01**	0.10	0.08	-0.75	**-0.64**	-0.55	0.05	0.42	**0.46**	0.50	0.02	0.42	**0.48**	0.51	0.03
S. clarias (17)	-0.19	**0.15**	0.35	0.12	-0.73	**-0.55**	-0.32	0.10	0.16	**0.21**	0.29	0.04	0.29	**0.36**	0.44	0.03
S. schall (25)	-0.04	**0.10**	0.28	0.08	-0.67	**-0.55**	-0.42	0.07	0.29	**0.37**	0.48	0.04	0.32	**0.40**	0.46	0.04
S. filamentosus (7)	0.05	**0.11**	0.17	0.05	-0.88	**-0.70**	-0.56	0.11	0.32	**0.38**	0.42	0.03	0.44	**0.48**	0.51	0.02
S. courteti (9)	-0.04	**0.03**	0.21	0.08	-0.86	**-0.66**	-0.53	0.10	0.40	**0.45**	0.51	0.03	0.45	**0.52**	0.56	0.04
S. violaceus (10)	-0.03	**0.08**	0.24	0.09	-0.98	**-0.79**	-0.63	0.12	0.36	**0.43**	0.48	0.04	0.47	**0.56**	0.60	0.04
S. ocellifer (5)	0.02	**0.07**	0.17	0.06	-0.49	**-0.45**	-0.42	0.04	0.27	**0.30**	0.34	0.03	0.33	**0.35**	0.37	0.02
S. eupterus (2)	-0.08				-0.39		-0.33		0.13		0.22		0.32		0.33	

Variable used for the log-shape ratio	**5 – maximum width of the posterior notch**				**6 – maximum depth of the bone**				**7 – log "(3)/(4)"**			
Species (no. of specimens)	**min**	**mean**	**max**	**sd**	**min**	**mean**	**max**	**sd**	**min**	**mean**	**max**	**sd**
S. membranaceus (13)	-0.44	**-0.35**	-0.29	0.04	-0.02	**0.09**	0.17	0.05	-0.06	**0.02**	0.11	0.06
S. sorex (13)	-0.19	**-0.13**	-0.04	0.05	-0.24	**-0.18**	-0.07	0.04	-0.21	**-0.16**	-0.13	0.02
S. batensoda (16)	-0.33	**-0.24**	-0.14	0.06	-0.14	**-0.05**	0.09	0.06	-0.05	**0.00**	0.03	0.03
S. nigrita (12)	-0.05	**0.07**	0.13	0.07	-0.43	**-0.36**	-0.30	0.05	-0.06	**-0.02**	0.01	0.02
S. clarias (17)	-0.18	**-0.04**	0.05	0.06	-0.28	**-0.12**	-0.04	0.05	-0.19	**-0.15**	-0.05	0.03
S. schall (25)	-0.23	**-0.07**	0.09	0.07	-0.40	**-0.25**	-0.08	0.09	-0.09	**-0.03**	0.03	0.03
S. filamentosus (7)	-0.01	**0.07**	0.14	0.06	**-0.43**	**-0.34**	**-0.30**	**0.04**	-0.15	**-0.10**	-0.08	0.03
S. courteti (9)	0.01	**0.13**	0.22	0.07	-0.56	**-0.46**	-0.33	0.08	-0.11	**-0.07**	-0.04	0.02
S. violaceus (10)	0.09	**0.19**	0.27	0.06	-0.56	**-0.47**	-0.37	0.06	-0.20	**-0.13**	-0.07	0.04
S. ocellifer (5)	-0.16	**-0.13**	-0.06	0.04	-0.17	**-0.14**	-0.12	0.02	-0.07	**-0.05**	-0.02	0.02
S. eupterus (2)	-0.17		-0.06	-0.08		0.04			-0.20		-0.10	

APPENDIX 9

Values of variables that allow distinguishing the dorsal spine of *Synodontis* Cuvier, 1816 species: **1**-**6**, log-shape ratios obtained from linear dimension; **7**, **8**, log transformed variables. The measurements taken to calculate the variables are shown in Figure 47 and described in the figure caption. Abbreviation: **sd**, standard deviation.

Variable used for the log-shape ratio	**1 – width of the head of the spine**				**2 – width of the spine at the basis of the head**				**3 – distance between the inflexion point of the anterior median crest and the most proximal edge of the spine**				**4 – width of the median articular process**			
Species (no. of specimens)	**min**	**mean**	**max**	**sd**	**min**	**mean**	**max**	**sd**	**min**	**mean**	**max**	**sd**	**min**	**mean**	**max**	**sd**
S. membranaceus (12)	0.62	**0.68**	0.79	0.01	-0.20	**-0.05**	0.07	0.03	0.66	**0.78**	0.83	0.02	-0.43	**-0.31**	-0.19	0.02
S. sorex (13)	0.71	**0.78**	0.84	0.01	-0.33	**-0.23**	-0.13	0.02	0.59	**0.73**	0.86	0.03	-0.17	**-0.08**	-0.03	0.01
S. batensoda (16)	0.67	**0.72**	0.83	0.02	0.00	**0.07**	0.16	0.02	0.69	**0.80**	0.91	0.02	-0.24	**-0.19**	-0.13	0.01
S. nigrita (12)	0.91	**0.98**	1.03	0.01	0.00	**0.08**	0.16	0.02	0.54	**0.61**	0.67	0.01	-0.22	**-0.11**	-0.03	0.02
S. clarias (20)	0.70	**0.77**	0.86	0.01	-0.17	**-0.06**	0.10	0.03	0.65	**0.75**	0.82	0.01	-0.26	**-0.15**	-0.08	0.01
S. schall (28)	0.82	**0.90**	1.00	0.02	-0.03	**0.01**	0.09	0.01	0.56	**0.67**	0.78	0.02	-0.29	**-0.15**	-0.05	0.02
S. filamentosus (7)	0.95	**0.97**	1.01	0.01	-0.17	**-0.12**	-0.03	0.02	0.64	**0.70**	0.79	0.02	-0.20	**-0.08**	0.00	0.03
S. courteti (9)	0.90	**0.97**	1.04	0.02	-0.22	**-0.09**	0.00	0.02	0.58	**0.63**	0.68	0.01	-0.24	**-0.15**	0.01	0.03
S. violaceus (10)	0.97	**1.01**	1.08	0.01	-0.14	**-0.03**	0.12	0.03	0.54	**0.67**	0.76	0.02	-0.13	**-0.03**	0.11	0.02
S. ocellifer (5)	0.85	**0.87**	0.91	0.01	0.06	**0.13**	0.20	0.03	0.48	**0.59**	0.65	0.03	-0.24	**-0.13**	-0.03	0.04
S. eupterus (2)	0.85		0.85		0.06		0.10		0.68		0.73		-0.27		-0.27	

Variable used for the log-shape ratio	**5 – depth of the median articular process**				**6 – width of the foramen**				**7 – log "(2)/(1)"**				**8 – log "(1)/(5)"**			
Species (no. of specimens)	**min**	**mean**	**max**	**sd**	**min**	**mean**	**max**	**sd**	**min**	**mean**	**max**	**sd**	**min**	**mean**	**max**	**sd**
S. membranaceus (12)	-0.36	**-0.22**	-0.13	0.02	-1.17	**-0.88**	-0.63	0.04	0.61	**0.73**	0.89	0.03	0.80	**0.90**	1.05	0.03
S. sorex (13)	-0.29	**-0.20**	-0.12	0.02	-1.10	**-1.01**	-0.72	0.03	0.91	**1.01**	1.08	0.02	0.90	**0.98**	1.10	0.02
S. batensoda (16)	-0.37	**-0.22**	-0.13	0.03	-1.29	**-1.18**	-1.05	0.03	0.58	**0.65**	0.73	0.02	0.81	**0.94**	1.20	0.04
S. nigrita (12)	-0.36	**-0.33**	-0.28	0.01	-1.34	**-1.24**	-1.09	0.03	0.81	**0.90**	0.98	0.02	1.24	**1.31**	1.37	0.02
S. clarias (20)	-0.32	**-0.24**	-0.15	0.01	-1.22	**-1.08**	-0.86	0.03	0.67	**0.83**	0.94	0.03	0.93	**1.01**	1.11	0.02
S. schall (28)	-0.35	**-0.23**	-0.12	0.02	-1.34	**-1.17**	-0.94	0.03	0.72	**0.88**	1.03	0.02	0.94	**1.13**	1.26	0.03
S. filamentosus (7)	-0.30	**-0.23**	-0.14	0.03	-1.44	**-1.25**	-1.04	0.07	1.01	**1.09**	1.16	0.02	1.12	**1.20**	1.25	0.02
S. courteti (9)	-0.47	**-0.35**	-0.26	0.02	-1.22	**-1.00**	-0.78	0.05	0.99	**1.07**	1.13	0.01	1.20	**1.33**	1.47	0.03
S. violaceus (10)	-0.47	**-0.38**	-0.26	0.02	-1.52	**-1.24**	-1.05	0.05	0.88	**1.04**	1.19	0.03	1.24	**1.39**	1.47	0.02
S. ocellifer (5)	-0.35	**-0.26**	-0.16	0.03	-1.31	**-1.20**	-0.95	0.07	0.68	**0.75**	0.79	0.02	1.01	**1.13**	1.21	0.03
S. eupterus (2)	-0.32		-0.24		-1.12		-1.04		0.75		0.79		1.09		1.17	